

# **IN SITU CO<sub>2</sub> EOR MECHANISM AND CO<sub>2</sub>-OIL PHASE BEHAVIOR**

A

**THESIS**

Presented to the Graduate Faculty of Petroleum Engineering

African University of Science and Technology

In Partial Fulfillment of the Requirements

For the Degree of

**MASTER OF SCIENCE IN PETROLEUM ENGINEERING**

By

**ABDULRASHEED, Rukayat Titilayo**



[JUNE, 2019]

## **CERTIFICATION**

This is to certify that the thesis titled “IN SITU CO<sub>2</sub> EOR MECHANISM AND CO<sub>2</sub>-OIL PHASE BEHAVIOR” submitted to the school of postgraduate studies, African University of Science and Technology (AUST), Abuja, Nigeria for the award of the Master's degree is a record of original research carried out by Abdulrasheed, Rukayat Titilayo in the Department of Petroleum Engineering.

**INSITU CO<sub>2</sub> EOR MECHANISM AND CO<sub>2</sub>-OIL PHASE BEHAVIOR**

By

**ABDULRASHEED, RUKAYAT TITILAYO**

**A THESIS APPROVED BY THE PETROLEUM ENGINEERING DEPARTMENT**

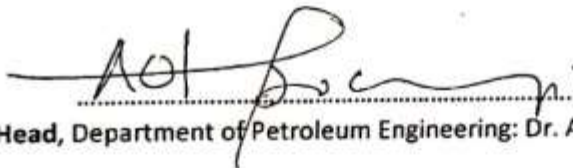
**RECOMMENDED:**



.....  
**Supervisor: Dr. Xingru WU**



.....  
**Committee Member: Prof. David Ogbe**



.....  
**Head, Department of Petroleum Engineering: Dr. Alpheus Igbokoyi**

**APPROVED:**

.....  
**Chief Academic Officer**

.....  
**Date**

## **DEDICATION**

This work is dedicated to my late Father, Alhaji IBRAHIM, Abdulrasheed for his tireless effort to ensure I am where I am today.

## ACKNOWLEDGEMENT

All praises are due to Almighty Allah, who in His infinite mercies has guided me throughout the course of my study at African University of Science and Technology, Abuja.

I would like to appreciate all those who has contributed to the success of this work:

- ✚ Foremost is my supervisor, Dr. Xingru Wu who has taken out time to listen to my ideas and gave me a professional supervision, constructive criticism and passion for doing a quality research.
- ✚ I will also like to mention my able Professor and instructor, Professor David Ogbe who birthed me with the fundamental knowledge of Reservoir Engineering and Simulation, his lectures motivated me to do research in area of study.
- ✚ To my Head of Department, Dr. Alpheus Igbokoyi who gave the courage to finish this work within the limited time available.
- ✚ My appreciation will be incomplete without appreciating my lovely husband; Engr. Abdulwahab Sa'ad for his full support from the beginning till the end of the program.
- ✚ To the wonderful members of Petroleum MSc class of 2019 for making the program worthwhile.
- ✚ To all my family – Mum, Siblings for their prayers and encouragement.
- ✚ To the entire members of AUST community, thank you all for making it a success.

## **ABSTRACT**

Numerical reservoir simulators are employed to obtain meaningful and reliable solutions for an actual case due to extreme complexity of the reservoirs systems. Wilcox formation is a reservoir in the gulf of Mexico with various development challenges, to better maximize the resources in the reservoir, simulation studies is needed to make better informed decision. For this study, a compositional simulator model is developed for comparing CO<sub>2</sub> injection in different API oil reservoir. The fluid samples were characterized using PVT simulator and so also is the swelling factor and the viscosity reduction test. The E300 eclipse simulator was used for determining the MMP by developing a 1-D slimtube experiment model and a CO<sub>2</sub> injection model for the case studied. The estimated MMP of 6500 psia is less than the reservoir pressure so a miscible flooding was achieved. Four API oil samples (22°, 29°, 38° and 45°) was simulated and compared considering different scenarios. The viscosity reduces with increasing injection rate for the light oil samples and from the swelling test, increasing CO<sub>2</sub> injected will increase the oil swelling capability. Furthermore, sensitivity analysis was performed to investigate which of the samples is best candidate for CO<sub>2</sub> flooding and results shows that light oil reservoirs are better candidate for CO<sub>2</sub> flooding.

## Contents

CHAPTER ONE .....	1
1.1 Background Study .....	1
1.2 OBJECTIVE OF RESEARCH .....	3
1.3 Aims and Objective .....	3
1.4 The outlay of the Thesis .....	4
CHAPTER TWO .....	5
Literature Review .....	5
2.1 Geology of deep water Wilcox Formation .....	5
2.1.1 Turbidite Elements .....	5
2.1.2 Paleogene (Wilcox) Deposition .....	6
2.2 Reservoir Characterization and Development Challenges of Wilcox Formation .....	7
2.2.1 Reservoir Characterization .....	7
2.2.2 Obstacles to Exploration and Development GoM Wilcox Formation .....	11
2.3 Immiscible CO <sub>2</sub> Processes .....	11
2.4 IN SITU CO <sub>2</sub> GENERATION .....	13
2.4.1 Ammonium Carbamate as a gas generating agent .....	14
2.5 Kinetics and Mechanism of the Reversible Dissociation of Ammonium Carbamate .....	19
2.5.2 Urea as a gas generating agent .....	27
2.6 TRANSPORT AND STORAGE OF CO <sub>2</sub> .....	28
2.6.1 CO <sub>2</sub> flooding .....	28
2.6.2 Molecular Diffusion Governed Mass Transport .....	29
2.7 Mass Transfer of CO <sub>2</sub> -Crude Oil Systems .....	30
2.7.1 Mass Transfer without Reaction (Physical Absorption) .....	34
2.7.1.1 Film Theory .....	34
2.7.2 Mass Transfer with Chemical Reaction .....	37
2.7.1 Prediction of Diffusion Coefficient .....	39
CHAPTER THREE .....	40
RESERVOIR SIMULATION MODELING .....	40
3.1 INTRODUCTION TO ECLIPSE 300 .....	40
3.2 Data description and Model used .....	40
3.2.1 The phase behavior of the fluid composition .....	41
3.2.2 3-parameter Peng-Robinson Equation of State Model .....	41

3.3 Estimating Minimum Miscibility Pressure (MMP) .....	43
3.4 Urea Reaction and CO <sub>2</sub> Generation Kinetics .....	44
3.5 CO <sub>2</sub> Swelling Factor .....	46
3.5.1 CO <sub>2</sub> swelling factor for different API oil .....	46
3.6 CO <sub>2</sub> -Oil Viscosity Reduction .....	47
3.7 Lohrenz, Bray and Clark Viscosity Reduction Correlation .....	48
3.8 Reservoir Model and Rock Properties .....	49
3.8.1 Grid System .....	49
3.8.2 Computational Process .....	50
3.8.3 Simulation Model .....	50
CHAPTER FOUR .....	52
RESULTS AND DISCUSSION .....	52
4.1 Grid sensitivity Analysis. ....	52
4.2 Simulation Result and Discussion .....	54
4.3 Sensitivity Analysis .....	67
CHAPTER FIVE .....	72
CONCLUSIONS AND RECOMMENDATIONS .....	72
5.2 Recommendations .....	73
REFERENCES .....	80



## LIST OF TABLES

Table 2. 1: The Reservoir and Fluid Properties of the Deepwater Wilcox Formation. ....	8
Table 2. 2: Reservoir Properties of the Lower and Upper Wilcox formation .....	10
Table 3. 1: Urea hydrolysis kinetic Parameters.....	45
Table 3. 2: Input Parameters for the rock and fluid Properties. ....	51
Table A.1: Reservoir Fluid (API @ 21°) Component and their Properties used for study after grouping ..	74
Table A.2: Reservoir Fluid (API @ 38°) Component and their Properties used for study after grouping ..	74
Table A 3: Reservoir Fluid (API @ 38°) Component and their Properties used for study after grouping...	75
Table A 4: Reservoir Fluid (API@ 45°) Component and their Properties used for study after grouping ...	75
Table A.5: The critical properties of the pseudocomponents for the heavy crude oil sample.....	76
Table A.6: The critical properties of the pseudocomponents for the heavy crude oil sample.....	76
Table A.7: The critical properties of the pseudocomponents for the heavy crude oil sample.....	77
Table A. 8: The critical properties of the pseudocomponents for the heavy crude oil sample.....	77
Table A.9: The Binary Interaction Coefficients of the pseudo-components for the heavy oil. ....	78
Table A.10: The Binary Interaction Coefficients of the pseudo-components for the medium oil. ....	78
Table A.11: The Binary Interaction Coefficients of the pseudo-components for the intermediate oil.....	79
Table A.12: The Binary Interaction Coefficients of the pseudo-components for the light oil.....	79

## LIST OF FIGURES

Figure 2. 1: Turbidite classification (Sylvester & Lowe, 2004). .....	5
Figure 2. 2: Major Paleogene producing formations, deep-water Gulf of Mexico (Paul & Meyer, 2001). ..	6
Figure 2. 3: Depositional/structural style of the Tertiary section along the Texas Gulf Coast. ....	9
Figure 2. 4: CO <sub>2</sub> concentration as a function of distance (Steffens, 2010). ....	15
Figure 2. 5: Two semi-infinite regions of CO <sub>2</sub> mass transfer from the water phase into the oil phase with a moving interface. ....	31
Figure 2. 6: Mass transfer of CO <sub>2</sub> progress from Carbonated Water into Oil due to the solubility difference between the aqueous phase and oil phase.....	33
Figure 2. 7: Schematic of the film theory for gas absorption into the liquid.....	35
Figure 2. 8: Mass transfer of CO <sub>2</sub> into the bulk liquid with a fast chemical reaction.(Cullinane, 2005). ....	38
Figure 3. 1: The plot recovery factor of against pressure for predicting MMP. ....	44
Figure 3. 2: the graph of CO <sub>2</sub> swelling factor for different API crude. ....	47
Figure 3. 3: The graph of viscosity reduction for different API crude.....	48
Figure 4. 1: Block oil viscosity graph for the 200 × 200 × 5, 100 × 100 × 5 and 50 × 50 × 5 grid system. ....	53
Figure 4. 2: Oil recovery efficiency for the 200 × 200 × 5, 100 × 100 × 5 and 50 × 50 × 5 grid system. ....	53
Figure 4. 4: Comparison plot of pressure, water-cut and oil production rate.....	56
Figure 4. 5: oil viscosity for the CO <sub>2</sub> injection three scenarios. ....	57
Figure 4. 6: Plots of water-cut against time for different CO <sub>2</sub> injection scenarios. ....	58
Figure 4. 7: Oil recovery factor versus time for the CO <sub>2</sub> injection Scenarios of case A .....	59
Figure 4. 8: Plot of recovery factor versus CO <sub>2</sub> mole fraction injected. ....	60

Figure 4. 9: The oil saturation grid model for CO <sub>2</sub> injection into a 29° API oil reservoir. ....	61
Figure 4. 10: The plot of pressure, production rate and water cut with time. ....	62
Figure 4. 11: The Cumulative recovery factor for 29° API crude sample. ....	63
Figure 4. 12: Plot of oil production rate and total water production with time. ....	63
Figure 4. 13: Oil saturation grid model of CO <sub>2</sub> injection scheme for (a) 50×50×5 grid system and (b) 100×100×5 grid system. ....	64
Figure 4. 14: Plot of pressure, oil production rate and water cut versus time ....	65
Figure 4. 15: Oil recovery factor of CO <sub>2</sub> injection for volatile oil reservoir. ....	66
Figure 4. 16: Plot of total water production and oil production rate versus time. ....	67
Figure 4. 17: Comparison plot of oil recovery factor for four API crude. ....	68
Figure 4. 18: Comparison plot of oil viscosity reduction for four API crude. ....	69
Figure 4. 19: Comparison plot of oil saturation for four API crude. ....	70
Figure 4. 20: Variation of water cut with time. ....	71

## CHAPTER ONE

### 1.1 Background Study

Only some fraction about (10%) of the initial hydrocarbon in place in a petroleum reservoir can be recovered by primary production using the reservoir's natural energy drive. In the turbidite system in the deepwater Wilcox formation of the Northwest Gulf of Mexico, there is a potential of 15Bbbl that covers over 34,000 mi<sup>2</sup> (54,740 km<sup>2</sup>) (Meyer, Zarra, Rains, Meltz, & Hall, 2005). This formation is characterized by high pressure and high temperature and a water depth of 3000-7000 feet, and the formation has an average permeability of about 15mD. Furthermore, the porosity is about 18%, crude gravity of 25<sup>0</sup> API, and viscosity of 6cP. The majority of the remaining oil is trapped by capillary forces, bypassed due to reservoir heterogeneity and mobility of the injected fluid to displace reservoir oil. Therefore, a significant fraction of the remnant oil is available as a target for Enhanced Oil Recovery (EOR) processes. This oil can be an energy source for years to come. However, as of date, there are new EOR technologies for producing the resource which includes Chemical, Water, Polymer, thermal flooding, and Gas Injection. Large research expenditure and efforts are being directed towards enhancing the recovery of this oil but with limited success. Although the complete recovery of all the trapped oil is difficult, the target resource base is very large. Of the major contending processes for this trapped resource, gas injection appears to be an ideal choice.

CO<sub>2</sub> injection is one of the most frequently used gas injection EOR methods and its application grows very fast because of its abundance, greenhouse effect and so forth. Secondary and tertiary recovery process based on gas injection can represent a very interesting solution to extend the life of the reservoirs and maximize the recovery. However, the injection strategy need to be carefully studied in order to optimize the overall sweep efficiency. The common challenges with CO<sub>2</sub> injection include CO<sub>2</sub> supply limitation, transportation, cost investment, and corrosion. For an offshore application, the critical challenge could be related to an extremely remote and significant increase in project cost. Different approaches have been employed to study the performance of CO<sub>2</sub> in increasing oil production including miscible/immiscible injection

carbonated water injection (CWI) and CO<sub>2</sub> injection into the aquifer. In these methods, different parameters can effect such as minimum miscible pressure (MMP), injection rate and so forth.

In situ CO<sub>2</sub> EOR (ICE) is a novel way of generating CO<sub>2</sub> in subsurface for flooding to increase oil recovery in hydrocarbon reservoirs. The process involves dissolving ammonium carbamate or urea in a brine solution as a gas generating agent. This chemical solution at reservoir condition liberates CO<sub>2</sub> and ammonia is generated as a by-product. CO<sub>2</sub> will reduce the viscosity of the crude oil resulting in oil swelling while the ammonia will benefit in terms of wettability alteration. These methods requires minimal capital investment upfront compared to supercritical CO<sub>2</sub> flooding. It reduces fingering because of the absence of free CO<sub>2</sub> phase and this makes it a potential tertiary oil recovery mechanism for both onshore and offshore fields. Chemical solvents methods have been widely studied and generally are recognized as the most effective technologies for CO<sub>2</sub> capture and separation (Bai & Yeh, 1997; Bonenfant, Mimeault, & Hausler, 2003; Chakma, 1995; McCann, Maeder, & Attalla, 2008; Wolsky, Daniels, & Jody, 1994).

CO<sub>2</sub> is absorbed in a chemical such solvent as amines to form bicarbonates (Khatri, Chuang, Soong, & Gray, 2006). In situ CO<sub>2</sub> generation has been studied for Enhanced Oil Recovery and it has been recognized that ammonium carbamate at a high temperature above 80°C will generate CO<sub>2</sub>. Studies have shown that when this ammonium carbamate at high temperature produced CO<sub>2</sub> in a sand pack column, it results in a decrease of oil viscosity and improve in oil recovery (Gumersky, Dzhafarov, Shakhverdiev, & Mamedov, 2000; Lei, Yang, Zu, Wang, & Li, 2016; Shiau, Hsu, Roberts, & Harwell, 2010; Wang, Kadhum, Chen, Shiau, & Harwell, 2017). Additionally, the mass transfer of CO<sub>2</sub> between water and hydrocarbon phase controls displacement efficiency and not MMP (Dong, Huang, & Srivastava, 2001).

Molecular diffusion of the CO<sub>2</sub> from the aqueous phase to the oil phase plays a key role in oil recovery processes. Modeling of the molecular diffusion becomes important in simulation of the reservoir for EOR. Two mechanisms are associated with the mass transfer of components: molecular diffusion and convective

bulk flow. The accurate prediction or measurement of the diffusion coefficient  $D$  is very crucial in determination of the diffusion flux.

## **1.2 OBJECTIVE OF RESEARCH**

Another novel technique of injecting  $\text{CO}_2$  for EOR is to inject it indirectly into the subsurface formation by injecting a solvent which is a  $\text{CO}_2$  generating species. Solvents like concentrated ammonium carbamate solution and urea are commercially available. The solvent when injected subsurface liberates  $\text{CO}_2$  and  $\text{NH}_3$  under reservoir condition. The  $\text{CO}_2$  liberated help reduce the interfacial tension, lowers the viscosity of the oil which results in oil swelling. The ammonia produced at high concentration leads to sand wettability reversal. The self-reaction ignition properties of the urea and ammonium carbamate make the single fluid injection possible and reduce the complexity of the injection system. Because of their  $\text{CO}_2$  producing capacity and reasonable cost-benefit, they appear to be a promising candidate for delivering  $\text{CO}_2$  to increase oil recovery. This work study the technical challenges for EOR of tight and viscous oil recovery of Wilcox formation, review in-situ  $\text{CO}_2$  generation and flooding and compare  $\text{CO}_2$  injection in different API crude through numerical simulation. Sensitivity study was also be carried out.

### **1.3 Aims and Objective**

This numerical study is directed towards studying of  $\text{CO}_2$  flooding for deepwater Wilcox formation. The aim is to investigate the technical limit for EOR of tight and viscous oil recovery using in-situ  $\text{CO}_2$  generation and flooding through numerical simulation and sensitivity study.

In order to accomplish the proposed objectives;

- The development challenges of the Wilcox formation will be studied.
- Review work on the development of in-situ hybrid  $\text{CO}_2$  for EOR.
- Develop a model to study  $\text{CO}_2$  injection in different API oil using a compositional simulator.
- Carry out sensitivity analysis on the study.

## **1.4 The outlay of the Thesis**

The thesis is organized as follows:

- Chapter two reviews literature on the development of Wilcox formation, characterization the formation, the in-situ generation of CO<sub>2</sub> from the gas generating species, extensive review on reaction kinetics and mechanism of dissociation of the generating species, mass transfer and molecular diffusion of CO<sub>2</sub>.
- Chapter three presents a brief description on the simulator used for the study, the properties of the rock and fluid, the methodology employed in this study and some model formulations.
- In Chapter four, the result of developed model obtained from simulation were presented and briefly discussed.
- Chapter five draws conclusions based on the results from chapter four and some useful recommendations were made for further studies.

## CHAPTER TWO

### Literature Review

#### 2.1 Geology of deep water Wilcox Formation

##### 2.1.1 Turbidite Elements

Turbidite used to describe sediment-gravity flow is the depositional system of the deepwater Wilcox formation. The deposition consists of density-driven and mass transport processes and can be classified as either low-density or high-density. The density is used to describe the velocity of the turbid fluid that transports sediment into deep water as shown in Figure 2.1. The low-density turbid flow is characterized by a muddy matrix while the high-density flow is characterized by a turbid flow that is sand rich and rapidly deposited. The properties of the reservoir are described using the flow of energy that transport sediments. The low-density flow is generally fine-grained and the high-density flow is coarse-grained with little or no clay matrix. The high-density type of flow makes the best hydrocarbon reservoirs

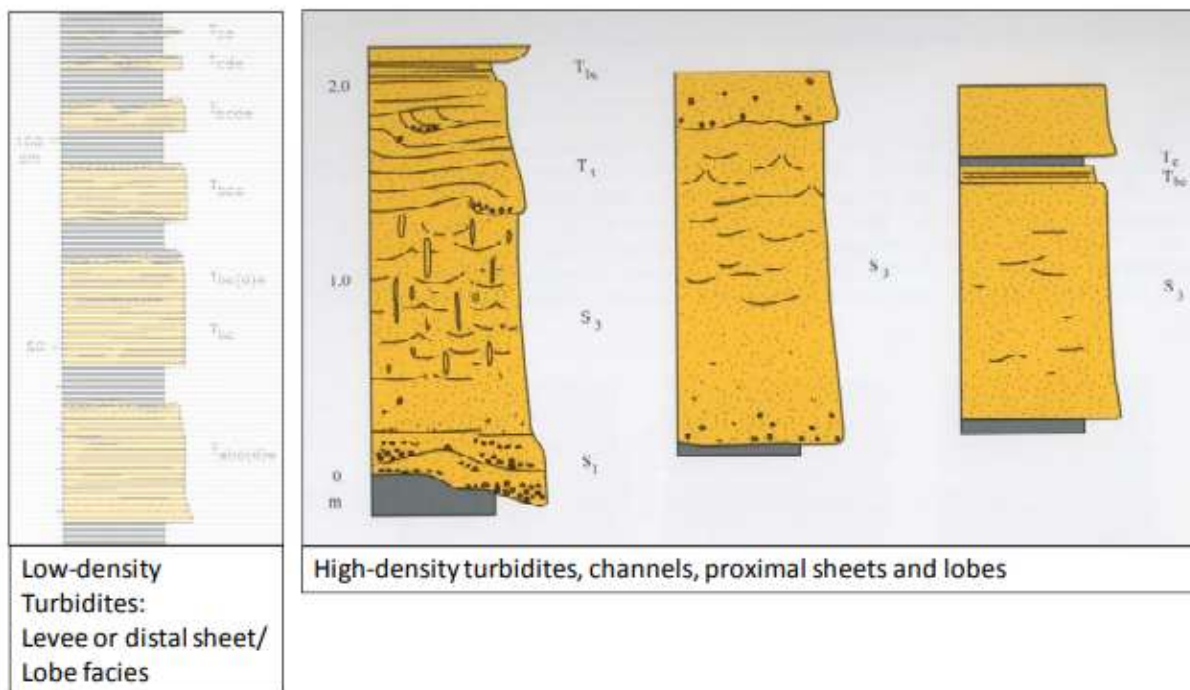


Figure 2. 1: Turbidite classification (Sylvester & Lowe, 2004).



### 2.1.2 Paleogene (Wilcox) Deposition

The deepwater Gulf of Mexico has three main reservoir targets: the Frio sandstone (Oligocene), the Upper Wilcox sandstone (Eocene) and the Lower Wilcox sandstone (Eocene to Paleocene) as shown in Figure 2.2. Frio and Upper Wilcox are found only in the western Gulf of Mexico whereas the Lower Wilcox occurs throughout the western and central basin. The three reservoirs occur in Alaminos Canyon fields and the primary pay sand is the Upper Wilcox. A model for the Wilcox shows that the primary sediment input was from the northwest in large Texas deltaic systems. Additional sediment was supplied by the proto-Rio Grande and other rivers from the southwest originating in Mexico. The clastic sediments from these rivers were deposited and occupied the central and western Gulf of Mexico. These deposits occur as the Lower Wilcox sands in the deeper portion of Alaminos Canyon wells. These tight sands at this depth are a future target for exploitation.

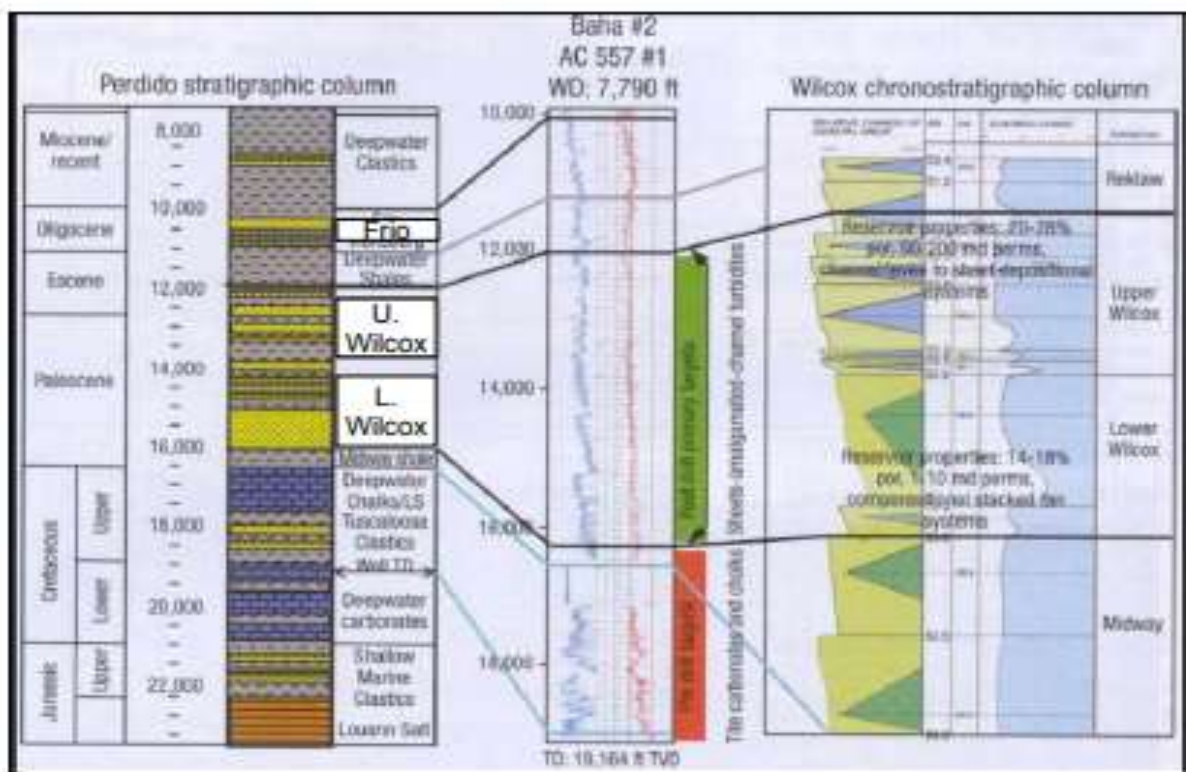


Figure 2. 2: Major Paleogene producing formations, deep-water Gulf of Mexico (Paul & Meyer, 2001).

### 2.1.3 Paleogene Trends (Wilcox Formation)

Paleogene reservoirs are reported to have a complex diagenetic history. Several factors control reservoir quality of Paleogene sands:

- I. **Reservoir mineralogy:** there are more unstable minerals in these reservoirs than in younger sands. The Frio sands exist with West Texas volcanic and have unstable glass shards in the sands which can break down into clay during diagenesis.
- II. **Heat flow:** there can be high heat flow and high temperatures in Paleogene reservoirs which could enhance breakdown of unstable minerals into clay and cement. The presence of salt canopies can lower reservoir temperature because heat is conducted by the salt away from the reservoir.
- III. **Pressure:** there can be overpressure beneath salt canopies. The pressure of the system can preserve properties and inhibit diagenesis.
- IV. **Early minerals:** some early type of cement, such as chlorite rims, inhibit further diagenesis.

## 2.2 Reservoir Characterization and Development Challenges of Wilcox Formation

### 2.2.1 Reservoir Characterization

The regional study of the distribution of sandstone within the Wilcox trend is part of the investigation to assess the potential for producing geothermal energy from the deep subsurface geopressured zone of the Gulf Coast. The study helps to identify areas along the coast that is most favorable for potential resources. It also identified the geopressured and geothermal reservoirs containing petroleum resource at commercial quantity. This includes a reservoir volume of  $3\text{m}^3$ , fluid temperature greater than  $300^\circ\text{F}$ , pressure gradient of at least 0.7 psi per foot, and permeability of more than 20md (Bebout, Loucks, Bosch, & Dorfman, 1976).

Table 2. 1: The Reservoir and Fluid Properties of the Deepwater Wilcox Formation.

Features / Reservoir & Fluid Properties	Properties
Total equivalent depth, feet	5000 – 40,000
The Thickness of pay, feet	Up to 1000
Geology <ol style="list-style-type: none"> <li>1. Age of deposits</li> <li>2. Depositional setting</li> <li>3. Lithology</li> <li>4. Rock texture</li> </ol>	<ol style="list-style-type: none"> <li>1. Paleogene</li> <li>2. submarine fan</li> <li>3. turbidites (interbedded sands &amp; shales)</li> <li>4. consolidated</li> </ol>
Initial Reservoir Conditions <ol style="list-style-type: none"> <li>1. Pressure, psia</li> <li>2. Temperature, °F</li> <li>3. Water saturation, %</li> <li>4. Gas-oil-ratio, scf/stb</li> <li>5. Saturation pressure, psia</li> <li>6. Over-pressured?</li> </ol>	<ol style="list-style-type: none"> <li>1. 7500 - 30,000</li> <li>2. 130 - 300</li> <li>3. 35</li> <li>4. 250-500</li> <li>5. 1239</li> <li>6. Yes</li> </ol>
Reservoir Rock Properties <ol style="list-style-type: none"> <li>1. Porosity, %</li> <li>2. Permeability to oil, md</li> <li>3. Rock compressibility, x E-06 psi-1</li> </ol>	<ol style="list-style-type: none"> <li>1. 7 - 29</li> <li>2. 15 or less</li> <li>3. 4.5</li> </ol>
Reservoir Fluid Properties <ol style="list-style-type: none"> <li>1. Oil gravity, °API</li> <li>2. Oil viscosity, cp</li> </ol>	<ol style="list-style-type: none"> <li>1. 29</li> <li>2. 8</li> </ol>
Structure	sheet sands of Wilcox turbidite trend
Compartmentalization Risk	Faulting
Lithofacies & Mineralogy	Fine-grained siliciclastic turbidites dominated by quartz, feldspar, and clays; cementation from quartz overgrowths, chlorite clay, carbonate minerals.

Growth faults developed near the shorelines of several of the larger delta lobes, where thick wedges of sand and mud were deposited on not consolidated offshore mud of the previous sediment wedge (fig. 2.3). Subsidence and displacement along these faults during burial isolated thick sandstone and shale sequences. Isolation of the sandstone units prevented the updip escape of pore fluids during subsequent compaction resulting from loading.

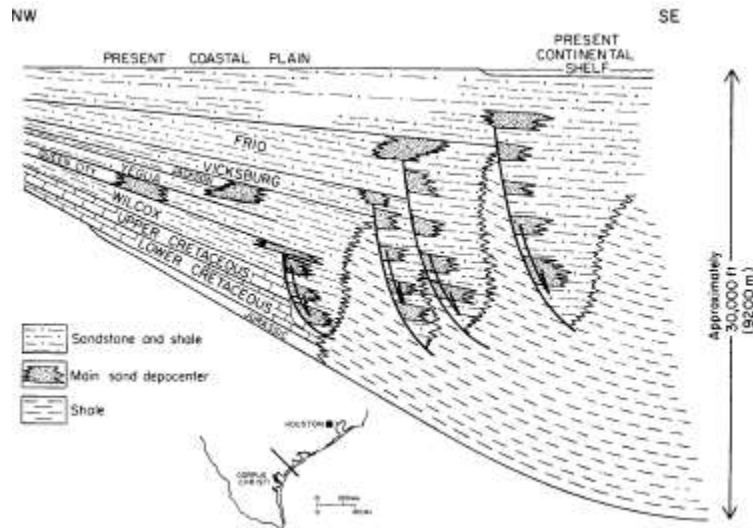


Figure 2. 3: Depositional/structural style of the Tertiary section along the Texas Gulf Coast.

Geopressed geothermal reservoirs occur downdip of major growth faults where deltaic sandstones were hydrologically isolated from surrounding rocks. Vertical escape of pore fluids was prevented by the low vertical fluid flow of superposed shales. Limited fluid circulation within these growth-faulted blocks caused the downward increase in pressure gradient from a normal hydrostatic pressure gradient of 0.465 psi per foot to between 0.7 and 1.0 psi per foot. The increased porosity and water content of sediments, caused by the buildup in fluid pressure and consequent reduction in overburden pressure, reduces the thermal conductivity and increases the geothermal gradient. Gradients in the hydro pressured zones range from 1.5 °F to 2.0 °F per 100 ft and from 2.0°F to more than 3.0°F per 100 ft in the geopressed zones. The faulted, downdip section of the Wilcox Group, which exhibits a high-pressure gradient and temperatures exceeding 300° F, constitutes the Wilcox geothermal corridor. Along with this corridor, six geothermal fairways were

outlined on the basis of sandstone distribution and isotherm maps. Table 2.2 Summaries the physical characteristics of the six Wilcox geopressed geothermal fairways.

With numerous leads, lessons learned, discoveries and prospective resources based upon hydrocarbon system analysis, and regional studies, the opportunities in Mexico's deepwater basins are large and underdeveloped. Viscosity varies vertically and laterally within individual structures, suggesting complex filling histories and fluctuating sand quality. The average API is between 22° to 41° API (Rains, Zarra, & Meyer, 2007). The Permeability very low less than 20md, Porosities between 7 to 29%, a temperature range of 130 to 350°F (54 -149°C), Pressure of about 7,000 to 30,000 psi (482 – 2068 bar) Thickness of about 1000ft and permeability-thickness (kh) of about 50,000md (from offshore magazines).

Table 2. 2: Reservoir Properties of the Lower and Upper Wilcox formation

	ZAPATA	DUVAL	LIVE OAK	DE WITT	COLORADO	HARRIS
Part of Wilcox	Upper	Upper	Upper	Lower	Lower	Lower
Depth to Top of Prospective Sandstone	9,600 to 10,500	11,000 to 12,000	9,200 to 11,000	10,490 to 10,660	10,960 to 11,400	12,500 to 13,300
Thickness of Prospective Sandstone	280 to 620	>600	>600	550	1,600	>2,000
Top of Geopressure (0.7 psi/ft)	10,700ft	10,000ft	9,960 ft	10,000ft	12,000ft	11,550 ft
Temperature °F	300 @ 11,400 ft	300 @ 10,750 ft	300 @ 11,000 ft	300 @ 10,850 ft	300 @ 11,780 ft	300 @ 12,990 ft
Porosity (%)	17 to 22	7 to 14	16 to 24	6 to 25	4 to 19	Average: 15
Permeability, mD	0 to 19 *SWC	0.1 to 44 **DC	5 to 40	0.01 to 242 DC	Most <5; locally up to 545 Dc	Most <1 DC

(Source: RPSEA).

### **2.2.2 Obstacles to Exploration and Development GoM Wilcox Formation**

The formation which is characterized by massive sand-rich deepwater turbidites reservoir has the following challenges in developing it:

1. Seismic Imaging: complex structures includes fold dominated kink bands and angularly folded strata.
2. Reservoir quality: the formation is of low porosity and permeability.
3. It is situated in an ultra-deep water environment.
4. It is more of a subsalt made formation.
5. The temperature and pressure can be classified to be in the high regime.
6. The correlation between sand sequences is challenging.
7. The acquisition of low-contaminated sample is difficult.
8. The fluid present in the reservoir is of low GOR, asphaltene gradient modeling is used as it is very informative because of the large variation in the composition of gas to liquid and there is a presence of high pressure to dissolve the asphaltene.

### **2.3 Immiscible CO<sub>2</sub> Processes**

In principle, there exist three categories of CO<sub>2</sub> flooding processes: miscible, near miscible and immiscible (Blunt, Fayers, & Orr Jr, 1993). Miscible displacement of crude oil by CO<sub>2</sub> is the most desirable scenario that can yield maximum recovery efficiency. This is ascribed to the favorable mechanisms initiated by forming a single-phase containing CO<sub>2</sub> and crude oil through multiple contacts. Oil swelling, oil viscosity reduction, reduction of interfacial tension, and vaporization and extraction of intermediate components from the crude oil all contribute to a low residual oil saturation (j. F. Orr & Taber, 1984). In general, minimum miscibility pressure (MMP) is decreased with the API gravity of crude oil (Alston, Kokolis, & James, 1985; Li, Qin, & Yang, 2012; Shokir, 2007). As for oil reservoir containing crude oil with 30°API or lower, the MMP would be too high to achieve such that only immiscible state could prevail during CO<sub>2</sub> injection processes in a hydrocarbon reservoir (Mangalsingh & Jagai, 1996). A light or medium crude oil reservoir operating at a very high pressure undergoes the miscible displacement mechanism.

Although the immiscible CO<sub>2</sub> flooding is a non-thermal recovery method, it shows considerable potential for a range of heavy oil reservoirs. During the immiscible flooding process, CO<sub>2</sub> is injected into the formation, highly mobilizing the oil contacted and displacing it towards the production wells. Oil mobility is improved due to the solubility of CO<sub>2</sub> in the oil that causes a reduction in the viscosity, and an increase in oil volume (Al-Abri & Amin, 2010). Recovery mechanisms related to immiscible CO<sub>2</sub> flooding consist of viscosity reduction, oil swelling effect, and interfacial tension reduction.

**Viscosity reduction:** It is mainly attributed to the dissolution of CO<sub>2</sub> into the crude oil. The viscosity of CO<sub>2</sub> saturated oil is a function of temperature, pressure, and concentration of dissolved CO<sub>2</sub>. A decrease in viscosity due to carbonation is generally unimportant for light oils but plays a significant role in the recovery of heavy oil. For example, when the temperature is set at 75°F, the viscosity of a Wilmington oil sample with 15°API is reduced from 2000 cP to 20 cP with pressure increasing from 0 psi to 1500 psi (Spivak & Chima, 1984).

**Oil swelling:** When CO<sub>2</sub> comes into contact with crude oil, it is expanded due to the dissolution of CO<sub>2</sub>. The degree of swelling depends on pressure, temperature, and oil composition. Swelling is important in that the residual oil saturation is inversely proportional to the swelling factor (Hatzignatiou & Lu, 1994; Mangalsingh & Jagai, 1996). The swelling factor for light oil has a swelling which increases rapidly with pressure at first before flattening out and decreasing due to the extraction of lighter hydrocarbons. The swelling factor for heavy oil responds linearly with CO<sub>2</sub> solubility in the oil. Temperature influences the solubility of CO<sub>2</sub> and ultimately the swelling of the oil, high temperatures reduce the amount of CO<sub>2</sub> present in the oil.

**Interfacial tension reduction:** Reduction of interfacial tension takes place due to the dissolution of CO<sub>2</sub> into heavy oil. For a heavy oil at moderate pressures (4-6 MPa) and temperature (293.15-298.15 K) with dissolved CO<sub>2</sub> of 50-100 m<sup>3</sup>/m<sup>3</sup>, a 30% reduction of interfacial tension can be observed (Mangalsingh & Jagai, 1996). Reduction of interfacial tension increases the capillary number and thus enhances oil recovery.

## 2.4 IN SITU CO<sub>2</sub> GENERATION

In situ CO<sub>2</sub> EOR (ICE) is a novel way of generating CO<sub>2</sub> in subsurface for flooding to increase oil recovery in hydrocarbon reservoirs. The process involves dissolving ammonium carbamate or urea in a brine solution and inject it into the reservoir as a gas generating agent, this chemical solution at reservoir condition liberates CO<sub>2</sub> and ammonia is generated as a by-product. The CO<sub>2</sub> because of high mobility will reduce the viscosity of the crude oil resulting in oil swelling while the ammonia will benefit in terms of wettability alteration because of its elevated alkalinity. These methods compare to other EOR techniques requires minimal capital investment upfront compare to CO<sub>2</sub> flooding, it reduces fingering because of the absence of free CO<sub>2</sub> phase and this makes it a potential tertiary oil recovery mechanism for both onshore and offshore fields.

Sometimes, the WAG-modified process is unlikely to become economically viable, largely due to the presence of thick formation (Mosavat & Torabi, 2014). Many optimization efforts are required for acceptable economic feasibility on the WAG process (Han & Gu, 2014; Rao & Girard, 2002). Carbonated Water Injection (CWI), viz. injecting water with dissolved CO<sub>2</sub>, offered an alternative to address the problem of the WAG. The CWI technique had been demonstrated both in laboratory studies (Rutqvist et al., 2011; Sohrabi et al., 2011) and field pilot tests (Christensen, 1961; Hickok, Christensen, & Ramsay Jr, 1960; Scott & Forrester, 1965). CWI is a single aqueous phase injection that has similar sweep efficiency as water flooding. In comparison with conventional CO<sub>2</sub> flooding and CO<sub>2</sub> WAG, the only minor modification of the existing water injection system is required using a CWI system. For example, a pressurized mixing tank for dissolving CO<sub>2</sub> at surface facilities can easily achieve the CWI modification for an ongoing water flooding project.

The potential benefits of the novel way, when compared to the older methods are:

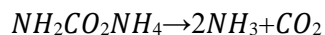
- Not relying on the natural CO<sub>2</sub> source and CO<sub>2</sub> transportation pipeline.
- Better sweep efficiency than that of CO<sub>2</sub> WAG.



- Self-initiation gas generation ability versus sequential injection of the gas generating reagents and acid slug system (a complex fluid system).
- Simple and cheap in operations (no additional polymer, surfactant or alkaline required).
- Reasonable recovery performance either above or below minimum miscibility pressure conditions.

#### 2.4.1 Ammonium Carbamate as a gas generating agent

Different variety of CO<sub>2</sub> generated compounds has been developed which includes aluminum carbamide, ammonium carbamate, sodium carbonate, and ammonium bicarbonate. Ammonium carbamate is a monovalent ammonium salt with chemical formula  $NH_2CO_2^-NH_4^+$ . Solid ammonium carbamate decomposes at a temperature above 60°C. It has a water solubility approximately 40 wt. % at room temperature. Ammonium carbamate in aqueous solution can largely decompose to generate CO<sub>2</sub> at 92°C and it has been selected as the simplest CO<sub>2</sub> gas generating agent (Shiau et al., 2010; Wang et al., 2017).



2.1

The formation of CO<sub>2</sub> in the system involves a complex chemical process and this been reported by previous researchers (Wen & Brooker, 1995). (Flury, Afacan, Tamiz Bakhtiari, Sjoblom, & Xu, 2013) reported that ammonia was a suitable replacement of sodium hydroxide on bitumen extraction. Ammonia had faster performance on bitumen liberation than the use of sodium hydroxide at the same pH value. The liberation of bitumen from the sand grains would lead to wettability reversal from oil-wet to water-wet. (Fjelde & Asen, 2010) also showed some evidence of more water wet surfaces generated during a CO<sub>2</sub>-WAG process in chalk rocks. Therefore, the effect of CO<sub>2</sub> generated in situ on wettability change cannot be neglected. The mass transfer of CO<sub>2</sub> generated which can be described by the two liquid film theory is the physical process in the formulation of in situ CO<sub>2</sub> generations. It involves the mass transfer of CO<sub>2</sub> from the aqueous phase to the oil phase with concentration difference being the driving force.

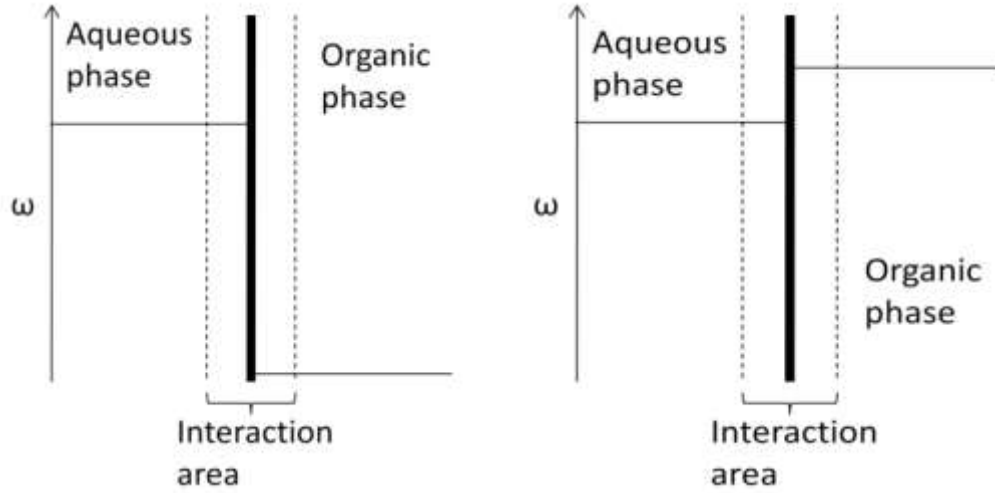


Figure 2. 4: CO<sub>2</sub> concentration as a function of distance (Steffens, 2010).

In Figure 2.4, the plot on the left shows initial condition and right is the condition after equilibrium. In the beginning, the CO<sub>2</sub> concentration is higher in the aqueous phase than in the oil phase. The direction of mass transfer is from the aqueous phase to the oil phase. Because of the intrinsic high solubility of CO<sub>2</sub> in oil, when the equilibrium is reached, the CO<sub>2</sub> concentration in the oil phase is much higher than it in the aqueous phase. It is controlled by the partition coefficient.

$$k = \frac{\omega_{CO_2}^{water}}{\omega_{CO_2}^{oil}} \quad (2.2)$$

Where  $\omega_{CO_2}^w$  and  $\omega_{CO_2}^o$  are the solubility of CO<sub>2</sub> in water and oil respectively.  $\omega_{CO_2}^o$  can be calculated from the model proposed by (Duan, Sun, Zhu, & Chou, 2006). (Hangx, 2005) summarized  $\omega_{CO_2}^o$  in the aqueous phase at the presence of  $K^+$ ,  $Mg^{2+}$ ,  $Ca^{2+}$  and  $SO_4^{2-}$  or DI water condition in CWI application.  $\omega_{CO_2}^o$  can be modeled by many EOS calculations (Elsharkawy & Foda, 1998). (Altunina & Kuvshinov, 2007) reported that the partition coefficient for CO<sub>2</sub> in oil/water system in the temperature range of 35-100°C and the pressure range of 10-40MPa is between 4 and 10 (i.e., dissolved mostly in oil). He also reported that the coefficient value for ammonia is extremely low and does not exceed  $6 \times 10^{-4}$ .

After the CO<sub>2</sub> equilibrated between aqueous and oil phase, higher CO<sub>2</sub> content results in oil swelling and viscosity reduction. The swelling factor (SF) is defined as the ratio of CO<sub>2</sub>-saturated oil volume at reservoir

pressure and the temperature to original oil volume measured at reservoir temperature and atmospheric pressure (Simon & Graue, 1965). When a significant amount of CO<sub>2</sub> is dissolved into crude, total oil volume will increase. This phenomenon can contribute to higher oil recovery. Increasing oil volume results in an apparent increase of oil saturation, thus allowing the discontinuous oil droplets previously trapped in the pores to merge with the mobile oil phase (Prosper & Ali, 1991). Assume that the residual oil saturation is the same whether the oil is carbonated or not. Then the same volume of oil will contain less pure oil if it is carbonated, due to oil swelling (De Nevers, 1964).

The dissolved CO<sub>2</sub> will cause a decrease in oil viscosity. The reduction level is mainly depending on CO<sub>2</sub> concentration in the oil. (Holm, 1982) stated that CO<sub>2</sub> could reduce the viscosity of oil at certain reservoir condition up to 5 to 10 times because of quite high CO<sub>2</sub> solubility. If the original oil has a higher initial viscosity, a larger percentage reduction in oil viscosity will realize when it is fully saturated by subcritical CO<sub>2</sub> (Rojas & Ali, 1988). The reduction of CO<sub>2</sub> saturated oil viscosity is higher at lower temperatures than at high temperatures because of higher solubility of CO<sub>2</sub> occurred at a lower temperature (Prosper & Ali, 1991).

The main mechanisms of the In situ CO<sub>2</sub> generation EOR is a combination of carbonated water flooding (oil swelling and viscosity reduction) and alkali flooding (wettability reversal and in situ surfactant generation (Southwick et al., 2016). The injection of the carbamate solution offers an effective route to deliver CO<sub>2</sub> to the targeted rock matrix. The aim of developing in situ CO<sub>2</sub> is to simultaneously lower the cost of both CO<sub>2</sub> capture and *in-situ* CO<sub>2</sub> generation for EOR operation.

(Wang et al., 2017) conducted laboratory studies on the development of in situ CO<sub>2</sub> for EOR and focused his research on checking the potentials of using ammonium carbamate and urea as a gas generating agent. In his study, four different types of oil were used as displaced fluid (Dodecane, Earlsboro, Deep Star) whose API and viscosity are (57.3 and 1.34 cP), (40, 4.6 cP) and (27, 22 cP) respectively. The gas generating agent (5-35 wt.% ammonium carbamate prepared in 5 wt. % NaCl solution) and base brine solution (5 wt. % NaCl) were dissolved in deionized water. The concentrate of the solution has a density of 1.13 g/ml for 5-

35 wt% ammonium carbamate and 1.042 g/ml for 5 wt. % NaCl. The highly concentrated chemical solution delivers an excessive amount of CO<sub>2</sub> and the free gas phase is eliminated at high pressure. At an operating temperature of 96°C and pressure of about 80psi the Earlsboro crude oil shows a residual oil saturation of 19.50% after brine injection, followed by Ammonium Carbamate injection which dropped the saturation to 16.78% and the estimated tertiary recovery of this formulation is about 13.50%.

A better result can be achieved if the reservoir temperature and other criteria for the decomposition of AC injected is met. This result provides evidence that in situ CO<sub>2</sub> generation will offer better recovery performance. The distribution of the generated gas was different from the injected gas. Gas water co-injection was largely affected by the gravity segregation and large mobility contrast. And liquid lamellar was stabilized by surfactant in foam injection. The state of generated gas was between the gas and water co-injection and foam injection. Therefore, the forming of the gas phase could promote sweep efficiency (Wang, Chen, Shiau, & Harwell, 2018). He also reported that the decomposition rate of AC and the mass transfer of CO<sub>2</sub> between oil and Aqueous phase were both a function of time-based on further tests carried out taking in to account the effects of residence time on the result obtained. The properties of the reservoir crude have impacted on recovery and so is the CO<sub>2</sub> partition coefficient. During the displacing process, mass transfer resistance and reaction rate were the limiting factors, and in general, heavier oil was quickly approaching its CO<sub>2</sub> solubility limit than lighter oil during the first AC injection period while higher API gravity oil leads to even larger CO<sub>2</sub> solubility, which would result in higher swelling factor.

A significant amount of ammonium carbamate could be converted to CO<sub>2</sub> and NH<sub>3</sub> at high temperature and high pressure depending on the reaction kinetics. When the effluent was cooled down, some of the produced CO<sub>2</sub> and NH<sub>3</sub> could re-associate back to some form of AC by-product (Darde, Thomsen, Van Well, & Stenby, 2009). The nature of this newly developed system may offer an opportunity of re-injecting/recycling the effluents for lowering the project cost.

In conclusion, the new formulation revealed the following;

1. The longer residence time for the gas generating agent can increase the tertiary recovery.
2. Better oil candidate for CO<sub>2</sub> flooding is also a favorable candidate using in situ CO<sub>2</sub> generation formulation.
3. A high acid number crude will inherit additional benefits due to wettability reversal and the alkaline produced (Buckley & Fan, 2007; Green & Willhite, 1998; Johnson Jr, 1976; Sharma et al., 2015).

The changing of the oil composition caused by in situ CO<sub>2</sub> generations EOR could be detected by gas chromatography analysis. In water flooding produced oil sample, the mole fraction of lighter components below C<sub>9</sub> was higher than them in situ CO<sub>2</sub> generation produced sample. Comparing to water flooding sample, in situ CO<sub>2</sub> generation produced oil sample contained more components heavier than C<sub>9</sub> and asphaltene liberation caused by ammonium was the reason of more heavy components in the tertiary recovered oil sample (Wang et al., 2018). Results of the oil saturation variation for different crudes under high-pressure condition are obtained as; for Earlsboro crude, the Sor was 29.28% after in situ CO<sub>2</sub> generation processes, the final oil saturation was 21.08% and Etr was 28%. For DeepStar crude, the Sor was 22.84%, the resulted final oil saturation reached 19.69% and total Etr was equal to 13.8%.

Based on the extensive studies of CO<sub>2</sub> flooding, the CO<sub>2</sub> miscible flooding could provide high tertiary recovery because of high microscopic displacement efficiency (Verma, 2015). (Wang et al., 2017) in his work used the modified high-pressure rating device to conduct tests above the estimated Earlsboro oil/CO<sub>2</sub> mixture Minimum Miscibility Pressure (MMP). He estimated the MMP values of Earlsboro and DeepStar crude based on the correlations proposed by (Emera & Lu, 2005). The estimated MMP of Earlsboro oil was 3,190 psi, and MMP of DeepStar oil was equal to 10,200 psi. The modified high-pressure rating sand pack can safely operate up to 4900 psi and 275 °F. Initially, he assumed that above the MMP condition, *in situ* CO<sub>2</sub> generation EOR might offer. A better performance of tertiary recovery, in analogy to conventional CO<sub>2</sub> flooding.

Surprisingly, tertiary recovery was not much greater than that in pressure below the MMP tests and this revealed the difference between CO<sub>2</sub> flooding and In situ CO<sub>2</sub> generation EOR. (Wang et al., 2017) established that unlike CO<sub>2</sub> flooding, there was no separate CO<sub>2</sub> phase involved in the in situ CO<sub>2</sub>

formulation. The system pressure controlled the CO<sub>2</sub> chemical potential in CO<sub>2</sub> flooding. In his work, (Wang et al., 2017) reported that In situ CO<sub>2</sub> generation formulation beyond the estimated MMP shows no benefit of miscible flooding but an increase of pressure above the MMP would only impact the values of CO<sub>2</sub> partition coefficient between the aqueous phase and the oil phase. Interphase mass transfer resistance thus became the controlled limitation for displacement, less depending on the CO<sub>2</sub> partition coefficient. He then concluded that;

1. Increasing pressure above MMP did not enhance the performance of In situ CO<sub>2</sub> generation significantly.
2. High pressure could provide more favorable CO<sub>2</sub> partition coefficient, especially for heavy crude.

Further investigation on the phase behavior of In situ CO<sub>2</sub> generation EOR system under high pressure needs to be explored (Wang et al., 2017). The formulation under intermediate pressure and high pressure largely eliminated the presence of free CO<sub>2</sub> gas phase but still exhibited satisfactory tertiary recovery, especially under high residual oil saturation conditions. The mechanisms of *In situ* CO<sub>2</sub> generation EOR involve multiple interactions such as oil swelling, viscosity reduction, wettability reversal and an increase in alkalinity. The tertiary recovery is a synergistic effect. The proposed system was an immiscible flooding process. Running *In situ* CO<sub>2</sub> generation EOR experiment above MMP does not show additional miscible flooding benefits (Wang et al., 2017).

## **2.5 Kinetics and Mechanism of the Reversible Dissociation of Ammonium Carbamate**

Ammonium carbamate, NH<sub>4</sub>CO<sub>2</sub>NH<sub>2</sub> (AC), is a solid material that coexists with its decomposition products, the small molecules CO<sub>2</sub> (C) and NH<sub>3</sub> (A). This heterogeneous equilibrium arises from the reversible dissociation process.



Above about 260.33°F, AC will dissociate into water and ammonia (Ramachandran, Halpern, & Glendening, 1998). At ambient temperature the equilibrium partial pressures of CO<sub>2</sub> and Ammonia are appreciable. For example, the equilibrium dissociation pressure, P<sub>eq</sub>, above solid AC is 1.546 psi at 76.73°F, and it reaches 14.7psi at 137.93°F. Furthermore, as these data imply, the dissociation pressure of

AC is strongly temperature dependent, with a temperature coefficient of about 12.8 kcal/mol, which is one-third of the enthalpy of reaction. The equilibrium properties of the AC system have been well characterized, and there are several reports in the literature concerning the temperature dependence of the vapor pressure of AC [2-4]. Several attempts have been made to analyze the kinetics of the  $AC \rightarrow 2A + C$  reactions. (Laurent & Kikindai, 1972) studied the time dependence of the formation of solid AC from A and C and obtained rate constants for this process between 296 and 433 K (a range that also encompasses the complication of urea formation). In the study, (Laurent & Kikindai, 1972) assumed an overall third-order process to account for the formation of solid AC (with partial orders of one and two with respect to A and C, respectively) and, furthermore, assumed a zero-order process for the reverse reaction decomposition. The results of this investigation are questionable because the temperature dependence of the equilibrium pressures reported by these workers does not agree with literature values and, furthermore, the validity of the termolecular elementary step was not substantiated.

(Frejacques, 1951) assumed an empirical second-order rate expression, i.e.,  $a - bP^2$ , for the decomposition of AC. Again, no mechanism was suggested to rationalize this rate law. (Lishnevskii & Madzievskaya, 1987) studied the formation of solid AC between 195 and 293 K and its decomposition between 263 and 303 K, by measuring initial rates of reaction. They allude to a mechanistic scheme that involves the initial adsorption of  $NH_3$  and  $CO_2$  onto the surface of the solid and a subsequent surface reaction, leading to the formation of AC. They also invoked the intermediacy of carbamic acid,  $NH_2CO_2H$  (CA), on the surface. Their kinetic analysis, however, is limited only to the temperature dependence of the initial rates of the forward and back reactions. No rate equation pertaining to any mechanism was presented.

(Claudel & Boulamri, 1988) studied the reaction kinetics in both the forward and reverse directions and fit the total pressure data to an empirical second-order polynomial represented by

$$\frac{dP}{dt} = k_{obs}(P - P_{eq})^2 \quad 2.4$$

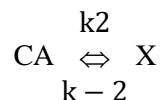
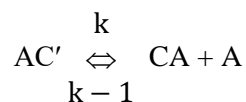
Where  $P_{eq}$  is the equilibrium pressure. No mechanism supporting this or any other rate law was presented. Furthermore, such a rate law is physically unacceptable because it breaks down for  $P > P_{eq}$ ; that is, it predicts that the pressure would increase in time and thus not decrease to approach  $P_{eq}$  under these circumstances. One additional difficulty with this study is the poor correlation between  $\ln k_{obs}$  and  $1/T$ , although Arrhenius behavior was observed for the initial rate of the reaction.

(Ramachandran et al., 1998) in his work study the mechanism by which this unusual reversible reaction occurs. This problem is especially interesting because carbamic acid, CA has been suggested as an intermediate in the reaction mechanism. CA has been the focus of theoretical calculations but direct evidence of its existence does not appear to have been reported. (Ramachandran et al., 1998) in his search for the mechanism of the reversible dissociation of AC performed a high-level ab initio calculations of CA and examined its structure and potential energy surface with respect to both unimolecular and bimolecular decomposition pathways and use the result of his study to determine the plausibility of various mechanism. He considered two generally different scenarios for the reversible decomposition of AC: a process involving the gas phase species A, C, and CA and a solid-state mechanism in which the postulated CA intermediate does not leave the surface of AC and present indirect arguments in support of the solid-state mechanism. The result of his study provides information on the time dependence of pressure over solid AC due to decomposition into A and C at 298 K. The mechanism that involves gas-phase CA in the  $AC \rightarrow 2A + C$  reaction was rejected because their rate laws failed to conform even to the observed result for all reasonable values of the relevant rate constants. He also evaluated several empirical differential rate laws and discarded the "one-step" mechanism involving the expulsion of  $2A + C$  from the AC surface and the termolecular reverse step because it predicts a rate law of the form  $P' = a - bP^3$ , which is not compatible with the observed rate data. Furthermore, his data are also incompatible with empirical first-, second-, and third-order rate laws, i.e.,  $P' = k(P_{eq} - P)$ ,  $P' = k(P_{eq} - P)^2$ , and  $P' = k(P_{eq} - P)^3$ , respectively.

## MECHANISMS



Mechanism 1 contains three reversible steps and accounts for the reversibility of the process. AC' symbolizes the ammonium carbamate formula unit as a solid-state species, which exists on the surface of the AC sample while all other entities are present in the gas phase.



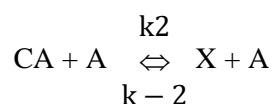
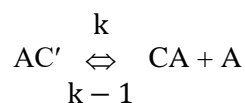
X represents a loose van der Waals complex formed between ammonia and carbon dioxide. The inclusion of this species avoids the necessity for assuming specific orientational requirements for the collisions between A and C to form CA. According to this mechanism, proton transfer from the ammonium ion to the carbamate ion forms carbamic acid and ammonia, which are then expelled from the surface into the gas phase. Carbamic acid then undergoes unimolecular isomerization to form the more loosely bound species, X, which itself then dissociates into NH<sub>3</sub> and CO<sub>2</sub>. Furthermore, he explained that the forward reaction in the first step, i.e., AC' ⇌ CA + A, is assumed to be a pseudo-zero-order process. Thus the rate constant k<sub>1</sub> is treated as an extensive quantity, i.e., k<sub>1</sub> = k<sub>1</sub>'S, where S is the effective surface area of the solid AC sample, which is assumed to be constant on the time scale of the experiment (ca. 40sec at higher temperatures and 2 min at the lowest one), and k<sub>1</sub>' is the true first-order rate constant. It is implicit in the above equation that k<sub>-1</sub> is also extensive in order that the equilibrium constant expressed by k<sub>1</sub> to k<sub>-3</sub> be intensive.

He reported that it is evident from mechanism 1 that C is formed sequentially (step 3), while A is produced both initially (step 1) and sequentially (step 3) after the onset of the reaction. The complex X is also formed sequentially (step 2), but its concentration is presumed to be very low (see below). After the ab initio

calculation the most significant outcome pertaining to mechanism 1, is that the gas phase CA molecule is remarkably stable with respect to the unimolecular decomposition. CA react via the in-plane transfer of the OH proton to the amino group, resulting in the scission of the CN bond to give A and C. Relative to the separated A and C product, CA has a free energy of 12.9 kcal/mol. The free energy of the transition state is significantly larger, 54.2 kcal/mol, corresponding to a considerable barrier to the decomposition of 41.4 kcal/mol. The thermodynamic stability of CA has been previously calculated by Wen and Brooker at the SCF level and by Remko and co-workers at higher levels of theory (MP2 to MP4). These calculations generally reveal that CA is either isoenergetic with or slightly more stable than the separated products A and C.

(Ramachandran et al., 1998) proceed by considering an alternative process for the decomposition of CA, namely, the bimolecular ammonia-assisted process,  $CA + A \rightarrow X + A$  due to the predicted kinetic stability of gas-phase CA, and hence its inability to be directly converted to products as indicated in mechanism 1, we were led to consider

## MECHANISM 2.



Because both mechanisms 1 and 2 require the presence of gas-phase carbamic acid, the direct evidence for the existence of this species was sought. He sought evidence of the van der Waals complex, X (see eq 4 and 8), by examining the vibrational features of the out-of-plane bending mode of  $NH_3$  in the 750-1250  $cm^{-1}$  region. In a comparison of the spectrum of  $NH_3$  in equilibrium with AC with that of  $NH_3$  itself, no evidence was found to suggest the presence of additional, shifted features that would be expected for the

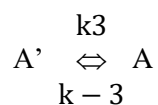
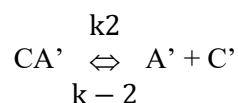
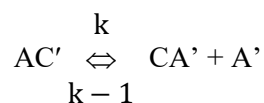
complex. He pointed out that, according to mechanisms 1 and 2, the steady state concentration of CA is expected to be very low, and thus, the failure to find direct IR evidence for this species does not necessarily rule out their existence.

This process is clearly less strongly activated than the unimolecular reaction, having a free energy of activation, 18.9 kcal/mol, which is significantly lower than that of the second step of mechanism 1. The reaction coordinate involves a double proton transfer, first from OH to the assisting ammonia molecule to form an ammonium cation and second from ammonium to the amino group. The second transfer simultaneously cleaves the CN bond of carbamate yielding a van der Waals complex of two A molecules with C. decomposition of CA is considerably more plausible than the unimolecular decomposition step of mechanism 1. Although the surface reaction of mechanism 2 (step 1) cannot be directly examined by calculation, its endothermicity can be judged from the enthalpy changes calculated for steps 2 and 3 and the overall endothermicity of the AC decomposition (38.0 kcal/mol).

Another difficulty he stated with Mechanisms 1 and 2 is that in the back reaction, solid AC must be produced through a bimolecular collision between CA and A, which, in view of the apparently low number density of CA, must correspond to a very low probability event.

### MECHANISM 3.

In this mechanism, the reaction steps leading to the formation of the small molecules A and C from solid AC are assumed to take place *on its surface*; i.e., A and C are the only gas-phase species present.





where the primed species represent surface-bound molecules. This mechanism contains eight rate constants. Furthermore, it shows that the dissociation of CA' is a first-order process. In view of the ab initio calculations supporting the stability of CA, this process is nevertheless reasonable because it is likely to be assisted by neighboring ammonium ions on the solid surface/matrix. In this context, it is useful to consider the solid-state structure of AC. The NH<sub>2</sub>COO<sup>-</sup> ions (denoted hereafter as CA<sup>-</sup>) form head-to-head, roughly planar, centro-symmetric dimers that are arranged in parallel layers. The NH<sub>4</sub><sup>+</sup> ions (denoted hereafter as A<sup>+</sup>) form interpenetrating double layers that are sandwiched between the anion layers. Each A<sup>+</sup> ion is hydrogen-bonded through its H-atoms to the O-atoms of four separate CA<sup>-</sup> ions (three on one side and one on the other) and each O atom of the CA<sup>-</sup> anion is hydrogen bonded to two A<sup>+</sup> ions. The A<sup>+</sup> ions thus cross-link the anion layers, as well as the anions within each layer. The N-H...O hydrogen bond distances range from 1.77 and 2.19 Å. Although the surface structure of solid AC may not exactly correspond to its interior structure as described in the previous paragraph, it is reasonable to assume that the dimeric anions hydrogen-bonded to the ammonium ions do exist on the surface.

Thus a surface (and maybe bulk) reaction leading to the reversible decomposition of AC' into A' and C' may be quite facile. Mechanism 3 is reasonably compatible with this solid-state structure of AC. The H atom of an A<sup>+</sup> ion, which is already hydrogen-bonded to the O-atom of an AC<sup>-</sup> ion, can readily undergo a transfer (as H<sup>+</sup>) to the anion, leading to the formation of carbamic acid (CA') and ammonia (A') on the surface (or within the matrix) of AC. The CA' species, assisted by the other CA<sup>-</sup> unit of the dimer, can then undergo decomposition into C' and a second A' molecule. Such a scheme may also be used to account for the reverse process, i.e., the formation of solid AC from gaseous A and C. Successive adsorption onto a surface, such as glass, of alternate layers of A and X (the van der Waals complex of A and C) can lead to the formation of CA' via hydrogen bonding and proton transfer. This CA' species can then react with A'

to produce AC. On the basis of infrared studies of AC formation from gaseous A and C that had been adsorbed on a surface at low temperature

(Hisatsune, De Courcy Jr, & Mudd, 1967) has suggested that crystalline AC may be formed from an unstable precursor consisting of a 2:1 complex between A and C in which the  $\text{NH}_3$  molecules are not equivalent. It thus seems possible that such a species, i.e.,  $(\text{NH}_3)_2\text{CO}_2$ , is involved as an intermediate in the decomposition of solid AC. Mechanism 3 is indeed consistent with this idea.

(Ramachandran et al., 1998) noted that although the  $\text{AC}^-$  anion-assisted decomposition of  $\text{CA}'$  may be viewed as a second-order process, the *local* concentration of the neighboring  $\text{AC}^-$  ions can be assumed to be a constant. Thus, the dissociation of  $\text{CA}'$  in mechanism 3 can be represented as a pseudo-first-order process. With reference to mechanism 3, we use the following approximations to simplify the kinetic treatment of this mechanism:

(a)  $k_3 \approx k_4 \equiv k_d$  and  $k_{-3} \approx k_{-4} \equiv k_a$ , and

(b)  $[\text{CA}']$ ,  $[\text{A}']$ ,  $[\text{C}']$ , i.e.,

$[\text{A}'] = 2 [\text{C}']$ , where  $[\text{CA}']$ ,  $[\text{A}']$ , and  $[\text{C}']$  are the time-dependent-surface concentrations of CA, A, and C, respectively.

(Ramachandran et al., 1998), concluded that from the three mechanism proposed for the reversible decomposition of ammonium carbamate, the first two “gas phase” mechanisms failed because it is incompatible with the ab initio calculation indicating that the carbamic acid intermediate postulated in these mechanisms is too stable to play the transient role that is required and was thus cast aside because he considers the calculations reliable enough, especially in view of the considerable stability that is associated with carbamic acid and of our failure to observe this species spectroscopically. The third mechanism (solid state) proposed seems more plausible, for it does not require the presence of carbamic acid in the gas phase, it is reasonable in the context of the known solid state structure of carbamic acid and it is qualitatively consistent with kinetic simulations based on reasonable values of the rate constants.

### **2.5.2 Urea as a gas generating agent**

Urea has been used as a potential source of generating CO<sub>2</sub> in situ because of its remarkable availability at bulk quantity and resistance to divalent cations. Urea is highly soluble in fresh water or brine and can decompose at reservoir conditions spontaneously to release carbon dioxide and ammonia. It exhibits very high water solubility (1,080g/L at 20 °C) and can be safely transported as a solid form or in concentrate solution with minimum hazard to human and environment. (Wang et al., 2018) in his study found that results of injecting urea solution (as low as 5 % solution) showed superior tertiary recovery performance (as high as 37.5%) as compared to the use of ammonium carbamate as a gas generating agent (29.5%) as well as similar in situ CO<sub>2</sub> generation EOR (2.4% to 18.8%) approaches proposed by previous studies. For the remarkable reservoir brine compatibility of urea, even under seawater levels of divalent ions, the floods showed no detectable effect of brine composition on the recovery and/or any occurrence of formation damage.

Furthermore, the preferable wettability reversal was indicated by recovered oil compositional analyses. In situ CO<sub>2</sub> EOR is a single aqueous phase injection and the sweep efficiency is better than water flooding when the oil viscosity was reduced and it also have many flexibilities on mobility control method like water flooding examples include formulations involved aluminum salt-carbamide-surfactant, ammonium carbamate-surfactant, sodium carbonate-acid surfactant, and ammonium bicarbonate-surfactant-polymer were developed (Altunina & Kuvshinov, 2007; Bakhtiyarov, Shakhverdiev, Panakhov, & Abbasov, 2007; Gumersky et al., 2000; Lei et al., 2016; Shiau et al., 2010; Wang et al., 2017)

The tertiary recovery based on in situ CO<sub>2</sub> generations is an immiscible flooding and mainly a synergistic effect involving oil swelling, viscosity reduction, and wettability alteration. Urea injection as a gas generating agent at a low flow rate achieved a high recovery when compared to injection at a high flow rate in tertiary recovery. The high recovery of low flow rate is attributed to the longer chemical residence time in the porous medium and the high recovery using urea is believed to be rendered either by mass transfer of CO<sub>2</sub> generated from the aqueous phase to the oil phase or urea hydrolysis rate, The longer residence time offers better oil recovery based on in situ CO<sub>2</sub> generation system (Wang et al., 2017). In conclusion, tertiary

recovery does not increase proportionally with an increase in urea concentration; running in situ CO<sub>2</sub> generation EOR above MMP does not show miscible flooding benefits and no separate CO<sub>2</sub> phase occurs during urea flooding and urea is a better gas generating agent than other carbonates because of its outstanding divalent cations resistance (Wang et al., 2018).

## **2.6 TRANSPORT AND STORAGE OF CO<sub>2</sub>**

Experience in CO<sub>2</sub> transportation has been gained from EOR. After separating CO<sub>2</sub> from flue gas, it is compressed to the high pressure of about 100 ~150 bar for ease of transport. High-density CO<sub>2</sub> is stored in geological formation deeper than 800m to achieve permanent sequestration (F. M. Orr, 2009). Water or moisture content in the CO<sub>2</sub> stream needs to be removed or greatly reduced to minimize corrosion rate of pipelines as well as the cost of pipeline materials (Seiersten, 2001). Removal of 13 other impurities such as N<sub>2</sub>, O<sub>2</sub>, H<sub>2</sub>S, and SO<sub>3</sub> avoids over-compression and lowers operational cost (Wilkinson et al., 2009). Many studies have been put forward to prove the feasibility of CO<sub>2</sub> storage in geological formation and information with experience gained from CO<sub>2</sub> injection activities in EOR and acid gas projects and studies has been positive and proven (Benson & Cole, 2008). The candidate geologic formation for the storage is depleted oil/gas reservoir, deep saline formation, and coal seams which provide a total capacity adequate for CO<sub>2</sub> storage for a long period into the future. The cost of storing CO<sub>2</sub> is generally small compared to the cost for capturing CO<sub>2</sub> which makes up to 70% or more of the total cost of CCS (House, Harvey, Aziz, & Schrag, 2009).

### **2.6.1 CO<sub>2</sub> flooding**

CO<sub>2</sub> flooding has been reported by many researchers to be promising and one of the most popular miscible gas flooding. CO<sub>2</sub> is injected into a reservoir which has undergone primary production and possibly water flooding and the natural pressure has been depleted. CO<sub>2</sub> is introduced into the reservoir either as a pure gas or as dissolved gas, this gas mixes with reservoir fluid to reduce viscosity and ultimately cause the oil to swell. The CO<sub>2</sub> could be miscible or immiscible, miscibility is achieved when two fluids combine and form a single phase; one fluid can completely displace the other phase leaving no residue behind. When miscible a zone of CO<sub>2</sub> and light hydrocarbon forms a front that is soluble with oil making the oil easier to

move towards the production well. Immiscible injection of CO<sub>2</sub> has an advantage when pressure required is not large, solvents are not expensive and recovery will still be achieved. For miscibility to be achieved, the reservoir pressure has to be above the Minimum Miscibility Pressure (MMP) which depends on temperature, pressure, solvent purity and the molecular weight of the heavy component in the reservoir fluid. CO<sub>2</sub> has a density which makes it behave like a liquid but a viscosity like gas in the reservoir at the supercritical conditions and make it a preferred solvent.

### **2.6.2 Molecular Diffusion Governed Mass Transport**

Molecular diffusion plays a key role in the recovery of oil in miscible gas injection. It tends to control mass transfer rate between two phases. In low matrix permeability, thin matrix blocks, or insignificant density difference between the oil and the injected gas, viscous forces and gravity drainage become inefficient. The diffusion of molecule is responsible for mixing at pore level and it has been shown to be an important rate controlling mechanism in gas flooding (Grogan, Pinczewski, Ruskauff, & Orr, 1988). It has been shown by both theory and experiments that diffusion can result from pressure gradients (pressure diffusion), temperature gradients (thermal diffusion), external force fields (forced diffusion), and concentration and chemical potential gradients (Reid, Prausnitz, & Poling, 1987).

Two models are widely used to describe the molecular diffusion flux for multicomponent mixtures. The first law is described using Fick's law. Fick's law presents molecular diffusion equation and states that the flux of a substance diffusing through a unit area of cross section is proportional to the concentration gradient. Self-concentration gradient with the diffusion coefficient is the driving force for the Fick's law.

$$J_i = -cD_i \frac{\partial x}{\partial d} \quad 2.8$$

The second model is developed from the irreversible thermodynamics of diffusion. This model assumes diffusion take place to minimize free energy and the condition for diffusion equilibria is the chemical potentials. The chemical potential is expected to be equal in the two phases for equilibrium to be achieved.



Diffusion flux is better presented using total potential given by chemical, gravity, and thermal forces (Robert Byron Bird, Lightfoot, & Stewart, 1960):

$$J_i = -cD_i^a x_i \frac{1}{RT} \frac{\partial}{\partial d} (\mu_i - M_i G(h - h_0) + M_i D_i^T \ln(T)) \quad 2.9$$

If the gravity and thermal diffusion term are neglected in the Eq. (2.9), the equation can be written as:

$$J_i = -cD_i^a x_i \frac{1}{RT} \frac{\partial \mu_i}{\partial d} \quad 2.10$$

Where  $\mu_i = \mu_0 + RT \ln f_i$

Substituting equation for chemical potential in Eq. (2.10) gives:

$$J_i = -cD_i^a x_i \frac{\partial (\ln(f_i) T, P)}{\partial d} \quad 2.11$$

Using the chain rule, Eq. (2.11) can be rewritten as

$$J_i = -cD_i^a \frac{\partial (\ln(f_i))}{\partial (\ln(x_i))} \frac{\partial y}{\partial d} \quad 2.12$$

Comparing Eq. (2.8) and Eq. (2.12). The activity-corrected diffusion coefficient (Reid, Prausnitz and Poling 1998) is given by:

$$D_i^a = \frac{D_i}{\partial \ln(f_i) / \partial \ln(x_i)} \quad 2.13$$

Where  $D_i$  and  $D_i^a$  is the classical Fickian and activity corrected diffusion coefficient respectively.

## 2.7 Mass Transfer of CO<sub>2</sub>-Crude Oil Systems

The mass transfer of CO<sub>2</sub> in crude oil is a complicated process because of crude oil multicomponent mixture, the multicomponent mixture can be treated reasonably as one pseudo component so that the mass transfer can be easily studied. The diffusion of the CO<sub>2</sub> into the oil can be described with the below equation with the concentration being a function of location, time and radius;

$$\frac{\partial C}{\partial t} = D \left( \frac{1}{r} \frac{\partial}{\partial r} \left( r \frac{\partial C}{\partial r} \right) + \frac{d^2 y}{d^2 x} \right) \quad 2.14$$

Where  $D$  is diffusion coefficient of  $\text{CO}_2$ ,  $C$  is the  $\text{CO}_2$  concentration in oil or water in ( $\text{kmol-3}$ ) which is a function of  $x$ ; the distance in (m) and  $t$ ; the time in (sec).

In One-Dimensional form, the radial form of the equation can be written as;

$$\frac{\partial C_i(x,t)}{\partial t} = D_i \frac{\partial^2 C_i(x,t)}{\partial x^2} \quad i = \text{oil or water} \quad 2.15$$

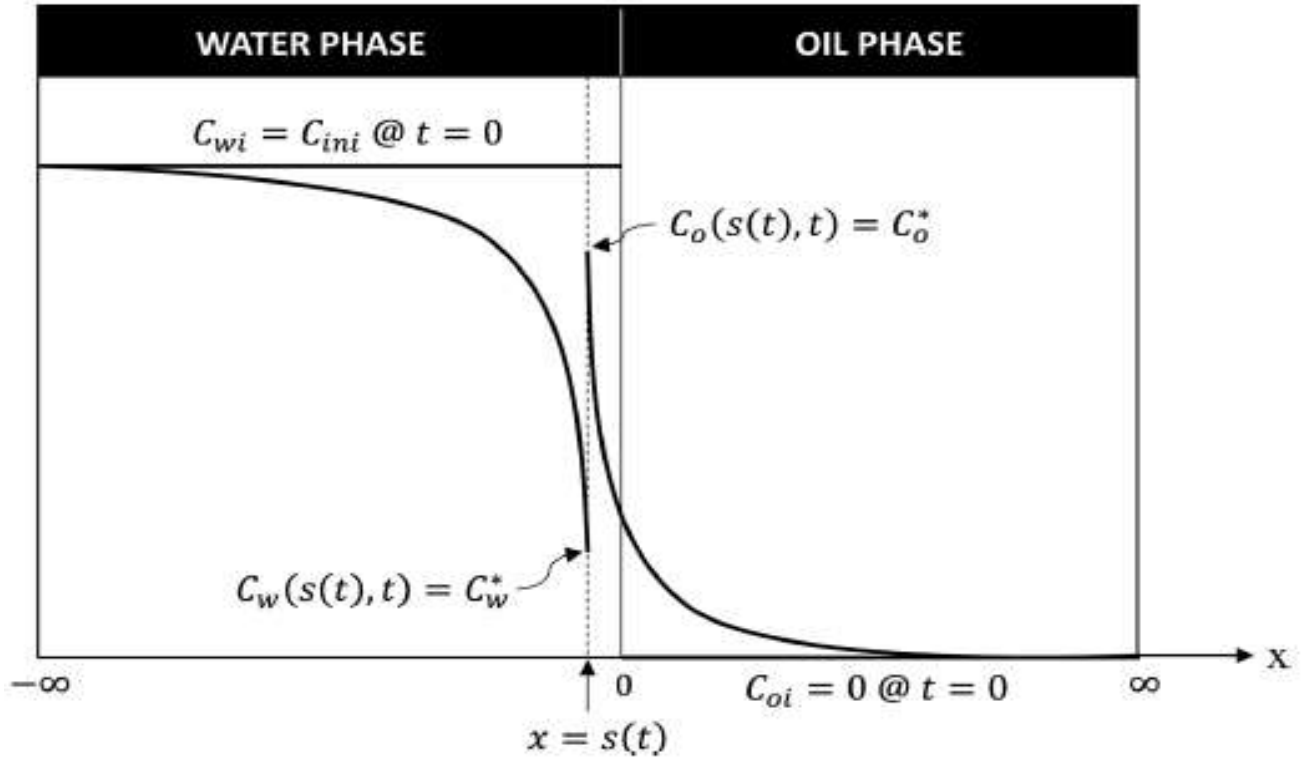


Figure 2. 5: Two semi-infinite regions of  $\text{CO}_2$  mass transfer from the water phase into the oil phase with a moving interface.

From the above figure, we can determine the Concentration of  $\text{CO}_2$  with respect to a location using the Fick's Law;

$$J = -D \frac{dC}{dz} \quad 2.16$$

Assume steady state:

$$In - Out = 0$$

At the interface of the two phases, we have;

The molar flow rate  $F$  flowing in and out of the system and can be written as

$$F_z - F_{z+\Delta z} = 0 \quad 2.17$$

The diffusive molar flux  $\vec{J}$  (mol / area.time) over the interface area is given as;

$$\frac{1}{A} \frac{F_z - F_{z+\Delta z}}{\Delta z} = 0 \quad 2.18$$

$$\frac{J_z - J_{z+\Delta z}}{\Delta z} = 0 \quad 2.19$$

From the Fick's Law above, if  $dC = k_0(-Ddz)$

On integrating both sides we have,

$$C(z) = -k_0 Dz + k_1 \quad 2.20$$

Using initial and boundary condition,

$$\text{When } z = 0, \quad C = C_0$$

$$z = L, \quad C = C_L \quad 2.21$$

solving for  $k_1$  and  $k_0$ , we have

$$C_0 = k_1$$

$$\frac{C_L - C_0}{-DL} = k_0 \quad 2.22$$

Therefore,

$$C(z) = \frac{z}{L}(C_L - C_0) + C_0 \quad 2.23$$

The transfer of  $\text{CO}_2$  in the reservoir has been explained in the literature by the mechanism of molecular diffusion, molecular diffusion is the process which defines the movement of molecules caused by Brownian

motion or composition gradients in a mixture of fluids. The main mechanism of transport is the concentration difference of CO<sub>2</sub> present between the injected fluid and the reservoir fluid. Many research has been conducted to consider the effect of diffusion coefficients on oil recovery and results have shown that it has a great significance on the CO<sub>2</sub> EOR. (Liu, Zhang, & Behrens, 2005) found out in his study that the dissolution of CO<sub>2</sub> in oil can affect the efficiency of CO<sub>2</sub> EOR by reducing the effect of viscous fingering, decelerating gas breakthrough, and improving oil production rate. (Shu, Dong, Chen, & Hassanzadeh, 2016) developed an analytical and experimental method of determining CO<sub>2</sub> diffusion coefficients in a carbonated water-oil system, the method measures pressure change for the liquid-liquid system and the diffusion coefficients of CO<sub>2</sub> in oil and water was determined simultaneously. The pressure build-up was observed as CO<sub>2</sub> is been transferred from the carbonated water to the oil phase.

Figure 2. 6: Mass transfer of CO<sub>2</sub> progress from Carbonated Water into Oil due to the solubility difference between the aqueous phase and oil phase.

(Al-Menhali & Krevor, 2016) modeled the formation of new fluid phase development in CWI. He reported that the continuous transfer of CO<sub>2</sub> to the oil phase after saturation leads to the development of a new phase (gas) in oil. The continuous transfer generates continuing expansion of the new phase which would postulate a continuous film flow of oil.

### 2.7.1 Mass Transfer without Reaction (Physical Absorption)

The absorption rate of CO<sub>2</sub> depends on the physical solubility of CO<sub>2</sub> in the solution when there are no reactive species in solution. The parameters used to quantify the solubility is Henry's constant, H<sub>CO2</sub> and the liquid phase mass transfer coefficient,  $k_l^0$ .

$$N_{CO_2} = k_l^0 ([CO_2] - [CO_2]^*) = k_l^0 \left( \frac{p_{CO_2}}{H_{CO_2}} - [CO_2]^* \right) \quad 2.24$$

$k_l^0$  is a function of both the CO<sub>2</sub> diffusivity and the liquid viscosity. Several important mass transfer models have been developed to describe the mechanism of absorption and the relationship between the mass transfer coefficient and the physical properties of the fluids. The models can be applied to both physical absorption and chemical reaction.

#### 2.7.1.1 Film Theory

At the interface between a liquid and a gas phase, there exists a thin film next to the interface as the two phases are trying to contact each other. The film is of finite thickness and stagnant with their thickness for the gas and liquid phase represented as  $\delta_g$  and  $\delta_l$ , respectively. The diffusion of the gas through the film determines the rate of absorption and the remaining gas that does not diffuse will mix with the liquid without a concentration gradient. At the interface, the liquid and the gas are assumed to be at equilibrium. The rate of mass transfer can be calculated using the Fick's law and the expression of the flux is given as;

$$N = k_l^0 (C_i^* - C_i) = \frac{D_l}{\delta_l} (C_i^* - C_i) \quad 2.25$$

where  $N$  is the flux,  $k_l^0$  is the physical liquid mass transfer coefficient and  $D_l$  is the diffusion coefficient of the solute in the liquid.

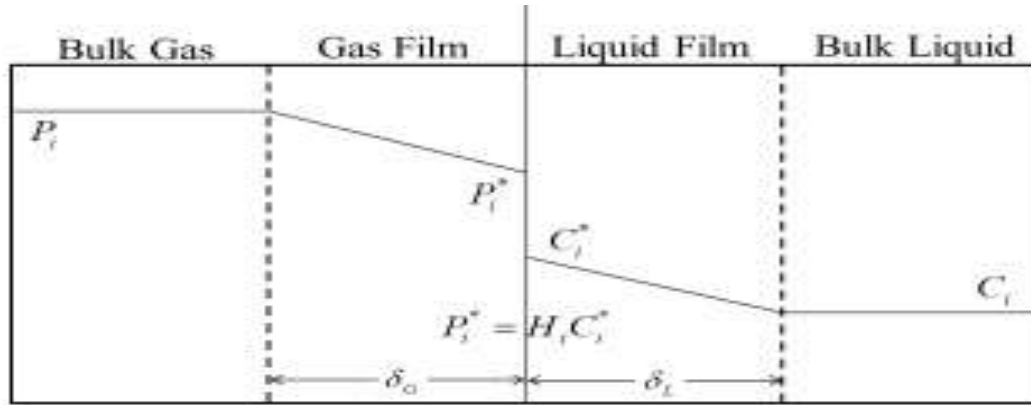


Figure 2. 7: Schematic of the film theory for gas absorption into the liquid.

(Danckwerts, 1970) reported that film theory does not consist of most experimental finding but it explains that gas must go into the liquid by molecular diffusion and dissolution before it can be transported by convection. The simplicity of the theory has made its widespread use in the modeling of gas-liquid mass transfer. In trying to improve the accuracy calculation for the concentration profile, films are further divided into segments. The mass transfer equations for those segments are solved independently especially if chemical reactions are involved.

### 2.7.1.2 Penetration Theory

Film theory with its steady flow is not valid for the penetration period that is of the same magnitude to or longer than the contact time between gas and liquid (Higbie, 1935). (Higbie, 1935), then proposed a theory describing the real mechanism of absorption, that absorption of gas by liquid only take place when the element of liquid is exposed to the gas. He said the time of exposure for each element is of the same length  $\theta$  and the element during this time is assumed to be stagnant and infinitely deep, also absorbs the same amount  $Q$  of gas per unit area. And the relationship between the transfer coefficient and the length is given as;

$$k_l^0 = \frac{Q}{\theta(c_i^* - c_i)} = 2 \sqrt{\frac{Dl}{x\theta}} \quad 2.26$$

The dependence of the physical mass transfer coefficient of gas diffusivity on square root is consistent with previous experiments, in which the order of 0.5-1 was observed on diffusion coefficient (Bishnoi & Rochelle, 2000).

### 2.7.1.3 Surface Renewal Theory

A theory similar to the penetration theory is the surface renewal theory but the only difference between the two is their length of exposure time. The same time of exposure is not realistic for all elements of the surface but the stationary normal distribution of time of exposure could be a better idea. The stationary normal distribution of time of exposure is expressed as:

$$\phi(\theta) = se^{-s\theta} \quad 2.27$$

S is the mean fractional rate of any element at the surface. This distribution leads to the following dependence of  $k_l^0$  on s:

$$k_l^0 = \sqrt{D_i s} \quad 2.28$$

### 2.7.1.4 Eddy Diffusivity Theory

(King, 1966) postulates that the eddy diffusivity for a liquid element near the interface of the gas-liquid system can be described using a power law model:

$$DE = a\delta^n \quad 2.29$$

$\delta^n$  is the distance normal to the interface. At the interface,  $\delta^n=0$  and the eddy diffusivity is zero. The mass transfer is completely dominated by molecular diffusion and therefore, the mass transfer behavior at the surface for a liquid element can be represented by the equation:

$$\frac{\partial C_i}{\partial t} = \frac{\partial}{\partial \delta} (D + D_E) \frac{\partial C_i}{\partial \delta} \quad 2.30$$

In this model  $a$  and  $n$  are independent of surface age  $t$ , which when high enough and  $n$  sufficiently large give rise to a steady-state mass transfer and the physical mass transfer coefficient becomes independent of  $t$ .

$$k_l^0 = a^{\frac{1}{n}} D_i^{1-\frac{1}{n}} \frac{n}{\pi} \sin \frac{\pi}{n} \quad 2.31$$

The eddy diffusivity model with  $n = 2$  was applied by (Bishnoi & Rochelle, 2000) and (Cullinane, 2005) the corresponding equation is:

$$k_l^0 = \frac{2}{\pi} \sqrt{a D_i} \quad 2.32$$

this theory allows for independence on time and its main advantage compared to the film theory is the continuous eddy diffusivity profile close to the interface, and the avoidance of the concept of a —film or a discontinuity in transport properties (King, 1966).

## 2.7.2 Mass Transfer with Chemical Reaction

### 2.7.2.1 Instantaneous Reactions

Equilibrium applies to the reaction between CO<sub>2</sub> and some highly reactive solvents like MEA and piperazine at high temperature because the reaction occurs very fast. With a reversible instantaneous reaction, CO<sub>2</sub> solubility is enhanced as a result of the presence of alkanolamines to first order approximation (Rochelle, Bishnoi, Chi, Dang, & Santos, 2001). The dissolved forms of gas such as carbamate and bicarbonate are added up and represent the total solubility of CO<sub>2</sub>. The rate of mass transfer [(flux) is expressed as:

$$N_{CO_2} = k_l^0 ([CO_2]_{i,T} - [CO_2] * T) = k_l^0 \left( \frac{P_{CO_2}}{H_{CO_2}} [CO_2] * T \right) \quad 2.33$$

$H_{CO_2}$  is the Henry's constant of CO<sub>2</sub> in the amine solvent;  $[CO_2]_{i,T}$  is the total concentration of the dissolved CO<sub>2</sub> species at the gas-liquid interface that would be in equilibrium with CO<sub>2</sub> Partial pressure in the gas phase (Pi).

### 2.7.2.2 Finite-Rate Reaction

The below figure represents the film analysis of how CO<sub>2</sub> is absorbed by a bulk liquid with a fast chemical reaction. Reaction rate, in this case, is not so fast for it to be instantaneous but still fast enough for most of the reaction to take place within a thin boundary near the gas-liquid interface. This is the scenario mostly



encounter in most CO<sub>2</sub> absorption using amine solvents. The concentration of CO<sub>2</sub> at the interface is related to the chemical reaction. The rate of absorption is a function of the reaction rate constant and thermodynamics.

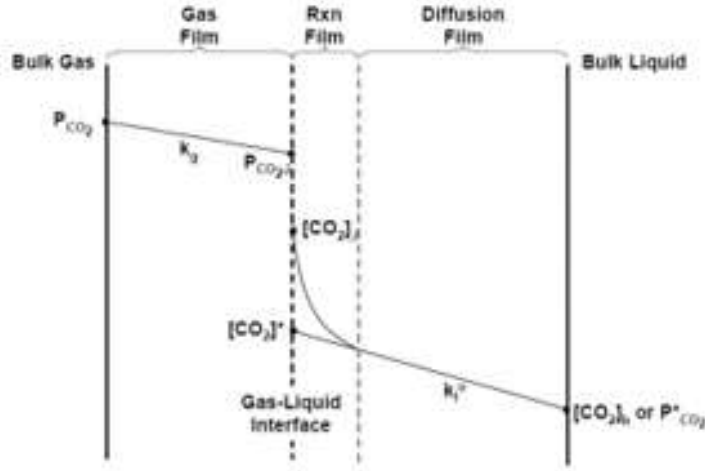


Figure 2. 8: Mass transfer of CO<sub>2</sub> into the bulk liquid with a fast chemical reaction.(Cullinane, 2005).

The total resistance to mass transfer consists of a series of resistances from the gas film, reaction film and diffusion film, represented by the following equation:

$$\frac{1}{K_G} = \frac{1}{k_g} + \frac{H_{CO_2}}{Ek_l^0} + \frac{1}{k_l^0 PROD} \frac{\partial P^*CO_2}{\partial [CO_2]_T} = \frac{1}{k_g} + \frac{1}{k'_g} \quad 2.34$$

$K_G$ ,  $k_g$  and  $k'_g$  are the overall, gas-side and liquid-side mass transfer coefficients with the driving force in gas partial pressure unit, respectively.  $E$  is the enhancement factor defined as the ratio of CO<sub>2</sub> flux with chemical reaction and CO<sub>2</sub> flux with only physical absorption.  $\partial P^*CO_2 / \partial [CO_2]_T$  represents the slope of the equilibrium curve for CO<sub>2</sub> in amine-CO<sub>2</sub>-water.

CO<sub>2</sub> flux is usually calculated by solving the steady-state differential equation on CO<sub>2</sub> mass balance in the boundary layer, followed by applying the Fick's law to the CO<sub>2</sub> concentration profile at the interface.

$$DCO_2 \frac{\partial^2 [CO_2]}{\partial x^2} + rCO_2 = 0 \quad 2.35$$

$$NCO_2 = - DCO_2 \frac{\partial [CO_2]}{\partial x} \quad 2.36$$

### 2.7.1 Prediction of Diffusion Coefficient

Diffusion coefficients are function of pressure, temperature and the species been diffused. Kinetic theory models are sufficient and accurate for calculation of binary diffusion coefficients in gases at low pressure but not for predicting liquid phase diffusion coefficients (R Byron Bird, Stewart, & Lightfoot, 2007).

(Wilke & Chang, 1955) developed a correlation for the liquid phase and is given below:

$$D_{AB} = 7.4 \times 10^{-8} \frac{\sqrt{\psi_B M_B T}}{\mu V_A^{0.6}}$$

Where  $\psi_B$  is called an association parameter with value of 2.6 for water

$M_B$  is the molecular weight of species B

$\mu$  is the solution viscosity in cP

$V_A$  (cm<sup>3</sup>/gmol) is the molar volume of species A at its normal boiling point as liquid.

## CHAPTER THREE

### RESERVOIR SIMULATION MODELING

#### 3.1 INTRODUCTION TO ECLIPSE 300

Eclipse 300 is a compositional simulator with cubic Equation of State, pressure dependent k-value and black-oil treatments. The program can run in fully implicit, IMPES and adaptive implicit (AIM) modes. It has four equations of state; the Redlich-Kwong, Soave-Redlich-Kwong, Peng-Robinson and Zudkevitch-Joffe EoS. In the simulator, adaptive implicit scheme would be used to tackle problems which makes cells implicit only where necessary. The linear equation systems from linearization are solved using Nested Factorization accelerated by orthomin Matrix conditioning iterative method. The method conserves mass balance accurately at each iteration and therefore Nested Factorization is particularly well suited to the solution of large problems. It can be used to model different types of reservoir problems including; CO<sub>2</sub> storage, chemical reaction, gas injection, coal bed methane, multi-phase flash, diffusion, modeling miscible displacement scheme with compositional gradient with depth among others (Eclipse Technical Description, 2010).

#### 3.2 Data description and Model used

The data used for this work is a representative fluid composition data from literature (Hashemi Fath & Pouranfar, 2014) having the characteristics API gravity of 22°, 29°, 38° and 45° which was simulated at a temperature similar to that of the Wilcox formation in the deepwater Gulf of Mexico. The other characteristic of the reservoir formation are presented in Table 2.1 for the properties of the formation needed for modeling the reservoir. The raw fluid components and their compositions in mole fraction before and after grouping into pseudo components are presented in tables in appendix. The grouping was done by lumping some of the components together to reduce the number of components to improve computation efficiency. The carbon number of two to five were grouped together as C<sub>2</sub>-C<sub>5</sub> and the carbon number of seven to twelve plus fraction were grouped together as C<sub>7+</sub>.

### 3.2.1 The phase behavior of the fluid composition

The phase envelope (pressure-temperature) diagram of the fluid composition was developed using a PVT simulator. The package is used to determine the phase behavior of reservoir fluids. The 3-parameter Peng-Robinson EoS was used for the analysis and the Lohrenz-Bray-Clark viscosity model. Table A5-A9 in appendix summaries the critical pressures and temperatures of used components for the heavy, medium, intermediate and light oil crude samples. The binary interaction parameters obtained is also presented in the Appendix.

### 3.2.2 3-parameter Peng-Robinson Equation of State Model

Equation of states EoS, help to predict the volumetric behavior of a fluid for given pressure and temperature. Pressure term of the semi-empirical van der Waals equation was modified by Peng and Robinson (1976) which result in the PR EoS. The EoS can be used for both phase and volumetric behavior when applied to binary, ternary or multi-component system. For any number of component system, the PR EoS is as follow:

$$P = \frac{RT}{V-b} - \frac{a\alpha}{V^2+2b-b^2} \quad 3.1$$

$\alpha$  is a repulsion term which is temperature dependent and  $b$  is an attraction parameter.

The terms in the above equation which is for both single component system or single component in a binary, ternary or multi-component system is defined as below:

$$a = \frac{0.457235R^2T_c^2}{P_c} \quad 3.1b$$

$$b = \frac{0.077796RT_c}{P_c} \quad 3.1c$$

$$\alpha = (1 + k(1 - T_r^{0.5}))^2 \quad 3.1d$$

The  $k$  in Eq. 3.1d is a quadratic function and defined in equation 3.1e below while the reduced temperature  $T_r$  is given by equation 3.1f. The  $k$  value initially estimated from Wilson's method.

$$k = 0.37464 + 1.54226\omega - 0.2699\omega^2 \quad 3.1e$$

$$T_r = \frac{T}{T_c} \quad 3.1f$$

Where the  $T_c$  (K) is the critical temperature.

In a multi-component system,  $a$  and  $b$  are computed for the phases present not component and therefore makes the parameters a function of all the constituent components of the phase. For the liquid phase, the terms  $a\alpha^L$  and  $b^L$  are used whereas for the vapor phase the term  $a\alpha^V$  and  $b^V$  are used. The van der Waal mixing rule is given as:

$$a\alpha^L = \sum_{i=1}^{N_c} \sum_{j=1}^{N_c} x_i x_j (a\alpha)_{ij} \quad 3.1g$$

Where:

$$(a\alpha)_{ij} = (1 - \delta_{ij}) \sqrt{(a\alpha)_i (a\alpha)_j} \quad 3.1h$$

$x_i$  and  $x_j$  are the liquid phase mole fraction of component  $i$  and component  $j$  respectively.  $\delta_{ij}$  is the binary interaction parameters used to adjust the interaction between unlike components (Okuno, Johns, & Sepehrnoori, 2010). The van der Waals mixing rule is given as  $b^L$  which is represented as below:

$$b^L = \sum_{i=1}^{N_c} x_i b_i \quad 3.1i$$

Analogous equations are used for the vapor phase calculations  $a\alpha^V$  and  $b^V$ , where the liquid phase mole fractions  $x_i$  and  $x_j$  are replaced by the vapor phase mole fraction  $y_i$  and  $y_j$ .

Because hydrocarbon usually have its critical compressibility less than 0.29 and the PR EoS calculates the critical compressibility as  $Z_c^{PR} = 0.307$ , with the two free parameters  $a$  and  $b$  while the third parameter  $Z_c$  is fixed. A third parameter  $c$  is introduced and treated as a volume shift, the corrected 3-parameter volume is the observed volume from the 2-parameter EoS less the volume shift. The volume shift leads to a reduced  $Z$ -factor.

$$V(3) = V(2) - \sum_{i=1}^N x_i c_i \quad 3.1j$$

The values of  $c_i$  is determined via variety of techniques, PVT uses the method of comparing the liquid molar volume of a component at standard conditions  $V^{obs}(P_{st}, T_{st})$  to that predicted by the 2-parameter at the same conditions,  $V^{EoS}(P_{st}, T_{st})$ . The difference between the two volumes gives the shift parameters.

$$c_i = Vi^{EoS}(P_{st}, T_{st}) - (Vi^{Obs}(P_{st}, T_{st}))$$

### 3.3 Estimating Minimum Miscibility Pressure (MMP)

MMP is the pressure above which gas displaces nearly 100% of oil in the swept zone. There are two main methods of determining MMP or MME (minimum miscibility enrichment): Analytical techniques and Experimental methods. The analytical techniques are based on numerical computations which could be derived from empirical correlations and compositional simulations. Three compositional simulation methods are frequently used which are: the tie-line method, 1-D slim-tube simulation, mixing cell method. The experimental methods used is the slim-tube method and Rising bubble apparatus method. The MMPs calculated from empirical correlations can have large errors and they should be used with caution.

For this study, the MMP was determined for the representative fluid sample at the reservoir temperature and pressure assuming pure CO<sub>2</sub> injection into the reservoir. Slim-tube simulation was carried out using eclipse 300 and First Contact Miscibility Pressure experiment was run using the PVT. The resulting MMP from the PVT package is 689.88 atm (10,134.8psia). In a slim-tube simulation, the estimated MMP is the pressure at which the oil recovery is between 95-98%. Simulation of 1-D slim-tube experiment with grid dimension of 200×1×1, porosity of 12% and permeability of 15 mD, 10 cm slim-tube, Peng-Robinson EoS and FULLIMP solution method. The estimated MMP from the Simulation is about 6500psia, above this pressure, the recovery factor begins to fall. Figure 3.2 shows the plot of how recovery changes with pressure.

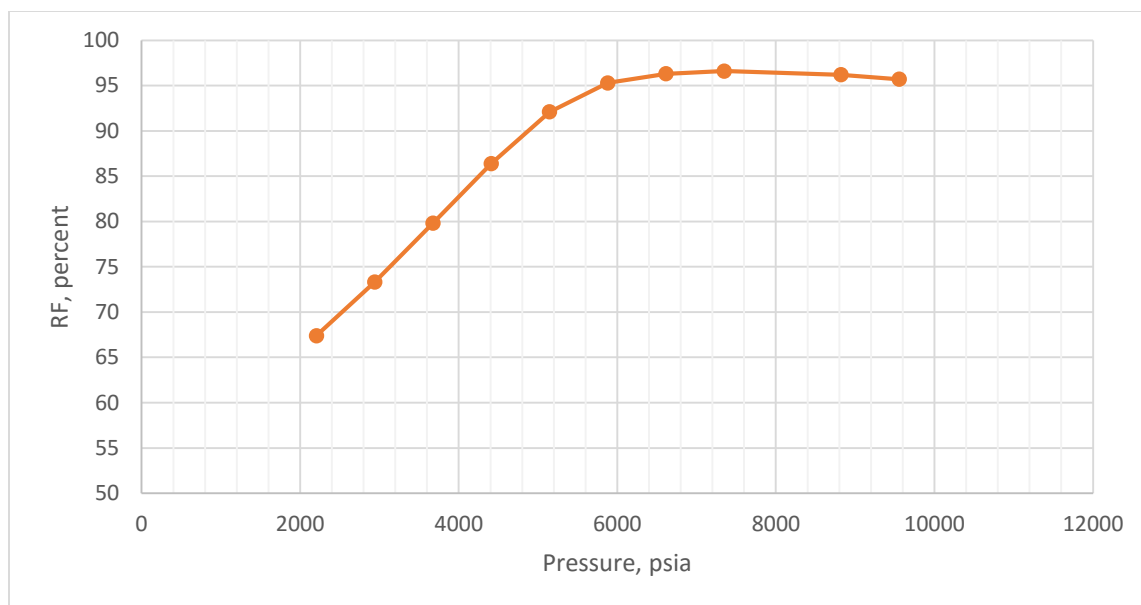


Figure 3. 1: The plot recovery factor of against pressure for predicting MMP.

### 3.4 Urea Reaction and CO<sub>2</sub> Generation Kinetics

The generation of CO<sub>2</sub> from urea has been demonstrated using the Arrhenius plot of thermal hydrolysis. (Wang et al., 2018) generated a plot at reservoir condition for a catalyzed and un-catalyzed reaction, the equation of the relationship between the reaction constant,  $k$  and the activation energy,  $E_A$  for both process show a linear reaction. He used sodium hydroxide (NaOH) as a homogeneous catalyst and this result in higher kinetics of urea hydrolysis. Literature (Clark, Gaddy, & Rist, 1933; Claudel & Boulamri, 1988; Kaminskaia & Kostić, 1997; Khan, Rafiquee, Niaz, & Khan, 1996; Ramachandran et al., 1998) has reported numbers of work on urea hydrolysis to generate CO<sub>2</sub> and NH<sub>3</sub> using different catalyst, like metal oxide, Aluminum Oxide and fly ash. The report of the metal oxide (Vanadium, Chromium, molybdenum) did not give details of the reaction parameters but concluded that there was no significant catalytic activity. The thermal hydrolysis of urea has been concluded to be a first order reaction and the rate constant increases with temperature. The reported kinetic parameters affecting CO<sub>2</sub> generation from urea hydrolysis is summarized in table 3.3 below. (Wang et al., 2018) generated the equation for the hydrolysis for both catalyzed and non-catalyzed reaction respectively as shown below and states that the equation is valid for temperature up to 300°C.

$$\ln k = -10445 \times \frac{1}{T} + 19.611 \quad 3.2a$$

$$\ln k = -11337 \times \frac{1}{T} + 21.248 \quad 3.2b$$

k is the reaction rate constant in  $\text{min}^{-1}$

T is temperature in kelvin

The parameters affecting the hydrolysis reported have shown similar trend. Catalyzed reaction are faster and tends to achieve notable decomposition which guarantee high conversion of urea to  $\text{CO}_2$  and  $\text{NH}_3$ .

For this study, Wilcox formation is considered and the temperature in the formation is  $250^\circ\text{F}$ . Using the relationship equation of (Wang et al., 2018), the rate constant expected in the hydrolysis of urea reaction with and without catalyst (1% NaOH) in the formation is 0.001026 and 0.000549 respectively. This will be useful in simulation study of in situ  $\text{CO}_2$  flooding considering the reaction happening subsurface.

Table 3. 1: Urea hydrolysis kinetic Parameters.

Author	Temperature, $^\circ\text{F}$	Catalyst	Rate constant $\text{min}^{-1}$	Activation energy $\text{kJ/mol}$	Pre-exponential factor $\text{min}^{-1}$	Half-life minutes
Sahu et al. (2009)	140	Fly ash	0.00457	129.48	$9.378 \times 10^{13}$	N/A
	150		0.00764			
	160		0.02120			
	170		0.06044			
	180		0.10483			
Ganghadaran et al. (2011)	150	$\text{Al}_2\text{O}_3$	0.00288	61	$9.089 \times 10^5$	N/A
	160		0.00387			
	170		0.00630			
Wang et al. (2018)	120	No catalyst	0.000506	94.26	$1.7 \times 10^9$	1290
		NaOH	0.000952	86.84	$3.3 \times 10^8$	
	250	Catalyst	0.000533			1300
	250	No catalyst	0.000553			1253



### 3.5 CO<sub>2</sub> Swelling Factor

One of the parameter used to measure the efficiency of CO<sub>2</sub> flooding is the swelling factor, this can be determined empirically, experimentally and by simulation. The swelling factor (SF) is defined as the ratio of CO<sub>2</sub>-saturated oil volume at reservoir pressure and the temperature to original oil volume measured at reservoir temperature and atmospheric pressure (Simon & Graue, 1965).

$$SF = \frac{V_{CO_2-oil}(P_R, T_R)}{V_{oil}(P_{atm}, T_R)} \quad 3.3$$

Where,  $V_{CO_2-oil}$  is the volume of CO<sub>2</sub>-oil mixture and  $V_{oil}$ , the volume of oil.

Also, PVT simulator can be used to carry out the swelling test of an injection fluid or gas to determine the swelling factor of the injected fluid by simulation. This can be used to predicting the flooding performance or efficiency of a particular solvent or gas.

#### 3.5.1 CO<sub>2</sub> swelling factor for different API oil

With PVT simulator having the fluid sample data and injection data like mole fraction, reference pressure, temperature and the saturation pressure, various PVT test can be simulated to obtain other needed data. To determine the swelling factor of CO<sub>2</sub> oil mixture, either the mole fraction or GOR of the injected fluid and temperature need to be specified. Different swelling test will be carried out on each oil sample and graphical result can be generated which could be used to establish a relationship between CO<sub>2</sub> and oil types used in study. For this work, oil sample with 22°, 29°, 38° and 45° was tested and the result obtained is shown below.

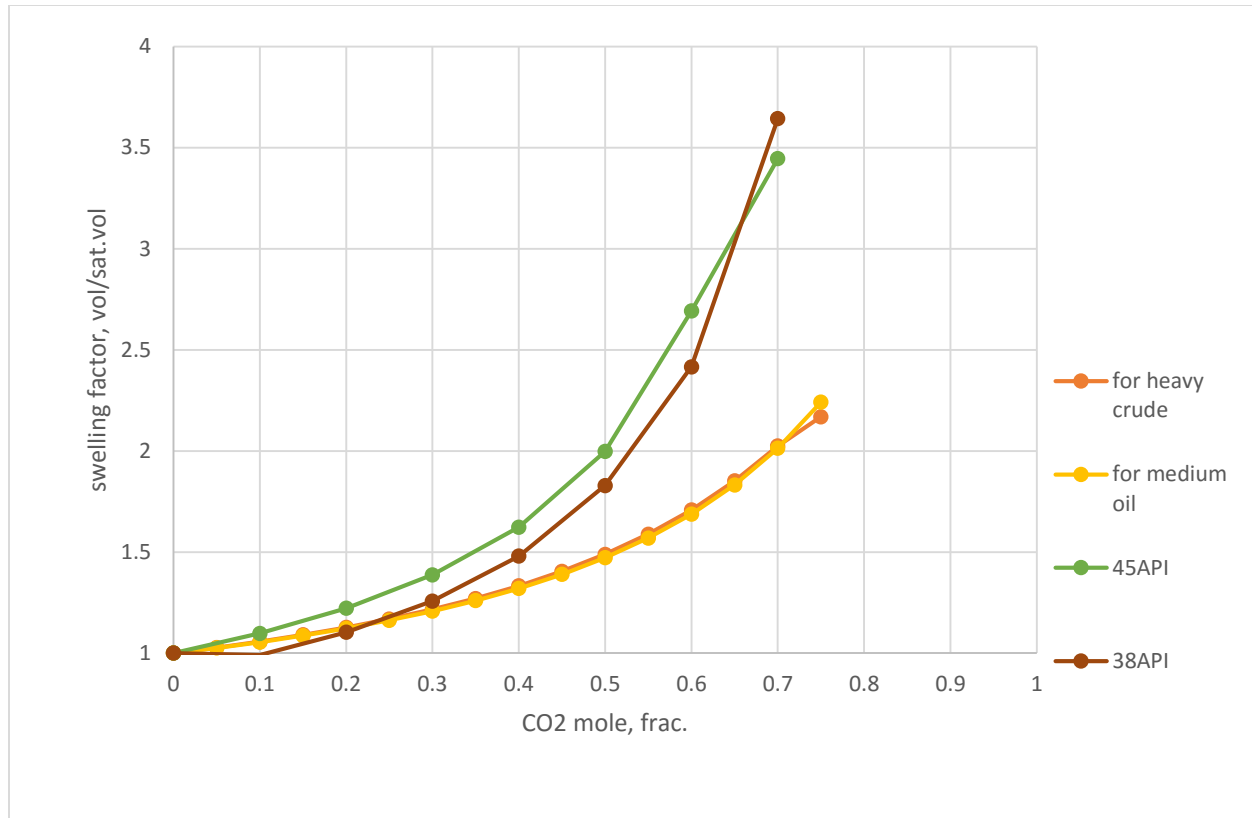


Figure 3. 2: the graph of CO<sub>2</sub> swelling factor for different API crude.

### 3.6 CO<sub>2</sub>-Oil Viscosity Reduction

Reservoir hydrocarbon fluid with high viscosity have been produced by injecting gas and solvents which helps to mobilize the oil towards the production well to maximize recovery. Many approach has been used to enhance production from heavy oil reservoirs and tight formations which includes water alternating gas (WAG), gas flooding, solvent flooding, thermal flooding, and chemical flooding among others.

Heavy crude oil is a hydrocarbon type with high specific gravity, low API value less than 22° and higher percentage of carbon number greater than 5. It is highly viscous, dense, has asphaltic nature with heavier molecular composition. The extraction, recovery and production of this heavy crude has remain a challenge and the reason for EOR. Medium oil type is a hydrocarbon type characterized with not very high specific gravity, average API value of about 25-30°, relatively low viscosity and with not too high percentage of carbon to hydrogen ratio . Light or volatile oil has a low density and flows freely at room temperature. The oil is characterized high API gravity due to the presence of a high proportion of **light** hydrocarbon fractions.

It generally has a low wax content as well. In this study, pure CO<sub>2</sub> and Impure CO<sub>2</sub> was injected and different grid dimension was considered.

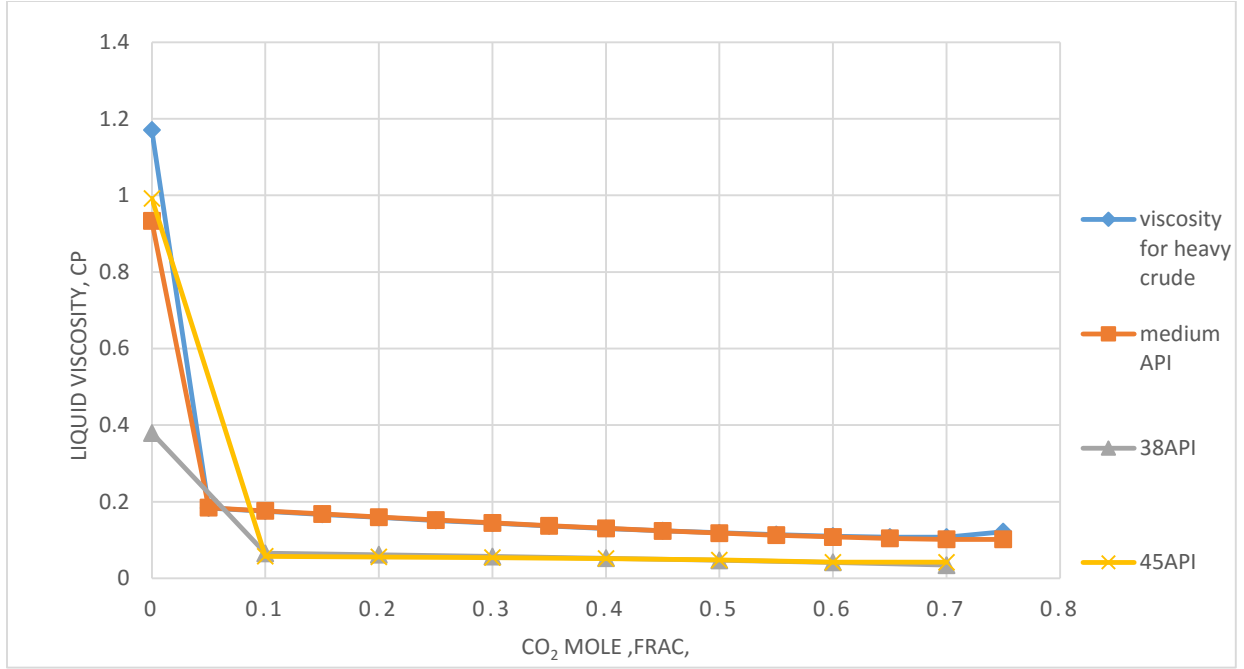


Figure 3. 3: The graph of viscosity reduction for different API crude.

### 3.7 Lohrenz, Bray and Clark Viscosity Reduction Correlation

The Lohrenz, Bray and Clark viscosity model is a correlation capable of predicting both oil and gas viscosities. It is the most widely used in reservoir engineering tool. It relates the residual viscosity to the reduced density via a fourth-degree polynomial and the relationship is shown below:

$$\rho_r = \frac{\rho}{\rho_c} \quad 3.4a$$

$$[(\eta - \eta^*)\xi + 10^{-4}]^{\frac{1}{4}} = a_1 + a_2\rho_r + a_3\rho_r^2 + a_4\rho_r^3 + a_5\rho_r^4 \quad 3.4b$$

Where

$$a_1 = 0.102300$$

$$a_2 = 0.0233640$$

$$a_3 = 0.0585330$$

$$a_4 = -0.0407580$$

$$a_5 = 0.0093324,$$

$\eta^*$  is the low-pressure gas mixture viscosity.

$\xi$  is the reduced viscosity parameter and is given for a fluid mixture as below:

$$\xi = [\sum_{i=1}^N Z_i T_{ci}]^{1/6} [\sum_{i=1}^N Z_i M_{wi}]^{-1/2} [\sum_{i=1}^N Z_i P_{ci}]^{-2/3} \quad 3.4c$$

The critical density  $\rho_c$  is evaluated from:

$$\rho_c = V_c^{-1} = (\sum_{i=1, i=C_{7+}}^N (Z_i V_{ci} + Z_{C_{7+}} V_{cC_{7+}}))^{-1} \quad 3.4d$$

Where the critical volume of the plus fraction is found from:

$$V_{cC_{7+}} = 21.573 + 0.015122M_{wC_{7+}} - 27.656\gamma_{C_{7+}} + 0.070615M_{wC_{7+}}\gamma_{C_{7+}} \quad 3.4e$$

The dilute gas mixture viscosity is as given by Herning and Zippener:

$$\eta^* = \left[ \sum_{i=1}^N Z_i \eta_i^* M_{wi}^{1/2} \right] \left[ \sum_{i=1}^N Z_i M_{wi}^{1/2} \right]^{-1} \quad 3.4f$$

Where the dilute gas viscosities of the individual components,  $\eta_i^*$  are derived from expressions due to Stiel and Thodos,

$$\eta_i^* = 34 \times 10^{-5} \frac{1}{\xi_i} T_{ri}^{0.94} \quad T_{ri} < 1.5 \quad 3.4g$$

$$\eta_i^* = 17.78 \times 10^{-5} \frac{1}{\xi_i} (4.58T_{ri} - 1.67)^{0.625} \quad T_{ri} > 1.5 \quad 3.4h$$

Where

$$\xi_i = T_{ci}^{1/6} M_{wi}^{-1/2} P_{ci}^{-2/3} \quad 3.4i$$

### 3.8 Reservoir Model and Rock Properties

#### 3.8.1 Grid System

The X and Y directions of a grid system are the areal co-ordinates and the positive Z direction is normal to the bedding plane in the downward direction. A block centered grid system was used for the simulation, the blocks are numbered in natural order and are first numbered within a row, then row by row and then plane by plane. There are NX blocks in each row, NY blocks in each column and NZ blocks (layers) in

each vertical column. So the entire system has a total of  $NX \times NY \times NZ$  blocks. For this study a  $50 \times 50 \times 5$ ,  $100 \times 100 \times 5$  and  $200 \times 200 \times 5$  grid system was simulated to know which one is best.

### **3.8.2 Computational Process**

The numerical computation is a sequence of steps. In a compositional model with number of components greater than five, Adaptive Implicit and IMPES (AIM) scheme is developed in ECLIPSE 300 to avoid using a fully implicit technique which has become prohibitive in both memory and CPU time. It is a compromise between fully implicit and IMPES methods, allowing cells in difficult regions to remain fully implicit while employing the advantage of an IMPES description in easy regions (Eclipse Technical Description 2010.1).

### **3.8.3 Simulation Model**

Four crude sample cases was considered and with different scenarios and three reported. A section of the reservoir was considered for simulation. The reservoir geometry considered is a symmetric model with an area of 100 acres and uniform reservoir thickness of 30ft. The absolute permeability of 15mD. The formation porosity of 12 percent was used. The initial reservoir pressure of the formation specified for simulation 75000psi. The rock, fluid and other properties used is presented in table 3.4 below.

Table 3. 2: Input Parameters for the rock and fluid Properties.

Properties	Value
Reservoir pressure, psia	7500
Reservoir temperature, °F	250
Thickness, ft	30
Model Area, acres	100
Permeability, mD	$\Delta x=15, \Delta y=13, \Delta z=10$
Porosity	12
Grid Dimension	$50 \times 50 \times 5$
Block Dimensions, ft×ft×ft	$\Delta x=42, \Delta y=42, \Delta z=6$
Rock Compressibility, psia <sup>-1</sup>	4.50E-06
Tops, ft	8000
gas injection rate, MSCF/day	250
Number of wells	5
Simulation time	10 years
Initial oil saturation	80%
connate water saturation	20%
Initial formation volume factor	1.34
Crude oil type, API gravity	22°, 29° and 38°

## CHAPTER FOUR

### RESULTS AND DISCUSSION

#### 4.1 Grid sensitivity Analysis.

This simulation study is targeted at observing how oil viscosity reduces with CO<sub>2</sub> injection and also how oil swells with CO<sub>2</sub>. However predicting reservoir performance can be challenging and one of the uncertainty sources is the spatial discretization of the model into grid blocks. The smaller the grid blocks used, the smaller the truncation error involved. The smaller the grid block, the more the number of grid cells in the model for the same length/ area/volume of investigation. Increasing number of grid cells in the model leads to increase in computation time (Shafikova, 2013). For this reason, it is crucial to have the optimum grids number and distribution so the model could be regard enough as the representative of the reservoir to meet the study objectives.

In this work, 100 acres section the reservoir was considered and two different grid sizing were simulated. The grid system are  $50 \times 50 \times 5$ ,  $100 \times 100 \times 5$  and  $200 \times 200 \times 5$ . After simulation, the oil viscosity and efficiency of the three grid system was compared. The trend of viscosity reduction is the same for all system but the time taken for each is different and this can be justified with the established fact that the more the number of grids, the less the error. This same trend was observed for the efficiency of the systems been considered. With an oil density of 22°API, the crude is classified as a heavy crude and efficiency peaks at 75% with CO<sub>2</sub> injection at the rate 250 MSCF/DAY for the  $100 \times 100 \times 5$  system and that was the highest obtainable recovery. Therefore, increasing the grids beyond  $100 \times 100 \times 5$  will only take more computation time with no additional recovery achieved. The result are shown in figure 4.1 and 4.2 below.

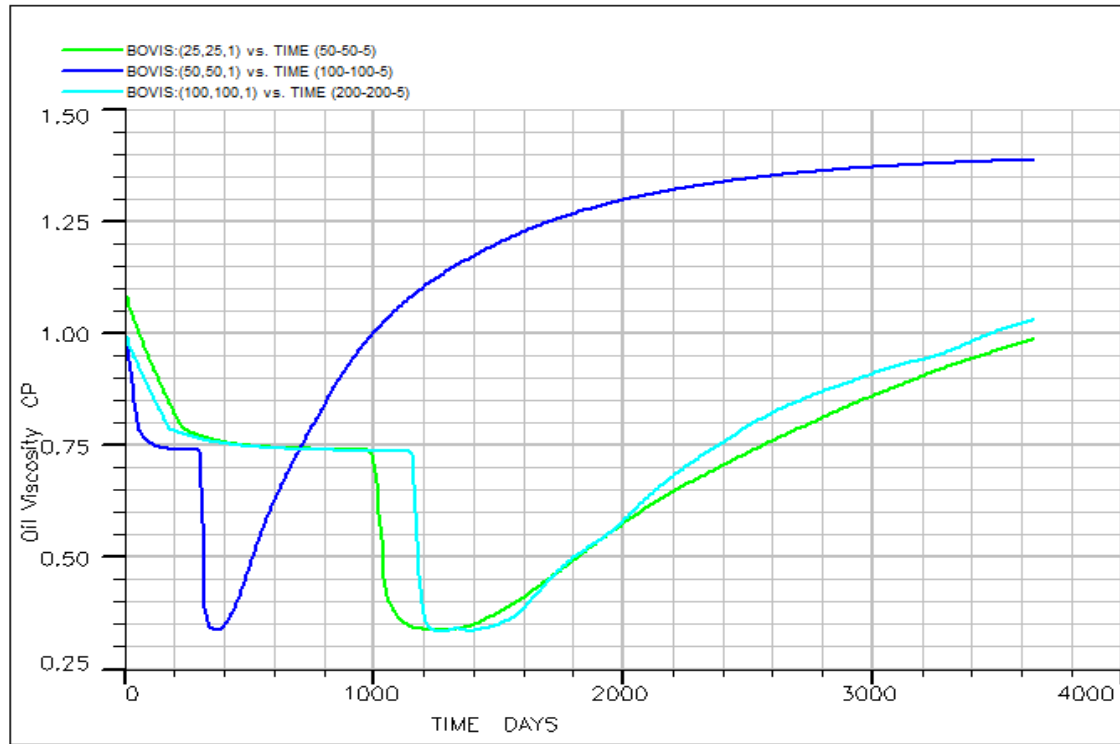


Figure 4. 1: Block oil viscosity graph for the  $200 \times 200 \times 5$ ,  $100 \times 100 \times 5$  and  $50 \times 50 \times 5$  grid system.

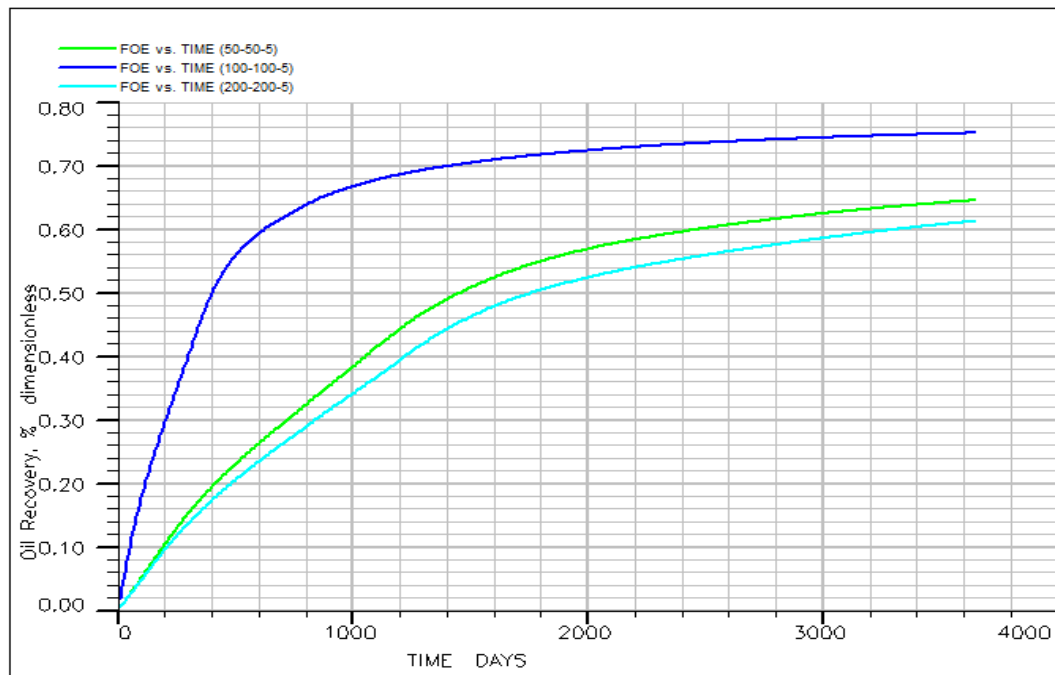


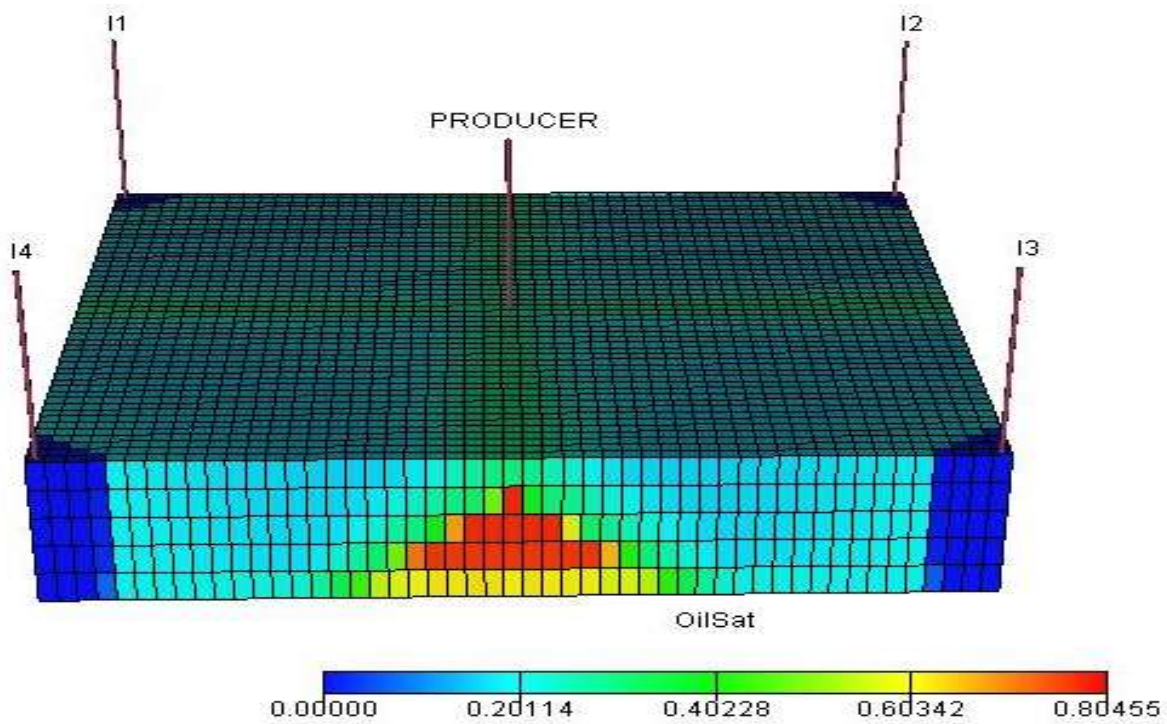
Figure 4. 2: Oil recovery efficiency for the  $200 \times 200 \times 5$ ,  $100 \times 100 \times 5$  and  $50 \times 50 \times 5$  grid system.



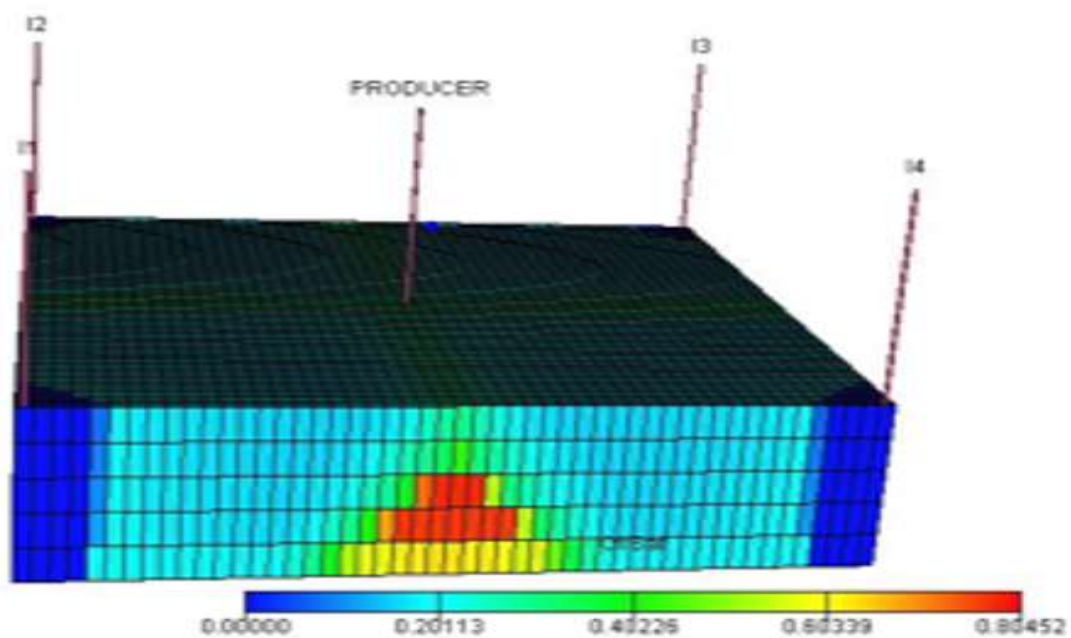
## 4.2 Simulation Result and Discussion

### Case A: 22° API Crude Sample

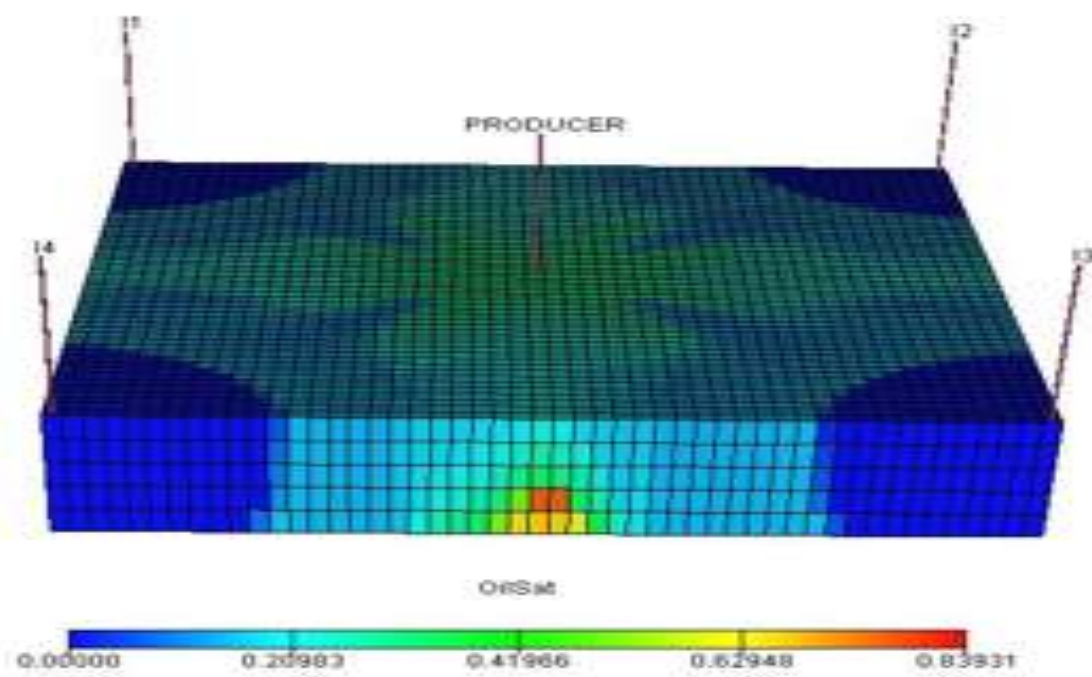
This crude sample is classified as heavy type, it has more of the heavy ends than the light ends. The sample is simulated for three different scenarios; the first scenario is the injection of pure CO<sub>2</sub> (100%) in to the reservoir at 250 MSCF/DAY, the second scenario is the injection of impure CO<sub>2</sub> (80% of CO<sub>2</sub> and 20% of H<sub>2</sub>S) at 250 MSCF/DAY and the last scenario is that of pure CO<sub>2</sub> (100%) injection at a rate of 1000 MSCF/Day. A 5-spot pattern model was considered and the result is present in figures below.



(a)



(b)



(c)

Figure 4. 3: The grid Model for case A CO<sub>2</sub> injection scheme for (a) 100% CO<sub>2</sub> injection, (b) for 80% CO<sub>2</sub> and 20% H<sub>2</sub>S and (c) high injection rate.

Referring to Figure 4.4, the pressure, water cut and the oil production rate on the same plot shows that with time, the rate of oil production reduces with pressure and water cut in to the production well increases. It was also observed on the same plot that any slight increase in pressure will result in production rate increasing and reduction in water cut. The rate at which pressure falls is gradual and this directly affect the rate of fall in production which means if pressure could be maintained the rate could also be maintained for this type of crude sample. For injection period of 10 years, the water cut was almost negligible and peaks at 0.13, the pressure reduces from 8000 psia to 2400 psia with rate from 1000 stb/day to almost 80 stb/day.

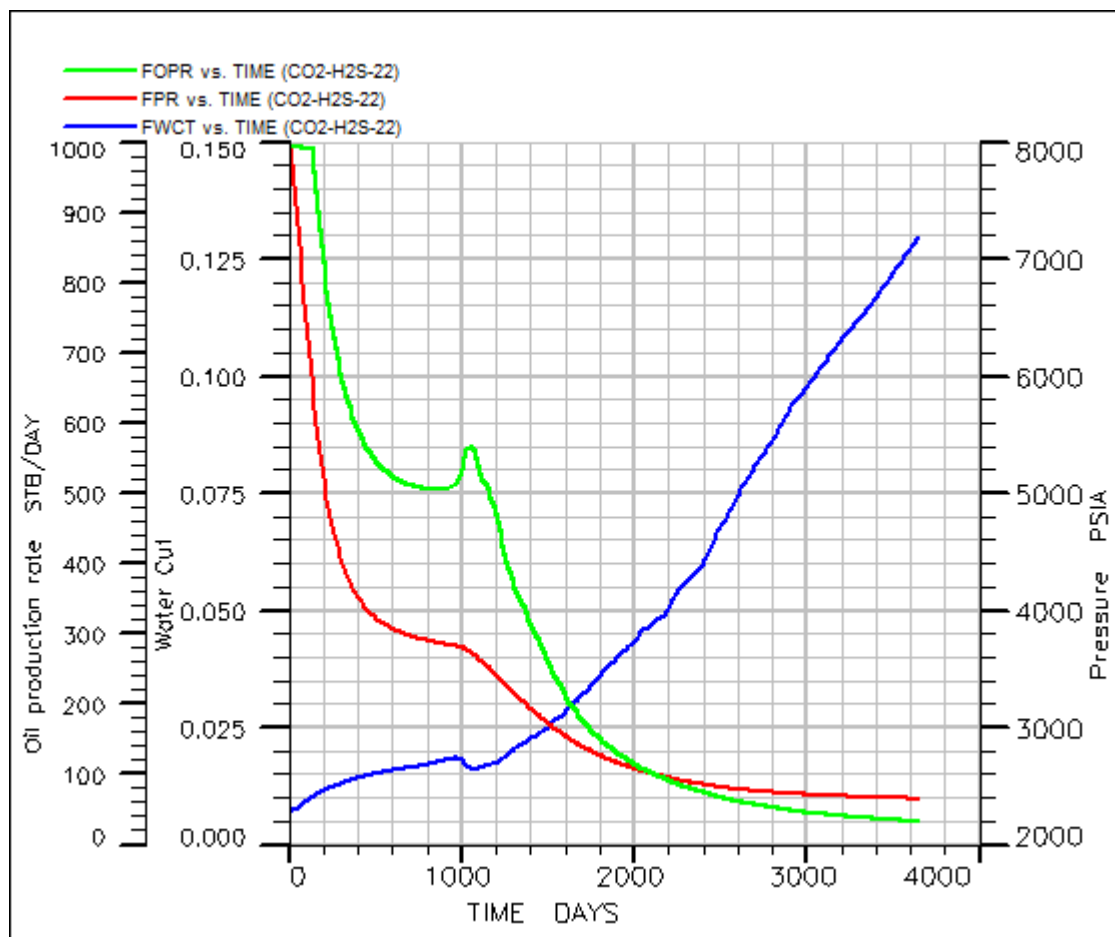


Figure 4. 4: Comparison plot of pressure, water-cut and oil production rate.

The comparison plot for CO<sub>2</sub>-Oil viscosity reduction is presented in figure 4.5. For pure CO<sub>2</sub> injection at 250MSCF/day, the oil viscosity reduces gradually for a period of 1300 days from 1.05 cP to 0.35 cP and then increases to a viscosity value of 1.2 cP after the simulation period of 10 years. The same trend was

observed for the impure CO<sub>2</sub> injection but with more viscosity reduction due to the presence of H<sub>2</sub>S in the injection stream and took about 1400 days before an increased in viscosity was observed which peaks at 0.9 cP after 10 years. With high injection rate, there was a viscosity overshoot for a period of about 600 days before experiencing rapid fall. The viscosity increases from 1.05 cP to 1.43 cP and then to 0.17 cP within a period of 100 days. Viscosity of the oil increases up to 1.2 cP after 10 years.

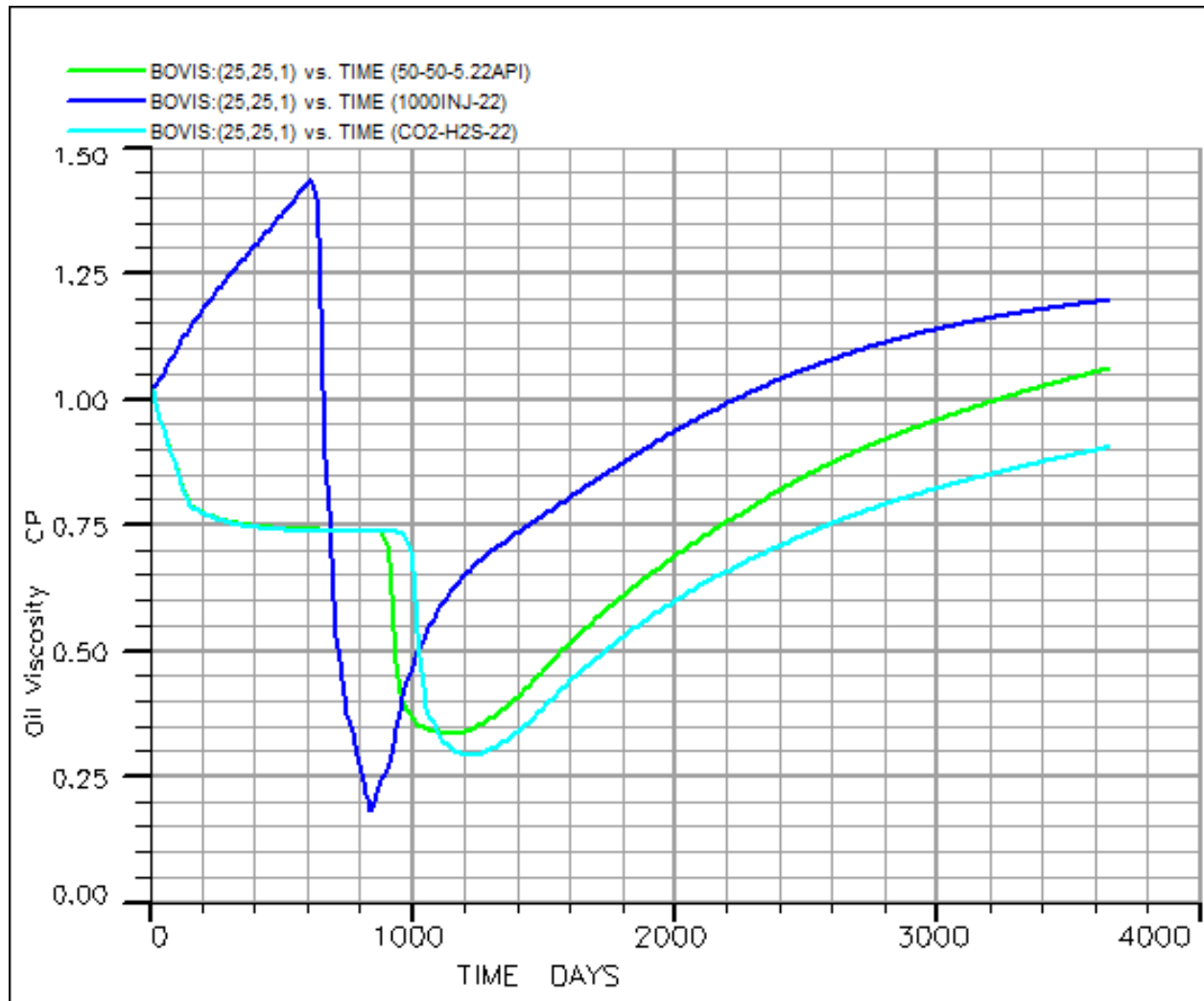


Figure 4. 5: oil viscosity for the CO<sub>2</sub> injection three scenarios.

From Figure 4.6 below, the water cut for the heavy oil crude production using CO<sub>2</sub> injection is plotted against time. The scenario of high gas injection rate (1000 MSCF/Day) present a sharp water cut after about 900 days of CO<sub>2</sub> injection when recovery was about 80% of OOIP. This support the claim that high injection

rate leads to high recovery and early water production. For the first 1000 days of oil production, the water cut was about 1% for both pure and impure CO<sub>2</sub> injection scenarios. For the next 1400 days, water cut increased from 1% to about 7% after which an insignificant different in water cut was observed between the two scenarios.

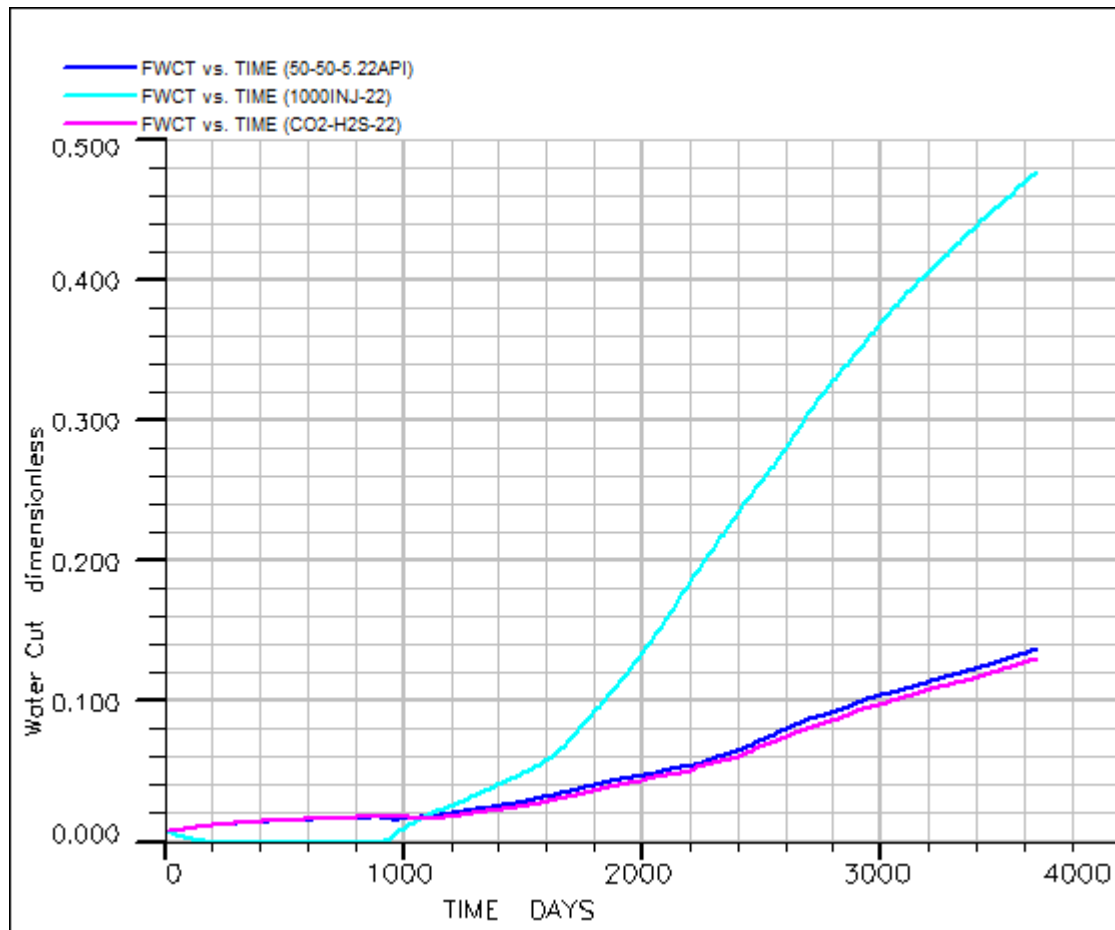


Figure 4. 6: Plots of water-cut against time for different CO<sub>2</sub> injection scenarios.

Figure 4.7 depicts the efficiency or the oil recovery factor with time for the three scenarios of case A injection scheme. In the figure, the high injection rate scenario has a recovery factor of 80% which compare to the two other scenarios is better option for the time of investigation. The efficiency of the pure and impure CO<sub>2</sub> injection has no significant difference as seen in Figure 4.7 but when compared with the third scenario whose injection rate 1000MSCF/day, the recovery efficiency can be concluded to increase with increasing injection rate.

The recovery factor increases with continuous injection of CO<sub>2</sub> and this is presented in Figure 4.8 for the pure CO<sub>2</sub> injection, the recovery factor peaked at 67% for 100 mole percent CO<sub>2</sub> injected in to the reservoir.

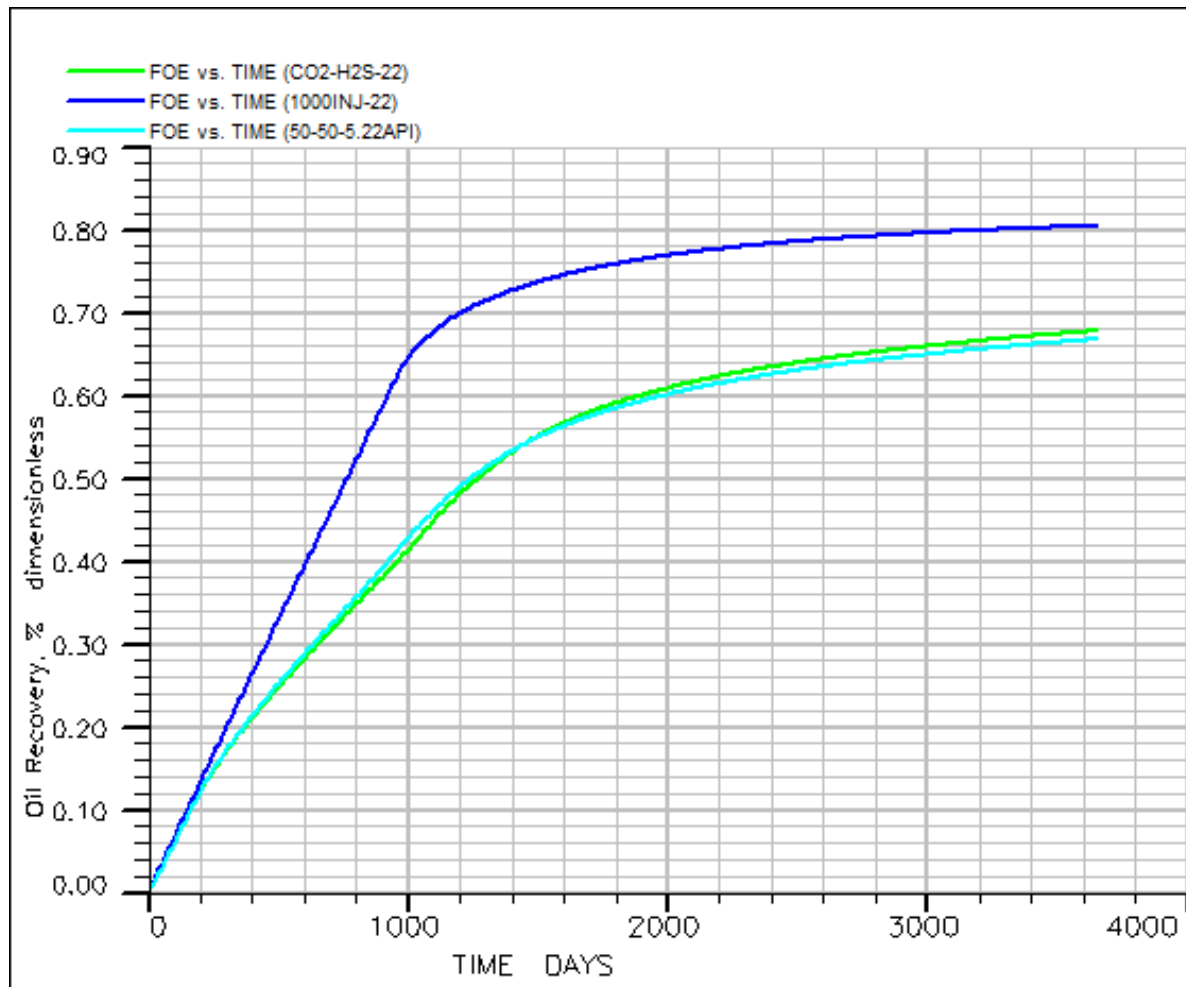


Figure 4. 7: Oil recovery factor versus time for the CO<sub>2</sub> injection Scenarios of case A

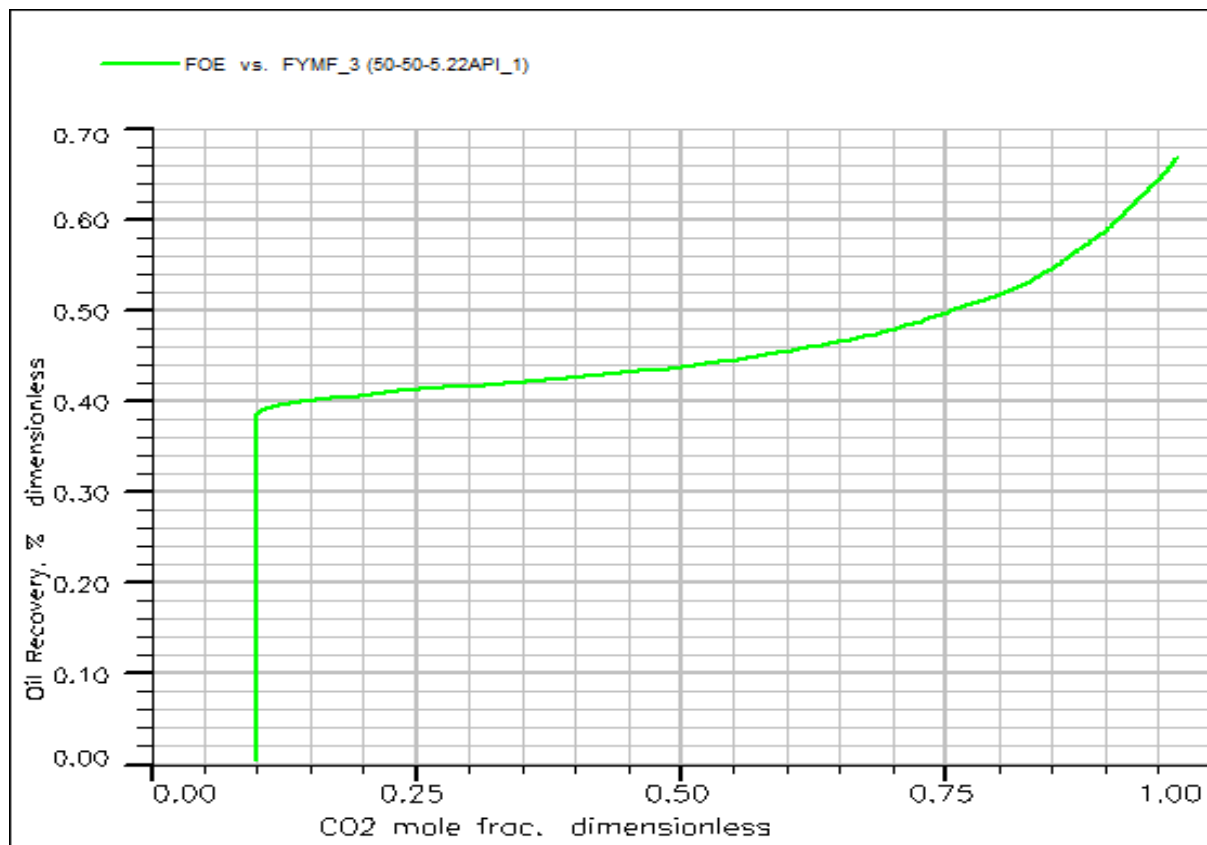


Figure 4. 8: Plot of recovery factor versus CO<sub>2</sub> mole fraction injected.

#### Case B: 29° API Crude Sample

CO<sub>2</sub> injection in to a reservoir with hydrocarbon fluid of 29° API oil is simulated with a  $50 \times 50 \times 5$  grid system for a period of 10 years. The injection rate of CO<sub>2</sub> in to the reservoir is 250 MSCF/Day and a 5-spot pattern model was considered. The model of oil saturation after 10 years of CO<sub>2</sub> injection in represented in figure 4.9.

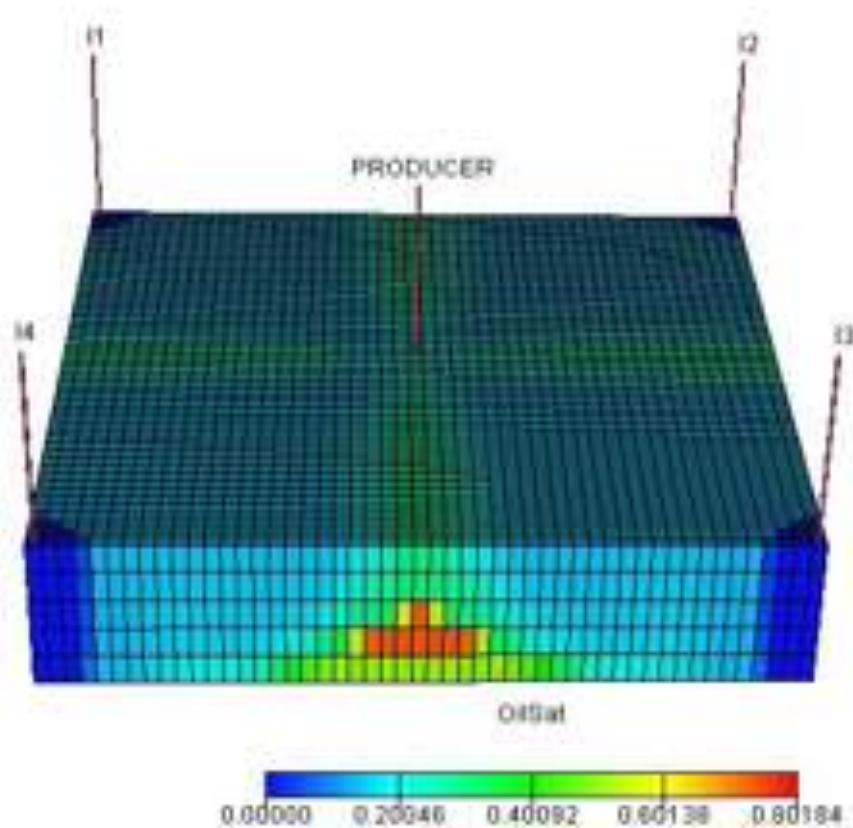


Figure 4. 9: The oil saturation grid model for CO<sub>2</sub> injection into a 29° API oil reservoir.

Referring to figure 4.10, the initial oil production rate (1000 stb/day) was maintained for about 150 days before experiencing decline. The maintenance of the production rate is as a result of minimal pressure drop probably because solution gas has not started evolving from the oil and the CO<sub>2</sub> injected as not reach miscibility with the reservoir oil. After 10 years, the reservoir pressure has dropped to 2400 psia resulting in production rate less than 100 stb/day and this gives about 70% recovery of OOIP as seen in figure 4.11. Also Figure 4.12 has a plot of how water production increases with decrease in oil production rate. The amount of water produced after 10 years of production is about 24000 STB.



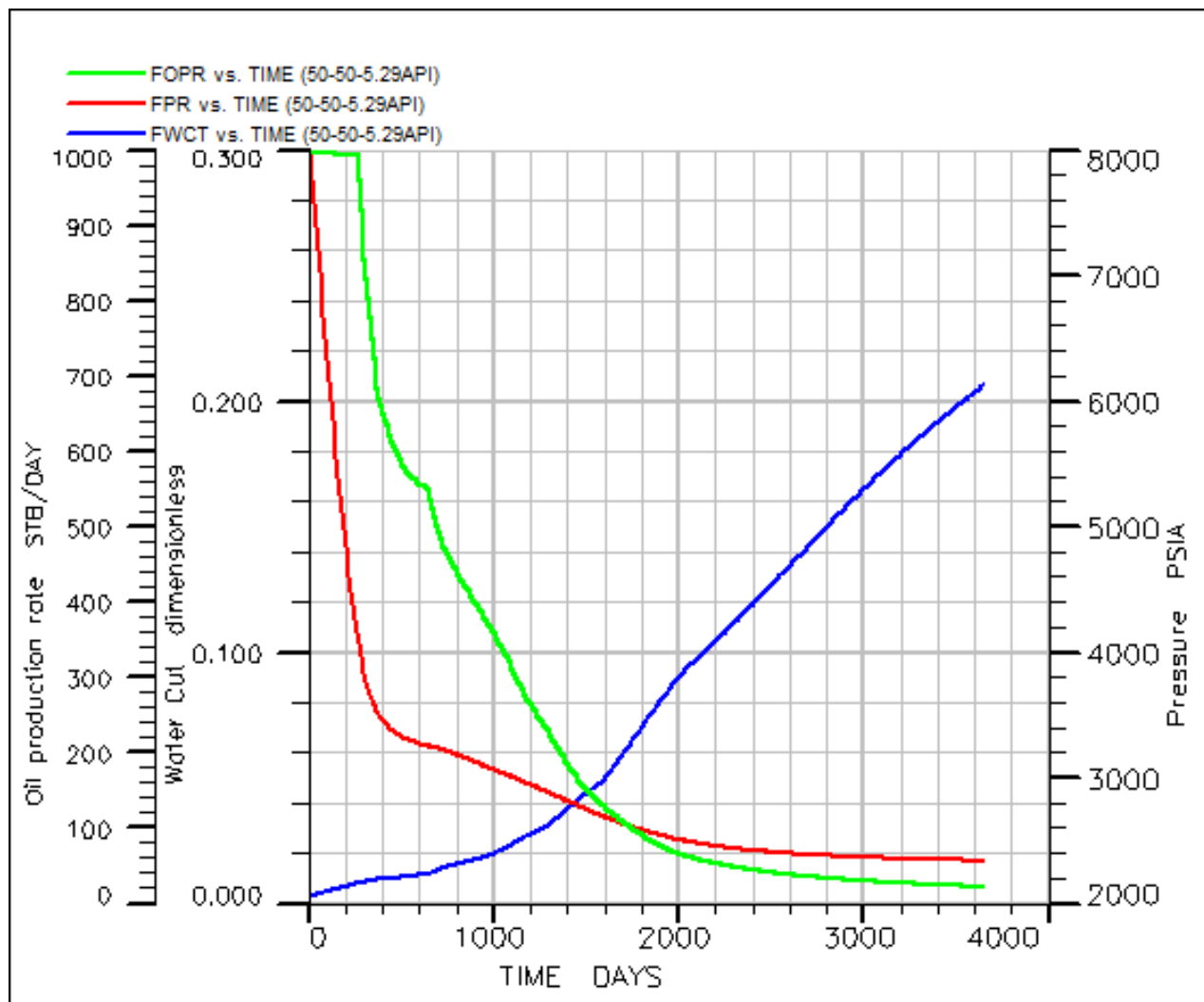


Figure 4. 10: The plot of pressure, production rate and water cut with time.

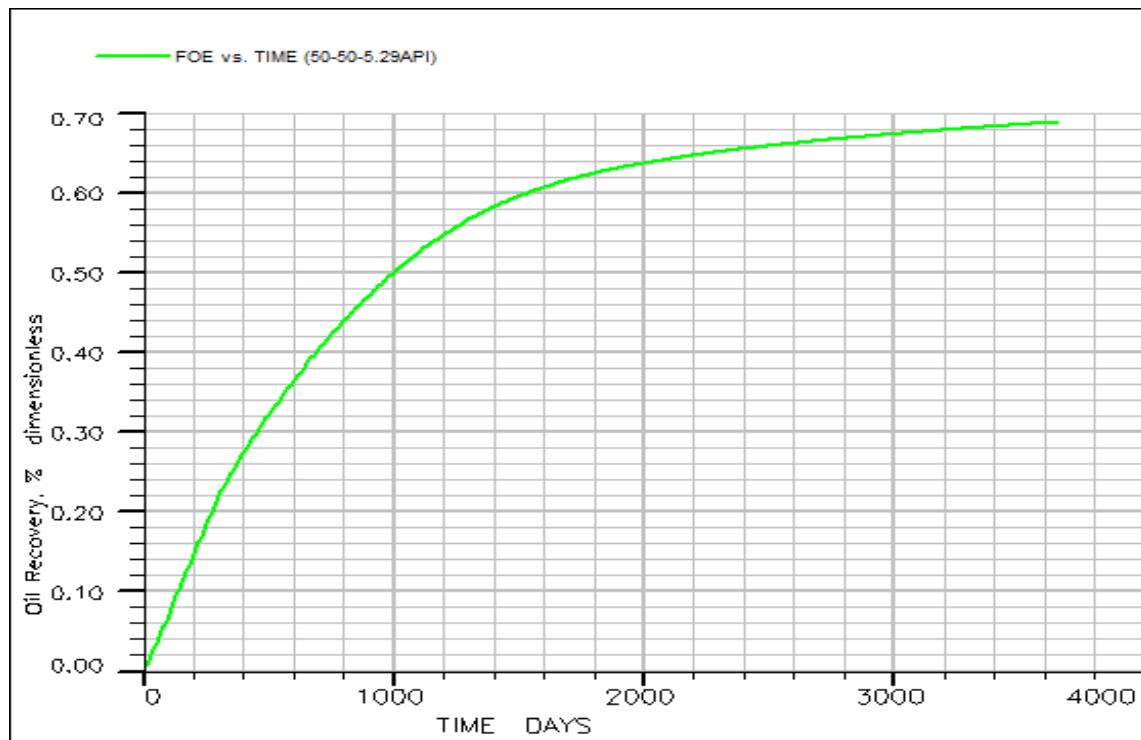


Figure 4. 11: The Cumulative recovery factor for 29° API crude sample.

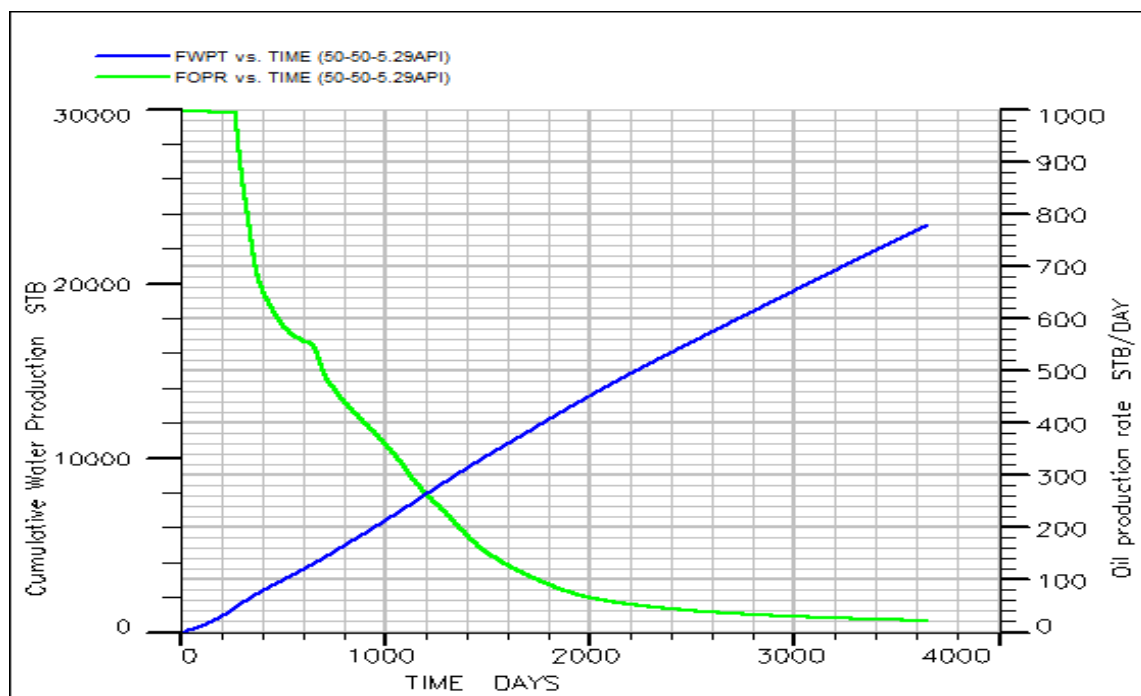
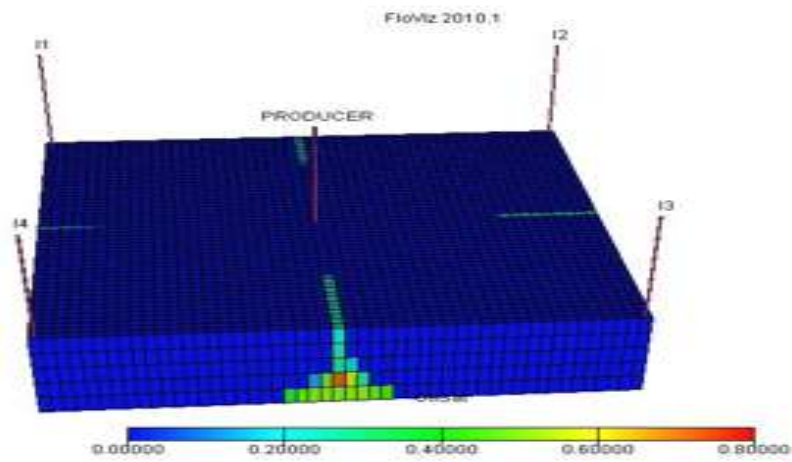


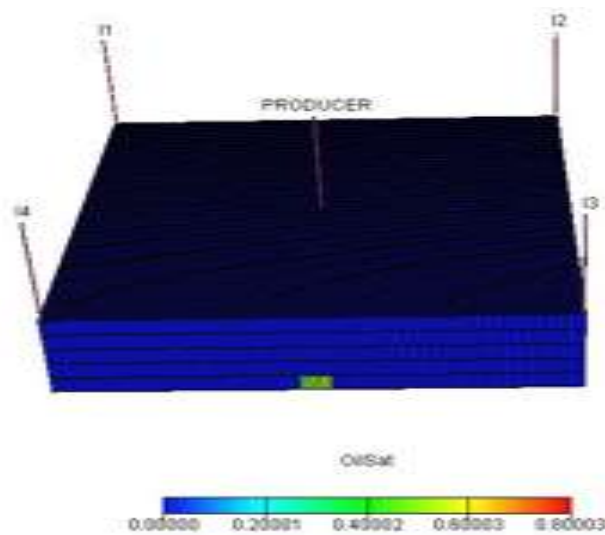
Figure 4. 12: Plot of oil production rate and total water production with time.

### Case C: 38° API Crude Sample

Pure CO<sub>2</sub> is injected into a reservoir with 38° API crude oil to enhance recovery via a 5-spot pattern model of injection. The simulation of this process was for ten years and the Cartesian oil saturation grid model is represented in figure 4.13 below.



(a)



(b)

Figure 4. 13: Oil saturation grid model of CO<sub>2</sub> injection scheme for (a) 50×50×5 grid system and (b) 100×100×5 grid system.

Represented in figure 4.14 below, the relationship between pressure, production rate and water cut with time in the reservoir shows that pressure decreases with production rate and production rate decreases with increase in water cut. The production rate was maintained for about 500 days with little or no pressure drop after which the pressure starts declining gradually with production rate. At about 800 days, production rate increases with constant pressure and no additional cumulative water produced. The water cut peaks at 100% with pressure of 2100psia and zero production rate after 10 years.

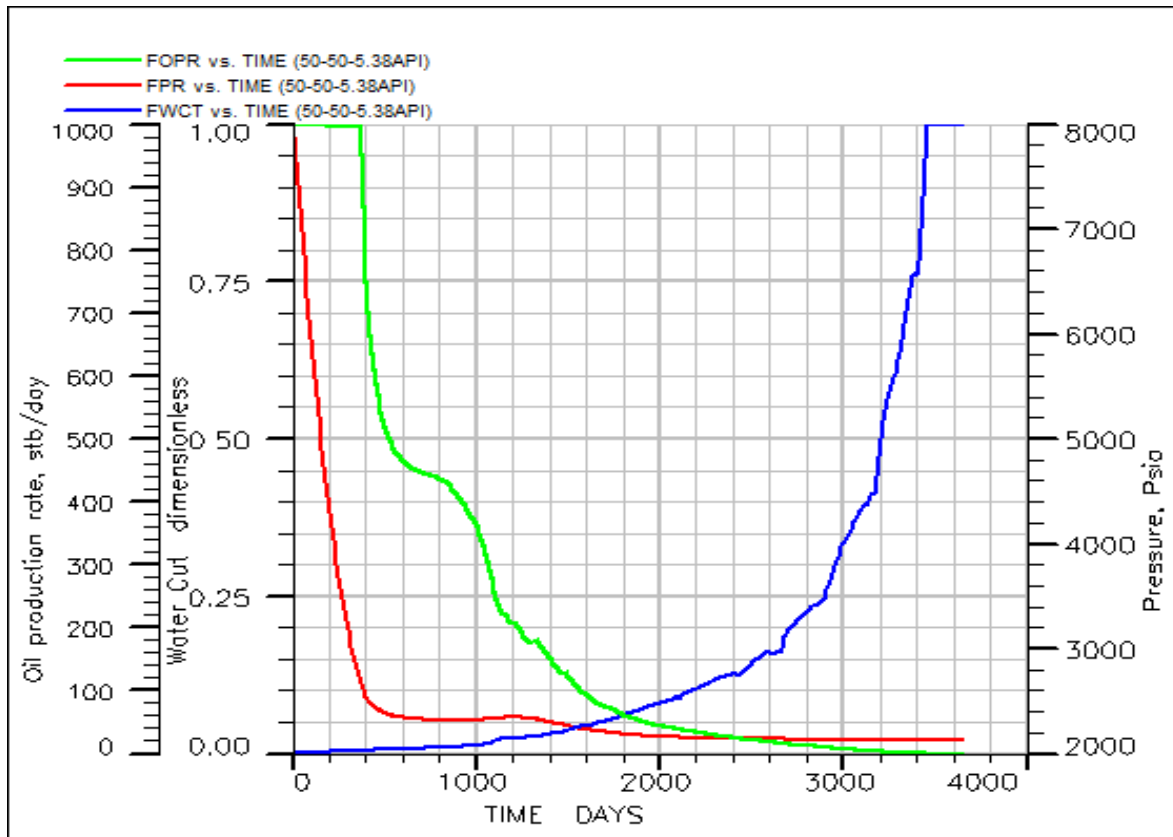


Figure 4. 14: Plot of pressure, oil production rate and water cut versus time

The recovery factor for CO<sub>2</sub> injection into a volatile oil reservoir with API gravity of 38° peaks after 10 years of CO<sub>2</sub> injection as presented in figure 4.15 below. High efficiency of this oil reservoir could be as a result of more light ends present in the hydrocarbon fluids which could be produced on its own without an additional support. Also, figure 4.16 below shows that the total water produced increases with time while production rate reduces with time for the simulation period of 10 years. The amount of water produced in

the reservoir is 14000 STB which is low compared to the 24000 STB produced in the medium crude oil reservoir. The higher efficiency of the two cases can be used to justify the low water production in the volatile oil reservoir.

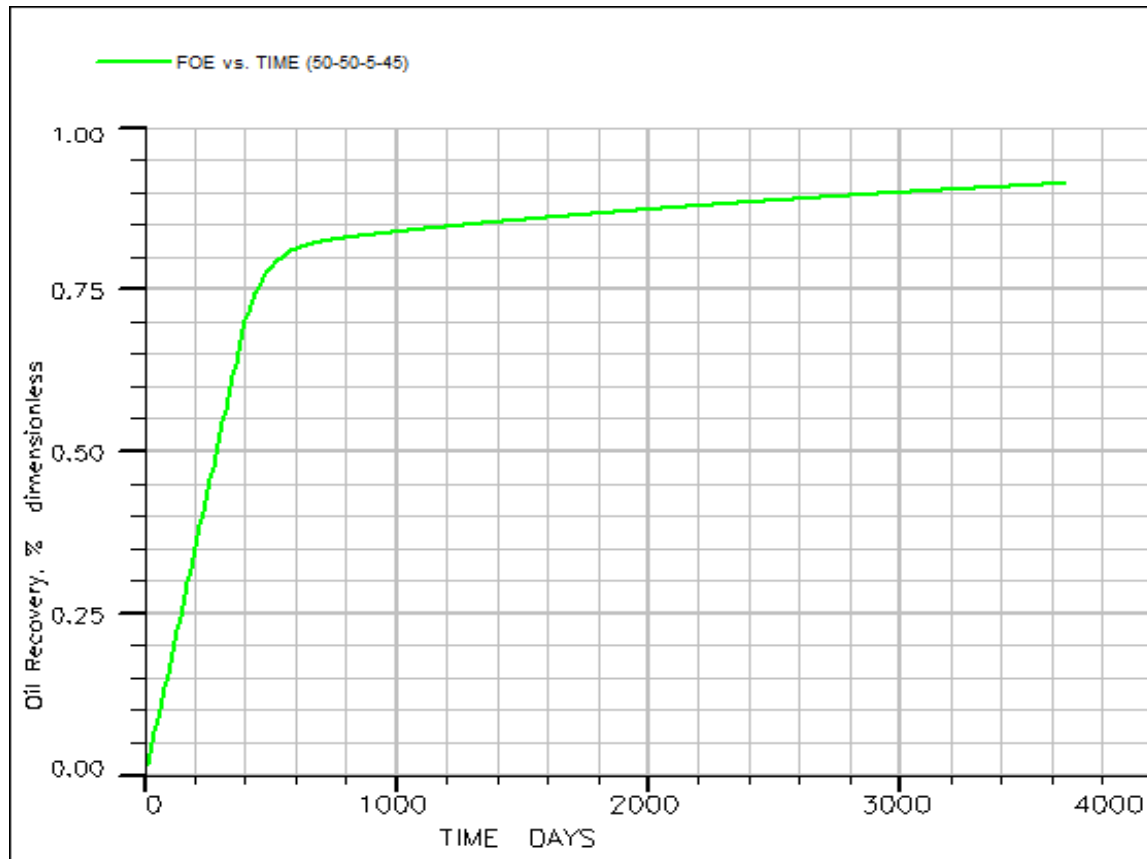


Figure 4. 15: Oil recovery factor of CO<sub>2</sub> injection for volatile oil reservoir.

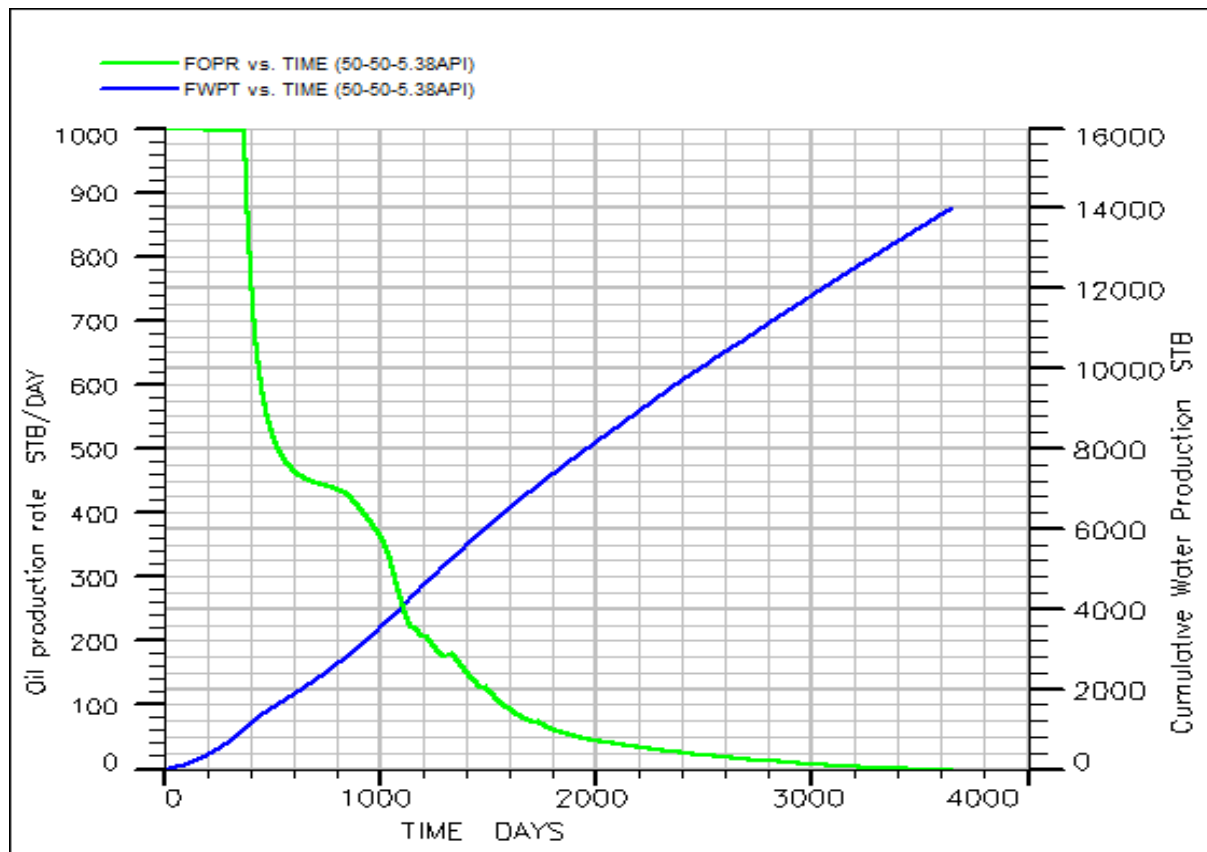


Figure 4. 16: Plot of total water production and oil production rate versus time.

#### 4.3 Sensitivity Analysis

Four different oil reservoirs having crude samples with API value of 22°, 29°, 38° and 45° are study for injection. Pure CO<sub>2</sub> is injected at the same injection rate and the formation properties kept constant for a period of 10 years. The output result from the simulation is studied and presented in figures.

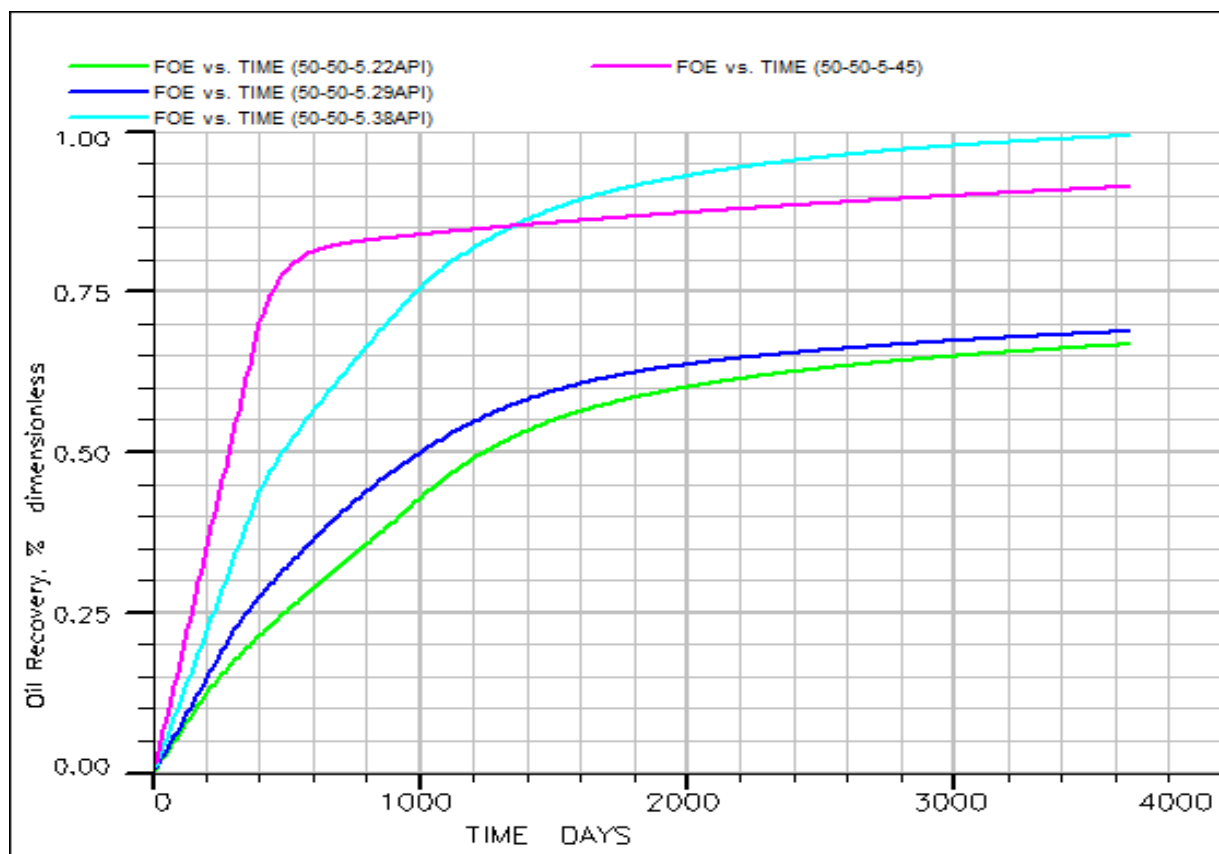


Figure 4. 17: Comparison plot of oil recovery factor for four API crude.

From figure 4.17, the recovery factor of the samples are presented graphically. The lightest crude (45° API) should have the highest recovery factor compare to the others but from the plot 38° API crude has the highest with RF of 100% while the 45° API has a RF of about 94% after 10 years of injection. The trend for all the samples was in order but an anomaly with the 45°API oil was observed after about 1300days of injection. Similar anomaly is noticed with water cut for the two samples of light oil studied as shown in figure 4.20 below. The two other samples (29° and 22°) follows the expected trend with the 38° API. The recovery factor for the heavy and medium oil samples corresponding to the 29° and the 22° API are 62% and 64% respectively.

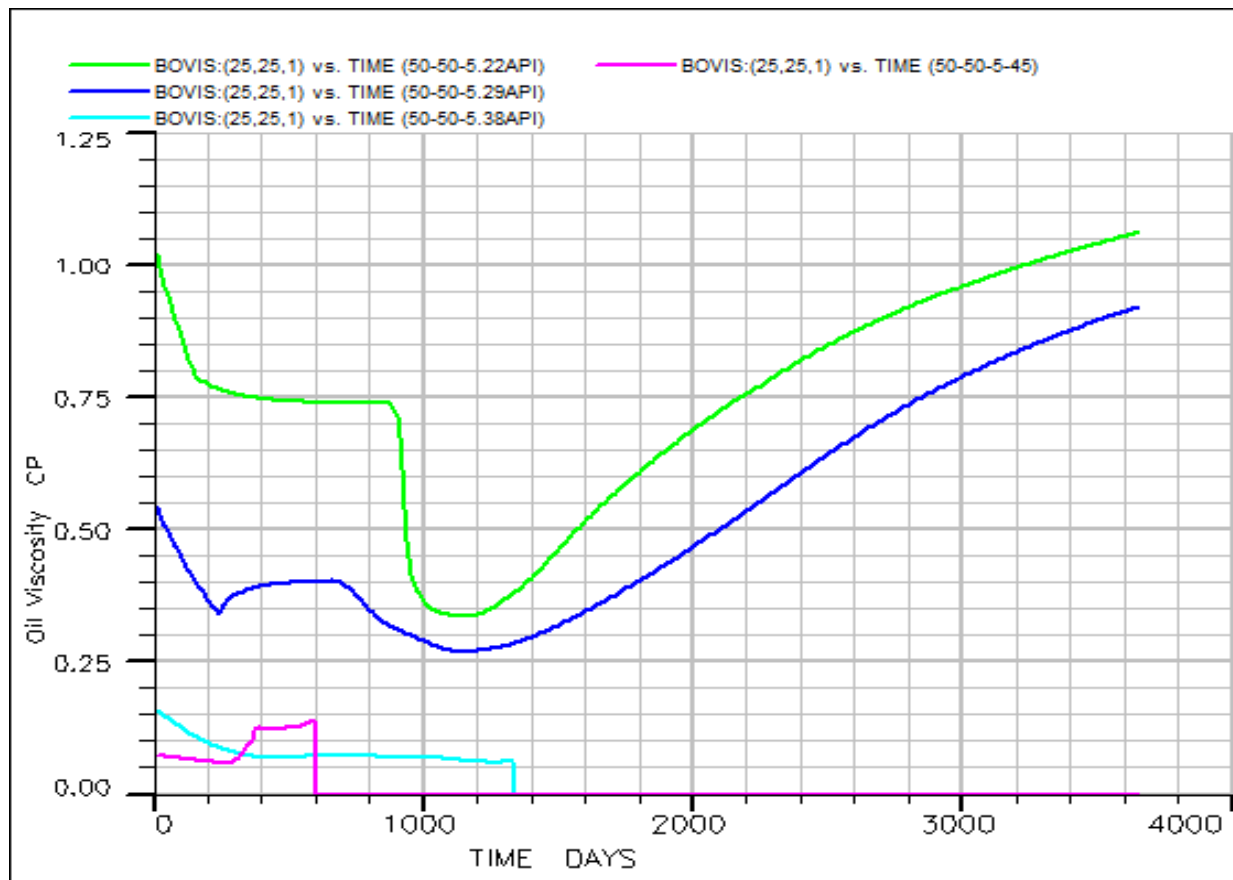


Figure 4. 18: Comparison plot of oil viscosity reduction for four API crude.

One of the major reason for carrying out tertiary recovery is to reduce the viscosity of the reservoir oil so as to increase mobility which ultimately increase recovery of hydrocarbon. The graphical representation of how oil viscosity reduces with continuous injection of CO<sub>2</sub> is shown in Figure 4.18 above. From the plot, the heavy crude has a higher viscosity than all other samples. The initial viscosities of the sample ranging from the heaviest to the lightest are 1.05 cP, 0.6 cP, 0.15 cP and 0.07cP. Two different observations are made, the heavy and the medium crude follow the same trend of CO<sub>2</sub>-Oil viscosity relationship with time. The viscosity was reducing and the minimum value reached is 0.32 cP and 0.27 cP after about 1200 days of injection, with continuous CO<sub>2</sub> injection viscosity continue increasing till the end of study.

For the other two light samples, the viscosity of 38° API oil was on continuous decrease with time while for the 45° API, the viscosity was zigzag patterned going up and down. After 600 days of injection, the



viscosity was zero for the lightest oil and compared with the efficiency from figure 4.15 there was a slight increase in recovery which flatten out after some days.

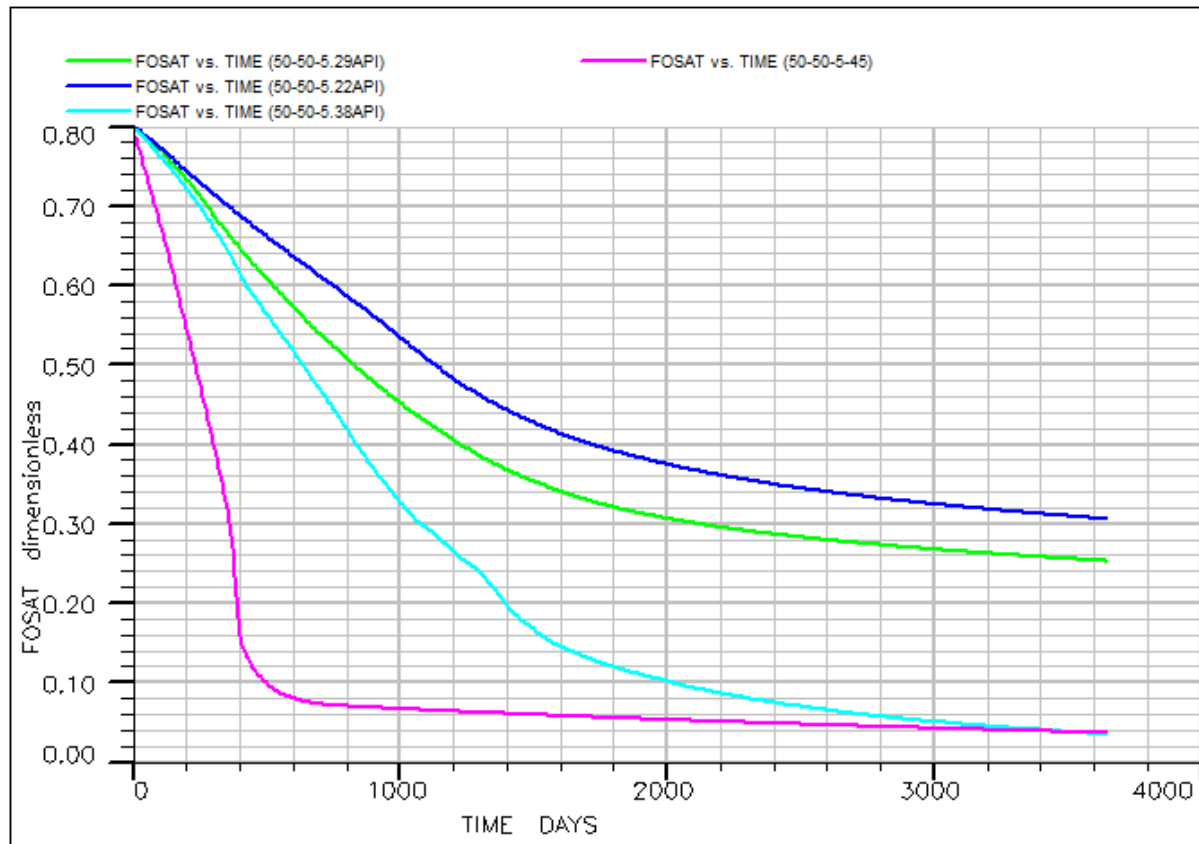


Figure 4. 19: Comparison plot of oil saturation for four API crude.

The initial oil saturation of the field was 80% as shown in figure 4.19 above. After ten years of CO<sub>2</sub> injection at the rate of 250 MSCF/DAY, the oil saturation for the four oil samples were 30%, 25% and 4% for the heavy, medium and the two light samples. The residual oil saturation of the heavy oil was reducible to 25% for additional simulation period of 10 years.

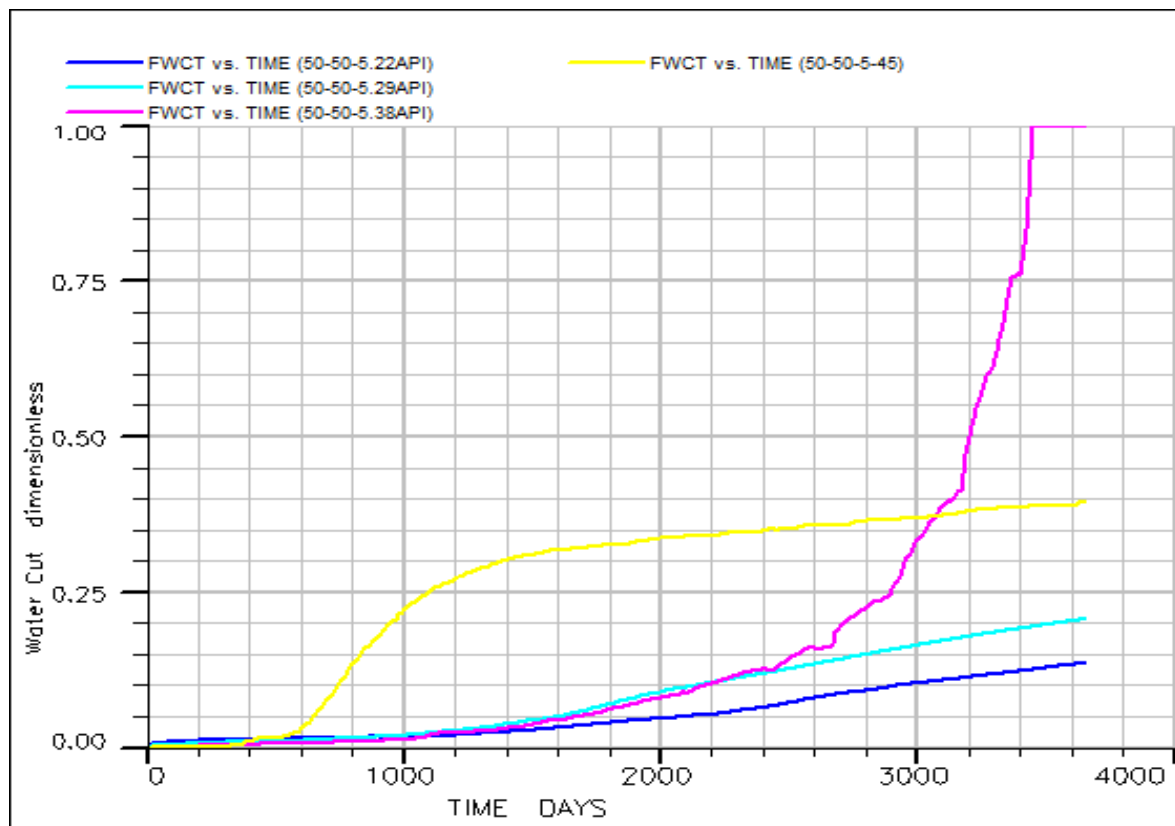


Figure 4. 20: Variation of water cut with time.

## CHAPTER FIVE

### CONCLUSIONS AND RECOMMENDATIONS

#### 5.1 Conclusions

Enhanced Oil Recovery is a method of recovering more oil from hydrocarbon reservoirs by injecting a fluid directly or indirectly which mobilizes the oil towards the producer well. CO<sub>2</sub> gas can be injected via different channels and methods to increase recovery, one of them is the in-situ generation method from CO<sub>2</sub> generating compounds. In this study, Eclipse 300 was used to characterize the fluid property. It was also used to test for CO<sub>2</sub>-Oil viscosity reduction and swelling. A compositional simulator was used to simulate CO<sub>2</sub> injection; a case study was considered and the properties of the formation were used for simulation of the process. The block oil viscosity, average reservoir pressure, oil saturation, recovery factor, water cut and cumulative water production are the key reservoir parameters considered. The following conclusions are drawn:

- The dissociation reaction of urea into carbon dioxide and ammonia is a first order linear reaction.
- Using more numbers of grid takes more computation time but the error is less.
- The swelling test from PVT simulator and efficiency from E300 simulator shows that recovery increases with increase in CO<sub>2</sub> injection.
- The CO<sub>2</sub>-oil viscosity relationship from PVTsim depicts that with increasing CO<sub>2</sub> injection viscosity reduces for all the crude samples tested, but the case was different with the E300 as the reduction was not continuous with the heavy and medium crude. With this, CO<sub>2</sub> injection could be considered best for volatile reservoirs.
- From the simulation of gas injection, high injection rate increases efficiency and improves recovery.

## 5.2 Recommendations

To better understand in situ CO<sub>2</sub> generation for flooding, the following recommendations were made;

- Simulation of the process has to be studied considering the molecular diffusion of CO<sub>2</sub> from the aqueous phase to the oleic phase.
- Practical field data should be used for simulation so as to obtain a publishable result which could be used in making decisions in the industry.
- The available compositional simulators could not simulate the chemical process hereby limiting the objective of this work, availability of the simulator software for research purpose should be considered.

## APPENDIX

Table A.1: Reservoir Fluid (API @ 21°) Component and their Properties used for study after grouping

Components	mole frac. (%)	Weight fraction (%)	Mol Weight (lb/mole)	Spec Gravity
	(percent)	(percent)		
H2S	2.19	0.49		
N2	0.24	0.04		
CO2	4.68	1.34		
C1	23.85	2.49		
C2-C4	16.40	4.37	40.86	0.56
C5-C6	2.88	1.43	76.22	0.64
C7-C9	14.33	9.77	104.51	0.74
C10-C11	5.89	5.37	139.52	0.78
C12+	29.54	74.69	387.5	0.89

Table A.2: Reservoir Fluid (API @ 38°) Component and their Properties used for study after grouping

Components	Mole frac. (%)	Weight frac.(%)	Mol Weight (lb/mole)	Spec Gravity
H2S	2.19	0.69		
N2	0.23	0.06		
CO2	4.68	1.91		
C1	38.72	5.77		
C2-C4	16.39	6.23	40.86	0.56
C5-C6	3.87	2.74	76.21	0.64
C7-C9	7.24	7.03	104.51	0.73
C10-C11	8.89	11.54	139.52	0.78
C12+	17.75	63.98	387.5	0.89

Table A 3: Reservoir Fluid (API @ 38°) Component and their Properties used for study after grouping

Components	mole, percent	Weight frac. Percent	Mol Weight	Spec Gravity
N2	0	0		
H2S	0	0		
CO2	0.35	0.28		
C1	40.08	11.73		
C2	7.45	4.08		
C3	7.49	6.03		
C4-C5	10.40	11.84	62.37	0.58
C6	3.56	5.46		
C7+	30.65	60.54	108.2	0.74

Table A 4: Reservoir Fluid (API@ 45°) Component and their Properties used for study after grouping

Components	mole , percent	Weight frac, percent	Mol Weight,lb/mole	Spec Gravity
H2S	0.31	0.25		
N2	0	0		
CO2	0.92	0.98		
C1	63.71	24.74		
C2	11.63	8.46		
C3	5.97	6.37		
C4-C5	5.11	7.78	62.95	0.58
C6	1.60	3.25		
C7+	10.75	48.14	185	0.80

Table A.5: The critical properties of the pseudocomponents for the heavy crude oil sample.

Components	Molecular weight,lb/mole	Crit. Pressure, psia	Crit. Temp., R	Crit. Volumes ,ft3/lbmole	Acentric Factors
'H2S'	34.07	1296.17	672.48	1.56	0.1
'N2'	28.01	492.31	227.16	1.44	0.04
'CO2'	44.01	1071.33	548.46	1.50	0.22
'C1'	16.04	667.78	343.08	1.56	0.01
C2-C4	40.86	641.88	633.72	3.02	0.13
C5-C6	76.21	471.72	863.69	5.18	0.26
C7-C9	104.50	414.62	1021.72	6.78	0.31
C10-C11	139.51	339.27	1143.60	8.91	0.39
C12+	387.50	121.00	1606.27	24.67	1.20

Table A.6: The critical properties of the pseudocomponents for the heavy crude oil sample.

Components	Molecular weight, lb/mole	Crit. Pressure, psia	Crit. Temperature, R	Crit. Volumes ,ft3/lbmole	Acentric Factors
'H2S'	34.076	1296.178	672.48	1.569809	0.1000
'N2'	28.013	492.3126	227.16	1.441661	0.0400
'CO2'	44.01	1071.331	548.46	1.505735	0.2250
'C1'	16.043	667.7817	343.08	1.569809	0.0130
'C2'	40.86353	641.8871	633.73	3.029178	0.1380
'C3'	76.21857	471.7203	863.69	5.187172	0.2602
'C4-C5'	104.5052	414.6209	1021.73	6.783325	0.3133
'C6'	139.5173	339.2748	1143.61	8.914171	0.3994
'C7+'	387.5007	121.0046	1606.27	24.67212	1.2017

Table A.7: The critical properties of the pseudocomponents for the heavy crude oil sample.

Components	Molecular weight, lb/mole	Crit. Pressure, psia	Crit. Temperature, R	Crit. Volumes ,ft3/lbmole	Acentric Factors
'H2S'	28.01	492.31	227.16	1.44	0.04
'N2'	34.08	1296.17	672.48	1.56	0.10
'CO2'	44.01	1071.33	548.46	1.50	0.22
'C1'	16.04	667.78	343.08	1.56	0.01
'C2'	30.07	708.34	549.77	2.37	0.09
'C3'	44.10	615.75	665.64	3.20	0.15
C4-C5	62.37	524.95	776.03	4.39	0.20
C6	84.00	436.61	913.50	5.62	0.29
C7+	108.20	429.26	1022.53	6.87	0.34

Table A. 8: The critical properties of the pseudocomponents for the heavy crude oil sample.

Components	Molecular weight, lb/mole	Crit. Pressure, psia	Crit. Temperature, R	Crit. Volumes ,ft3/lbmole	Acentric Factors
H2S	34.07	1296.18	672.5	1.57	0.10
N2	28.01	492.31	227.2	1.44	0.04
CO2	44.01	1071.33	548.5	1.50	0.22
C1	16.04	667.78	343.1	1.57	0.01
C2	30.07	708.34	549.8	2.37	0.09
C3	44.09	615.76	665.6	3.20	0.15
C4-C5	62.95	510.08	762.9	4.38	0.16
C6	84	436.62	913.5	5.62	0.29
C7+		275.55	1243.3	11.73	0.60



Table A.9: The Binary Interaction Coefficients of the pseudo-components for the heavy oil.

Components	'H2S'	'N2'	'CO2'	'C1'	C2-C4	C5-C6	C7-C9	C10-C11
'H2S'	0.176							
'N2'	-0.012	0.09						
'CO2'	0.1	0.05	0.1					
'C1'	0.1	0.05	0.1	0				
C2-C4	0.1	0.05	0.1	0.009	0.002			
C5-C6	0.1	0.05	0.1	0.035	0.007	0		
C7-C9	0.1	0.05	0.1	0.041	0.007	0	0	
C10-C11	0.1	0.05	0.1	0.066	0.007	0	0	0

Table A.10: The Binary Interaction Coefficients of the pseudo-components for the medium oil.

Components	'H2S'	'N2'	'CO2'	'C1'	'C2'	'C3'	C4-C5	C6
'H2S'	0.176							
'N2'		-0.01	0.09					
'CO2'		0.1	0.05	0.1				
'C1'		0.1	0.05	0.1	0			
'C2'		0.1	0.05	0.1	0.009	0.003		
'C3'		0.1	0.05	0.1	0.035	0.007	0	
'C4-C5'		0.1	0.05	0.1	0.041	0.007	0	0
'C6'		0.1	0.05	0.1	0.066	0.007	0	0

Table A.11: The Binary Interaction Coefficients of the pseudo-components for the intermediate oil.

Components	'H2S'	'N2'	'CO2'	'C1'	'C2'	'C3'	C4-C5	C6
'H2S'	0							
'N2'	0	0						
'CO2'	0	0	0.1					
'C1'	0	0	0.1	0				
'C2'	0	0	0.1	0	0			
'C3'	0	0	0.1	0	0	0		
C4-C5	0	0	0.1	0.03	0.01	0.01	0	
C6	0	0	0.1	0.06	0.01	0.01	0	0

Table A.12: The Binary Interaction Coefficients of the pseudo-components for the light oil.

Components	H2S	N2	CO2	C1	C2	C3	C4-C5	C6
H2S	0.18							
N2	0.09	-0.012						
CO2	0.05	0.1	0.1					
C1	0.05	0.1	0.1	0				
C2	0.05	0.1	0.1	0	0			
C3	0.05	0.1	0.1	0	0	0		
C4-C5	0.05	0.1	0.1	0.03	0.01	0.01	0	
C6	0.05	0.1	0.1	0.04	0.01	0.01	0	0

## REFERENCES

1. Al-Abri, A., & Amin, R. (2010). Phase behaviour, fluid properties and recovery efficiency of immiscible and miscible condensate displacements by SC CO<sub>2</sub> injection: experimental investigation. *Transport in porous media*, 85(3), 743-756.
2. Al-Menhali, A. S., & Krevor, S. (2016). Capillary trapping of CO<sub>2</sub> in oil reservoirs: Observations in a mixed-wet carbonate rock. *Environmental science & technology*, 50(5), 2727-2734.
3. Alston, R., Kokolis, G., & James, C. (1985). CO<sub>2</sub> minimum miscibility pressure: a correlation for impure CO<sub>2</sub> streams and live oil systems. *Society of Petroleum Engineers Journal*, 25(02), 268-274.
4. Altunina, L. K., & Kuvshinov, V. A. (2007). Physicochemical methods for enhancing oil recovery from oil fields. *Russian Chemical Reviews*, 76(10), 971.
5. Bai, H., & Yeh, A. C. (1997). Removal of CO<sub>2</sub> greenhouse gas by ammonia scrubbing. *Industrial & engineering chemistry research*, 36(6), 2490-2493.
6. Bakhtiyarov, S. I., Shakhverdiev, A. K., Panakhov, G. M., & Abbasov, E. M. (2007). *Effect of Surfactant on Volume and Pressure of Generated CO<sub>2</sub> Gas*. Paper presented at the Production and Operations Symposium.
7. Bebout, D., Loucks, R., Bosch, S., & Dorfman, M. (1976). Geothermal resources—Frio Formation, upper Texas Gulf Coast: The University of Texas at Austin. *Bureau of Economic Geology Geological Circular*, 76, 47.
8. Benson, S. M., & Cole, D. R. (2008). CO<sub>2</sub> sequestration in deep sedimentary formations. *Elements*, 4(5), 325-331.
9. Bird, R. B., Lightfoot, E. N., & Stewart, W. E. (1960). *Notes on Transport Phenomena*. *Transport Phenomena*. By RB Bird, Warren E. Stewart, Edwin N. Lightfoot. A Rewritten and Enlarged Edition of "Notes on Transport Phenomena": New York, London.
10. Bird, R. B., Stewart, W. E., & Lightfoot, E. N. (2007). *Transport phenomena*: John Wiley & Sons.
11. Bishnoi, S., & Rochelle, G. T. (2000). Physical and chemical solubility of carbon dioxide in aqueous methyldiethanolamine. *Fluid Phase Equilibria*, 168(2), 241-258.
12. Blunt, M., Fayers, F. J., & Orr Jr, F. M. (1993). Carbon dioxide in enhanced oil recovery. *Energy Conversion and Management*, 34(9-11), 1197-1204.
13. Bonenfant, D., Mimeault, M., & Hausler, R. (2003). Determination of the structural features of distinct amines important for the absorption of CO<sub>2</sub> and regeneration in aqueous solution. *Industrial & engineering chemistry research*, 42(14), 3179-3184.
14. Buckley, J. S., & Fan, T. (2007). Crude oil/brine interfacial tensions1. *Petrophysics*, 48(03).
15. Chakma, A. (1995). Separation of CO<sub>2</sub> and SO<sub>2</sub> from flue gas streams by liquid membranes. *Energy Conversion and Management*, 36(6-9), 405-410.
16. Christensen, R. (1961). *Carbonated waterflood results--Texas and Oklahoma*. Paper presented at the Annual Meeting of Rocky Mountain Petroleum Engineers of AIME.
17. Clark, K., Gaddy, V., & Rist, C. (1933). Equilibria in the ammonium carbamate-urea-water system. *Industrial & Engineering Chemistry*, 25(10), 1092-1096.
18. Claudel, B., & Boulamri, L. (1988). A new model of gas-solid kinetics: the case of ammonium carbamate formation and decomposition. *Thermochimica acta*, 126, 129-148.
19. Cullinane, J. T. (2005). *Thermodynamics and kinetics of aqueous piperazine with potassium carbonate for carbon dioxide absorption*.
20. Danckwerts, P. (1970). Chemical methods of measuring interfacial area and mass transfer coefficients in two-fluid systems. *Brit. Chem. Eng.*, 15, 522-526.
21. Darde, V., Thomsen, K., Van Well, W. J., & Stenby, E. H. (2009). Chilled ammonia process for CO<sub>2</sub> capture. *Energy Procedia*, 1(1), 1035-1042.

22. De Nevers, N. (1964). A calculation method for carbonated water flooding. *Society of Petroleum Engineers Journal*, 4(01), 9-20.
23. Dong, M., Huang, S., & Srivastava, R. (2001). A laboratory study on near-miscible CO<sub>2</sub> injection in steelman reservoir. *Journal of Canadian Petroleum Technology*, 40(02).
24. Duan, Z., Sun, R., Zhu, C., & Chou, I.-M. (2006). An improved model for the calculation of CO<sub>2</sub> solubility in aqueous solutions containing Na<sup>+</sup>, K<sup>+</sup>, Ca<sup>2+</sup>, Mg<sup>2+</sup>, Cl<sup>-</sup>, and SO<sub>4</sub><sup>2-</sup>. *Marine Chemistry*, 98(2-4), 131-139.
25. Elsharkawy, A. M., & Foda, S. G. (1998). EOS simulation and GRNN modeling of the constant volume depletion behavior of gas condensate reservoirs. *Energy & fuels*, 12(2), 353-364.
26. Emera, M., & Lu, J. (2005). *Genetic Algorithm (GA)-Based Correlations Offer More Reliable Prediction of Minimum Miscibility Pressures (MMP) Between the Reservoir Oil and CO or Flue Gas*. Paper presented at the Canadian International Petroleum Conference.
27. Fjelde, I., & Asen, S. M. (2010). *Wettability alteration during water flooding and carbon dioxide flooding of reservoir chalk rocks*. Paper presented at the SPE EUROPEC/EAGE Annual Conference and Exhibition.
28. Flury, C., Afacan, A., Tamiz Bakhtiari, M., Sjoblom, J., & Xu, Z. (2013). Effect of caustic type on bitumen extraction from Canadian oil sands. *Energy & fuels*, 28(1), 431-438.
29. Frejaques, C. (1951). The Kinetics of Decomposition of Nitric Acid in the Vapor Phase. *Compt. Rendus*, 232, 2206.
30. Green, D. W., & Willhite, G. P. (1998). *Enhanced oil recovery* (Vol. 6): Henry L. Doherty Memorial Fund of AIME, Society of Petroleum Engineers ....
31. Grogan, A. T., Pinczewski, V. W., Ruskau, G. J., & Orr, F. M., Jr. (1988). Diffusion of CO<sub>2</sub> at Reservoir Conditions: Models and Measurements. *SPE Reservoir Engineering*, 3(01), 93-102. doi:10.2118/14897-PA
32. Gumersky, K., Dzhabarov, I., Shakhverdiev, A. K., & Mamedov, Y. G. (2000). *In-situ generation of carbon dioxide: New way to increase oil recovery*. Paper presented at the SPE European Petroleum Conference.
33. Han, L., & Gu, Y. (2014). Optimization of miscible CO<sub>2</sub> water-alternating-gas injection in the Bakken formation. *Energy & fuels*, 28(11), 6811-6819.
34. Hangx, S. (2005). Subsurface mineralisation. Rate of CO<sub>2</sub> mineralisation and geomechanical effects on host and seal formations. Behaviour of the CO<sub>2</sub>-H<sub>2</sub>O system and preliminary mineralisation model and experiments.
35. Hashemi Fath, A., & Pouranfard, A.-R. (2014). Evaluation of miscible and immiscible CO<sub>2</sub> injection in one of the Iranian oil fields. *Egyptian Journal of Petroleum*, 23(3), 255-270. doi:<https://doi.org/10.1016/j.ejpe.2014.08.002>
36. Hatzignatiou, D., & Lu, Y. (1994). *Feasibility Study of CO<sub>2</sub> Immiscible Displacement Process In Heavy Oil Reservoirs*. Paper presented at the Annual Technical Meeting.
37. Hickok, C., Christensen, R., & Ramsay Jr, H. (1960). Progress review of the K&S carbonated waterflood project. *Journal of Petroleum Technology*, 12(12), 20-24.
38. Higbie, R. (1935). The rate of absorption of a pure gas into a still liquid during short periods of exposure. *Trans. AIChE*, 31, 365-389.
39. Hisatsune, K., De Courcy Jr, S. J., & Mudd, S. (1967). The immunologically active cell wall peptide polymer of Staphylococcus aureus. *Biochemistry*, 6(2), 595-603.
40. Holm, L. (1982). CO<sub>2</sub> flooding: its time has come. *Journal of Petroleum Technology*, 34(12), 2,739-732,745.
41. House, K. Z., Harvey, C. F., Aziz, M. J., & Schrag, D. P. (2009). The energy penalty of post-combustion CO<sub>2</sub> capture & storage and its implications for retrofitting the US installed base. *Energy & Environmental Science*, 2(2), 193-205.

42. Johnson Jr, C. (1976). Status of caustic and emulsion methods. *Journal of Petroleum Technology*, 28(01), 85-92.
43. Kaminskaia, N. V., & Kostić, N. M. (1997). Kinetics and mechanism of urea hydrolysis catalyzed by palladium (II) complexes. *Inorganic chemistry*, 36(25), 5917-5926.
44. Khan, Z., Rafiquee, M., Niaz, M. A., & Khan, A. A. (1996). Kinetics and mechanism of alkaline hydrolysis of urea and sodium cyanate.
45. Khatri, R. A., Chuang, S. S., Soong, Y., & Gray, M. (2006). Thermal and chemical stability of regenerable solid amine sorbent for CO<sub>2</sub> capture. *Energy & fuels*, 20(4), 1514-1520.
46. King, C. J. (1966). Turbulent liquid phase mass transfer at free gas-liquid interface. *Industrial & Engineering Chemistry Fundamentals*, 5(1), 1-8.
47. Laurent, V., & Kikindai, T. (1972). 2 REACTIONS WHICH CAN BE ACTIVATED BY INFRARED RAY OF A CO<sub>2</sub>-LASER. *BULLETIN DE LA SOCIETE CHIMIQUE DE FRANCE*(4), 1258-&.
48. Lei, H., Yang, S., Zu, L., Wang, Z., & Li, Y. (2016). Oil recovery performance and CO<sub>2</sub> storage potential of CO<sub>2</sub> water-alternating-gas injection after continuous CO<sub>2</sub> injection in a multilayer formation. *Energy & fuels*, 30(11), 8922-8931.
49. Li, H., Qin, J., & Yang, D. (2012). An improved CO<sub>2</sub>-oil minimum miscibility pressure correlation for live and dead crude oils. *Industrial & engineering chemistry research*, 51(8), 3516-3523.
50. Lishnevskii, V., & Madzievskaya, T. (1987). Kinetic Order of the Formation of Solid Ammonium Carbamate from Gaseous Mixtures of Ammonia and Carbon Dioxide. *Russian Journal of Physical Chemistry*, 61, 36.
51. Liu, Y., Zhang, Y., & Behrens, H. (2005). Solubility of H<sub>2</sub>O in rhyolitic melts at low pressures and a new empirical model for mixed H<sub>2</sub>O-CO<sub>2</sub> solubility in rhyolitic melts. *Journal of Volcanology and Geothermal Research*, 143(1-3), 219-235.
52. Mangalsingh, D., & Jagai, T. (1996). A laboratory investigation of the carbon dioxide immiscible process. Paper presented at the SPE Latin America/Caribbean Petroleum Engineering Conference.
53. McCann, N., Maeder, M., & Attalla, M. (2008). Simulation of enthalpy and capacity of CO<sub>2</sub> absorption by aqueous amine systems. *Industrial & engineering chemistry research*, 47(6), 2002-2009.
54. Meyer, D., Zarra, L., Rains, D., Meltz, B., & Hall, T. (2005). Emergence of the Lower Tertiary Wilcox trend in the deep-water Gulf of Mexico: American Association of Petroleum Geologists Search and Discovery Article# 10084. In.
55. Mosavat, N., & Torabi, F. (2014). Application of CO<sub>2</sub>-saturated water flooding as a prospective safe CO<sub>2</sub> storage strategy. *Energy Procedia*, 63, 5408-5419.
56. Okuno, R., Johns, R. T., & Sepehrnoori, K. (2010). Three-phase flash in compositional simulation using a reduced method. *Spe Journal*, 15(03), 689-703.
57. Orr, F. M. (2009). Onshore geologic storage of CO<sub>2</sub>. *Science*, 325(5948), 1656-1658.
58. Orr, J. F., & Taber, J. (1984). Use of carbon dioxide in enhanced oil recovery. *Science*, 224(4649), 563-569.
59. Paul, M. J., & Meyer, J. L. (2001). Streams in the urban landscape. *Annual review of Ecology and Systematics*, 32(1), 333-365.
60. Prosper, G. W., & Ali, S. (1991). *Scaled Model Studies Of The Immiscible Carbon Dioxide Flooding Process at Low Pressures*. Paper presented at the Annual Technical Meeting.
61. Rains, D., Zarra, L., & Meyer, D. (2007). The lower Tertiary Wilcox trend in the deepwater Gulf of Mexico: AAPG Search and Discovery article 110040. In.
62. Ramachandran, B., Halpern, A. M., & Glendening, E. D. (1998). Kinetics and mechanism of the reversible dissociation of ammonium carbamate: Involvement of carbamic acid. *The Journal of Physical Chemistry A*, 102(22), 3934-3941.

63. Rao, D., & Girard, M. (2002). Induced multiphase flow behaviour effects in gas injection EOR projects. *Journal of Canadian Petroleum Technology*, 41(07).
64. Reid, R. C., Prausnitz, J. M., & Poling, B. E. (1987). The properties of gases and liquids.
65. Riazi, M., Sohrabi, M., Jamiolahmady, M., & Ireland, S. (2009). *Oil recovery improvement using CO<sub>2</sub>-enriched water injection*. Paper presented at the EUROPEC/EAGE Conference and Exhibition.
66. Rochelle, G. T., Bishnoi, S., Chi, S., Dang, H., & Santos, J. (2001). Research needs for CO<sub>2</sub> capture from flue gas by aqueous absorption/stripping. *Final Report for DOE of DE-AF26-99FT01029*.
67. Rojas, G., & Ali, S. (1988). Dynamics of subcritical CO<sub>2</sub>/brine floods for heavy-oil recovery. *SPE Reservoir Engineering*, 3(01), 35-44.
68. Rutqvist, J., Liu, H.-H., Vasco, D. W., Pan, L., Kappler, K., & Majer, E. (2011). Coupled non-isothermal, multiphase fluid flow, and geomechanical modeling of ground surface deformations and potential for induced micro-seismicity at the In Salah CO<sub>2</sub> storage operation. *Energy Procedia*, 4, 3542-3549.
69. Scott, J., & Forrester, C. (1965). Performance of domes unit carbonated waterflood-first stage. *Journal of Petroleum Technology*, 17(12), 1,379-371,384.
70. Seiersten, M. (2001). Material selection for separation, transportation and disposal of
71. CO<sub>2</sub>. . *Proceedings Corrosion*.
72. Shafikova, G. M. (2013). *Analysis of Diffusion Models in Eclipse 300*. Institutt for petroleumsteknologi og anvendt geofysikk,
73. Sharma, H., Dufour, S., Arachchilage, G. W. P., Weerasooriya, U., Pope, G. A., & Mohanty, K. (2015). Alternative alkalis for ASP flooding in anhydrite containing oil reservoirs. *Fuel*, 140, 407-420.
74. Shiau, B. J. B., Hsu, T.-P., Roberts, B. L., & Harwell, J. H. (2010). *Improved chemical flood efficiency by in situ CO<sub>2</sub> generation*. Paper presented at the SPE Improved Oil Recovery Symposium.
75. Shokir, E. M. E.-M. (2007). CO<sub>2</sub>-oil minimum miscibility pressure model for impure and pure CO<sub>2</sub> streams. *Journal of Petroleum Science and Engineering*, 58(1-2), 173-185.
76. Shu, G., Dong, M., Chen, S., & Hassanzadeh, H. (2016). Mass transfer of CO<sub>2</sub> in a carbonated water-oil system at high pressures. *Industrial & engineering chemistry research*, 56(1), 404-416.
77. Simon, R., & Graue, D. J. (1965). Generalized Correlations for Predicting Solubility, Swelling and Viscosity Behavior of CO<sub>2</sub> -Crude Oil Systems. *Journal of Petroleum Technology*, 17(01), 102-106. doi:10.2118/917-PA
78. Sohrabi, M., Riazi, M., Jamiolahmady, M., Kechut, N. I., Ireland, S., & Robertson, G. (2011). Carbonated water injection (CWI)—A productive way of using CO<sub>2</sub> for oil recovery and CO<sub>2</sub> storage. *Energy Procedia*, 4, 2192-2199.
79. Southwick, J. G., van den Pol, E., van Rijn, C. H., van Batenburg, D. W., Boersma, D., Svec, Y., . . . Raney, K. (2016). Ammonia as alkali for alkaline/surfactant/polymer floods. *Spe Journal*, 21(01), 10-21.
80. Spivak, A., & Chima, C. (1984). *Mechanisms of immiscible CO<sub>2</sub> injection in heavy oil reservoirs, Wilmington Field, CA*. Paper presented at the SPE Enhanced Oil Recovery Symposium.
81. Steffens, A. (2010). Modeling and laboratory study of carbonated water flooding.
82. Sylvester, Z., & Lowe, D. R. (2004). Textural trends in turbidites and slurry beds from the Oligocene flysch of the East Carpathians, Romania. *Sedimentology*, 51(5), 945-972.
83. Verma, M. K. (2015). *Fundamentals of carbon dioxide-enhanced oil recovery (CO<sub>2</sub>-EOR): A supporting document of the assessment methodology for hydrocarbon recovery using CO<sub>2</sub>-EOR associated with carbon sequestration*: US Department of the Interior, US Geological Survey Washington, DC.

84. Wang, S., Chen, C., Shiau, B., & Harwell, J. H. (2018). In-situ CO<sub>2</sub> generation for EOR by using urea as a gas generation agent. *Fuel*, 217, 499-507.
85. Wang, S., Kadhum, M. J., Chen, C., Shiau, B., & Harwell, J. H. (2017). Development of in situ CO<sub>2</sub> generation formulations for enhanced oil recovery. *Energy & fuels*, 31(12), 13475-13486.
86. Wen, N., & Brooker, M. H. (1995). Ammonium carbonate, ammonium bicarbonate, and ammonium carbamate equilibria: A Raman study. *The Journal of Physical Chemistry*, 99(1), 359-368.
87. Wilke, C., & Chang, P. (1955). Correlation of diffusion coefficients in dilute solutions. *AIChE Journal*, 1(2), 264-270.
88. Wilkinson, M., Haszeldine, R. S., Fallick, A. E., Odling, N., Stoker, S. J., & Gatliff, R. W. (2009). CO<sub>2</sub>–mineral reaction in a natural analogue for CO<sub>2</sub> storage—implications for modeling. *Journal of Sedimentary Research*, 79(7), 486-494.
89. Wolsky, A., Daniels, E., & Jody, B. (1994). CO<sub>2</sub> capture from the flue gas of conventional fossil-fuel-fired power plants. *Environmental Progress*, 13(3), 214-219.